CONTINUOUSLY FREQUENCY-TUNABLE CW OPTICAL PARAMETRIC OSCILLATORS AND THEIR APPLICATION TO SPECTROSCOPY

Graham Martin Gibson

A Thesis Submitted for the Degree of PhD
at the
University of St Andrews

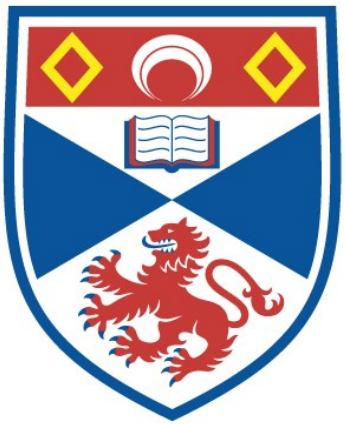

1999

Continuously frequency-tunable cw optical parametric oscillators and their application to spectroscopy

G. M. Gibson

J.F. Allen Physics Research Laboratories,
Department of Physics & Astronomy,
University of St. Andrews,
Fife, Scotland.

A thesis submitted to the University of St. Andrews
in application for the degree of Doctor of Philosophy

February 1999

ProQuest LLC.
789 East Eisenhower Parkway
P.O. Box 1346
Ann Arbor, MI 48106 – 1346

Declarations

I, Graham Martin Gibson, hereby certify that this thesis, which is approximately 22,000 words in length, has been written by me, that it is the record of work carried out by me and that it has not been submitted in any previous application for a higher degree.

Date 2/2/99 Signature of candidate _____

I was admitted as a research student in September 1995 and as a candidate for the degree of Doctor of Philosophy in September 1995; the higher study for which this is a record was carried out in the University of St. Andrews between 1995 and 1998.

Date 2/2/99 Signature of candidate _____

I hereby certify that the candidate has fulfilled the conditions of the Resolution and Regulations appropriate for the degree of Doctor of Philosophy in the University of St. Andrews and that the candidate is qualified to submit this thesis in application for that Degree.

Date 2/2/99 Signature of supervisors _____

_____

In submitting this thesis to the University of St. Andrews I understand that I am giving permission for it to be made available for use in accordance with the regulations of the University Library for the time being in force, subject to any copyright vested in the work not being affected thereby. I also understand that the title and abstract will be published, and that a copy of the work may be made and supplied to any bona fide library or research worker.

Date 2/2/99 Signature of candidate _____

Acknowledgements

I would firstly like to thank my supervisors, Professor Malcolm Dunn and Dr Miles Padgett, for their continued support and guidance over the last three years at St. Andrews. Their enthusiasm and commitment has been much appreciated.

I would like to thank the members of the research groups in the department that have been involved in collaboration work related to my PhD. I am grateful to the members of the Microchip Lasers group, Bruce Sinclair, Alan Kemp, and in particular Richard Conroy, for their co-operation in the collaborative work on the Cw Microchip-Laser Pumped OPO. I would also like to thank Graham Turnbull and Majid Ebrahimzadeh for their co-operation in the collaborative work on the Difference Frequency Generation in PPKTP. I am grateful to Majid for securing the collaboration with Håkan Karlsson and Fredrik Laurell on the PPKTP sample.

I would like to thank Cameron Rae for his help and advice on OPOs, and for the loan of equipment used in the experiments. I thank Gary Morrison for his help and support as a Research Assistant during the first year of my PhD.

I am grateful to the members of the CW-OPO group: Tom Edwards, Ian Lindsay, David Stothard and Graham Turnbull for their valuable discussions and advice concerning the work on OPOs.

Finally I would like to thank the other members of the Optical Science and Instrumentation group, both past and present, without whom my three years in St. Andrews would just not have been the same: Jochen Arlt, Mark Begbie, Johannes Courtial, Kishan Dholakia, Jacqueline Hewett, Paul Lesso, Tracy McKechnie, Anna O´Neil, Brett Patterson, Neil Simpson and Darren Steers.

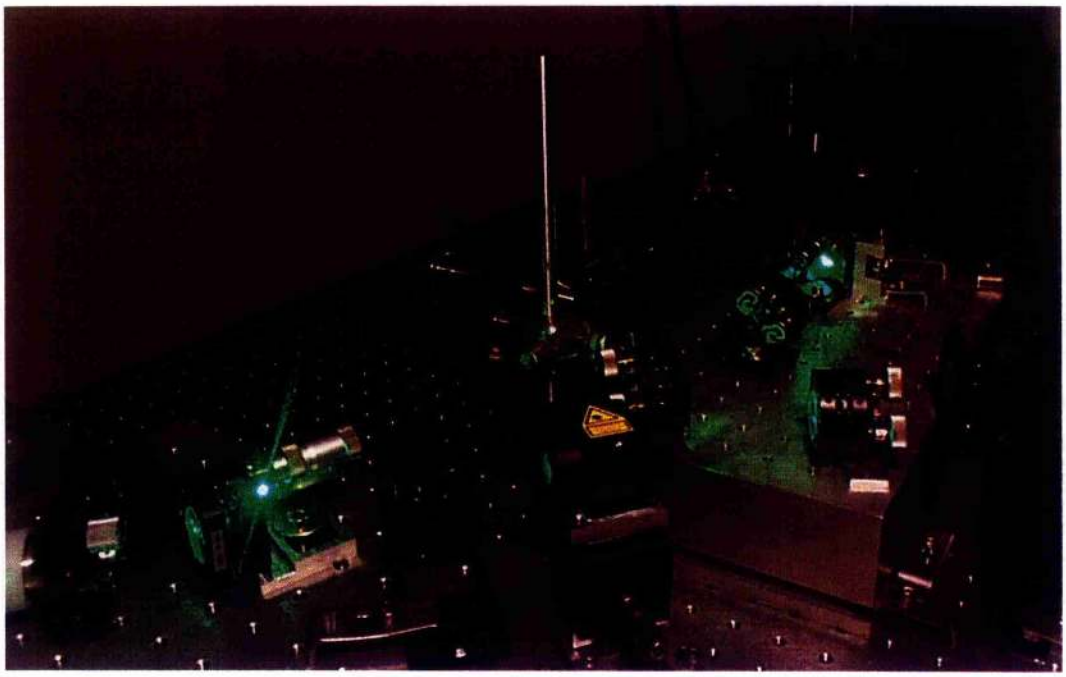

A Tunable Laser Source for Spectroscopy

Continuous Wave Optical Parametric Oscillators (cw OPOs) are solid-state sources of coherent light with broad tuning ranges. Applications of such devices include, quantum optics experiments, optical frequency division, and high-resolution spectroscopy. The doubly resonant OPO shown above provided single frequency light, around 1μm, that was coarsely tunable over ~50nm and smoothly tunable over ~5GHz. This configuration was used to demonstrate the DRO as a spectroscopic source by recording the transmission spectrum of the cesium molecule (Cs_2) in the 1μm region.

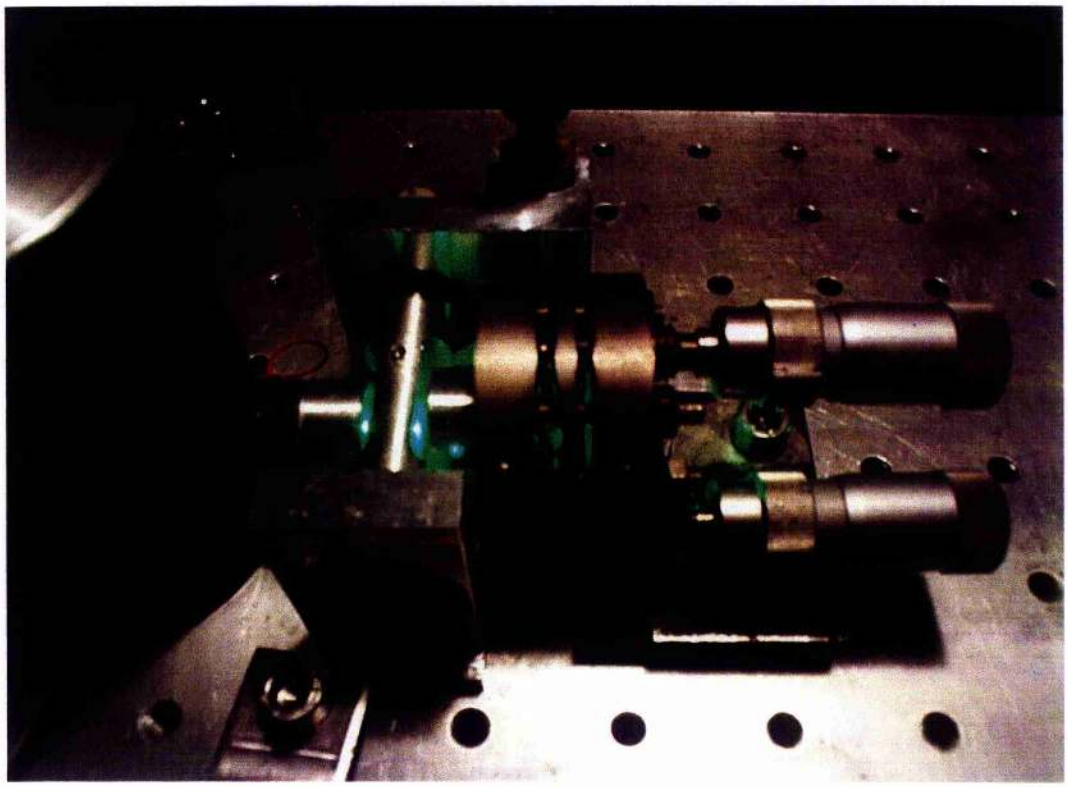

Doubly Resonant Optical Parametric Oscillator (DRO)

The DRO is stabilised using a cavity length servo system. The output power is monitored using a photodiode and a piezoelectric transducer provides the correction of the cavity length to maintain a constant output power and operation on a single mode-pair. This system maintains a constant cavity length to better than 0.5nm. Once stabilised, the DRO has the combination of good frequency selectivity and low pump power threshold (typically 10s of milliwatts or less).

All Solid-State, Diode-Pumped, Laser Source for OPOs

The OPO pump source comprises of a diode-pumped Nd:YLF laser with an intracavity KTP frequency doubler. This provides a few hundred milliwatts of single frequency light at 523nm. Piezoelectric control of the cavity length provides smooth tuning of the output frequency over a range of ~10GHz without mode-hops.

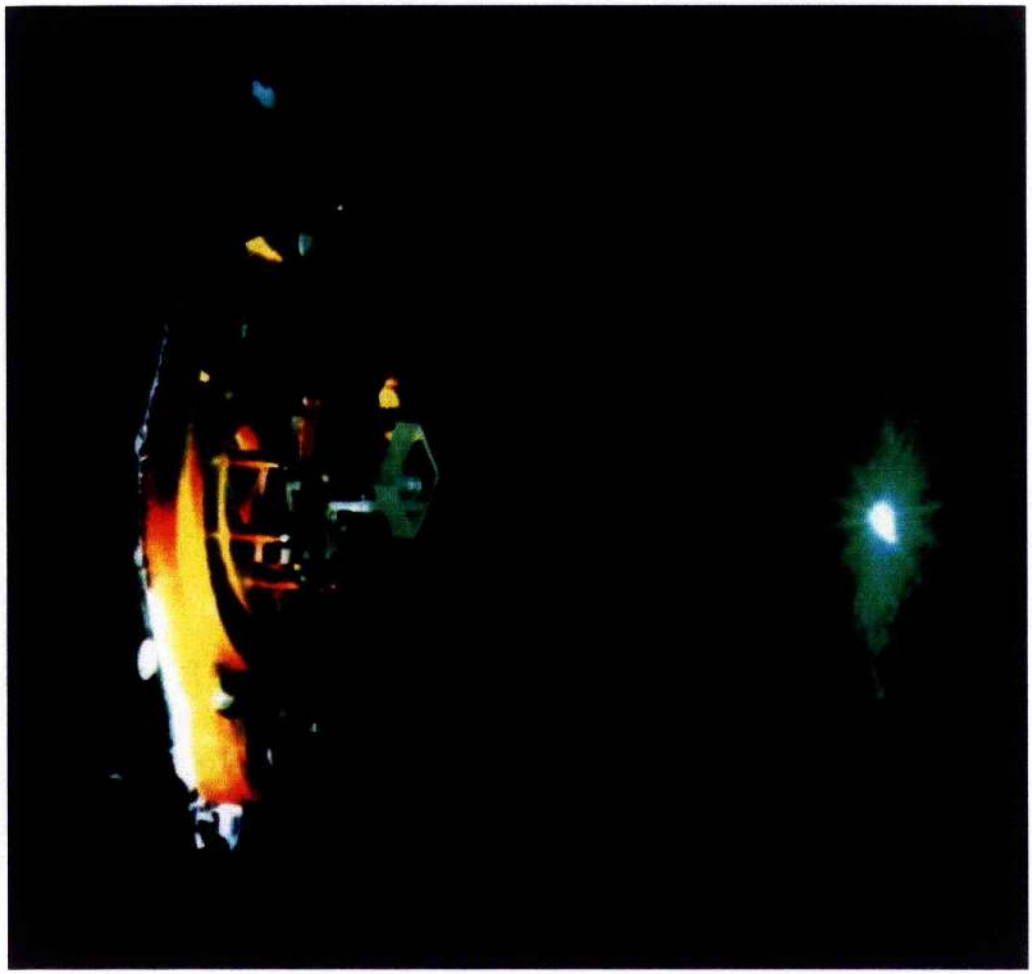

Compact Microchip Laser Pump Source for OPOs

An ultra-compact frequency-doubled microchip laser, based on a sandwich of Nd:YVO_4 and KTP, has been demonstrated as an alternative pump source for DROs. The OPO operated on a single mode-pair even when pumped using a multilongitudinal-mode laser. Such pump lasers, when combined with compact DROs, provide the opportunity of developing very compact sources of tunable light.

Abstract

This thesis describes the development and applications of single-frequency, continuously tunable, continuous-wave (cw), optical parametric oscillators (OPOs). Two doubly-resonant OPOs (DROs) are presented, one providing tunable light around 1μm, the other specifically designed as a spectroscopic source for methane near 1649nm. Once stabilised, the frequency-selective nature of the DRO ensures operation on a single mode-pair without the need for additional intracavity frequency-selective components. Both DROs are smoothly tunable by smoothly tuning the pump laser.

The 1μm DRO is based on a bulk KTP crystal cut for near-degenerate, type-II, critical phase-matching ($\theta = 90°$, $\phi = 37°$). Angle tuning the crystal provides coarse tuning of the output frequencies over a range of ~50nm. Small perturbations to the OPO cavity is sufficient to cause a systematic mode-hop and provides a method of tuning across the phase-matching bandwidth (~0.5THz). This DRO is demonstrated as a spectroscopic source by recording the absorption spectrum of cesium molecules near 1050nm.

The DRO as a potentially compact source of tunable light is demonstrated by using a frequency-doubled microchip laser as the pump source. The output consists of a single pair of signal and idler modes even when using a multilongitudinal-mode pump laser. Smooth tuning of the output frequencies is achieved by temperature tuning the pump laser.

The 1.65μm DRO is based on periodically poled $KTiOPO_4$ (PPKTP). The suitability of PPKTP for cw OPOs was first assessed by a difference frequency generation experiment from which the effective d_{33} coefficient was estimated to be ~5pm/V. The idler wavelength is coarsely tuned at a rate of 0.73nm/°C by varying the crystal temperature.

A combination of computer modelling and experimental observation is used to study the dynamic behaviour of a DRO. The numerical model calculates the time required for the OPO to build-up from the parametric fluorescence and is in excellent agreement with experimental observations.

Outline of the work within the thesis

Chapter 1 introduces the optical parametric oscillator as a source of tunable, coherent light and gives a brief history of the development of cw OPOs. It has only been in the last few years, with advances in pump lasers and new nonlinear optical materials, that many new cw OPO configurations have been investigated.

Chapter 2 gives the theoretical background starting with the parametric down conversion process and arriving at the three coupled equations which describe the pump, signal, and idler fields as they propagate through a nonlinear medium. The different cavity configurations for OPOs are discussed in terms of their associated pump power thresholds and stability requirements. A few different experimental OPO set-ups are discussed with the emphasis being on the single-cavity, doubly-resonant OPO (DRO) with single mode-pair output. Smooth, continuous frequency tuning from a single cavity DRO is also discussed.

Chapter 3 describes the experimental configuration of a cw, near degenerate, DRO operating in the 1μm spectral region. This OPO is based on a previously reported configuration and forms the basis of the main experimental work within this thesis.

Chapter 4 describes the study of the dynamic behaviour of a DRO using a combination of computer modelling and experimental observation. The computer model calculates the signal and idler fields as they build up from the spontaneous parametric fluorescence. The experimental observations are in excellent agreement

with the numerical modelling. The model is then used to predict the dynamic behaviour of systems for various design parameters of DROs and the implications this has on their stability. This work has been published in *Optics Communications*.

Chapter 5 reports the application of a smoothly-tunable, single-frequency, cw, OPO for high-resolution spectroscopy. The OPO is based on KTP and resonant for both signal and idler fields resulting in a device with a very low pump power threshold of 30mW. It is shown that the extremely stringent operating conditions normally associated with DROs aid the DRO in terms of single frequency output and smooth frequency tuning. This frequency selective nature ensures that the signal and idler modes can be tuned across the phase-matched bandwidth without the need for additional intracavity frequency selective components. Smooth frequency tuning of the OPO output is obtained by tuning the pump laser. The practicality of the OPO is demonstrated by recording the transmission spectrum of the cesium molecule (Cs_2) in the 1μm spectral region. Mode-hopping, which has long been regarded as a major disadvantage in DROs, can be successfully controlled to provide a reliable means of tuning over the phase-matched bandwidth of the nonlinear material. The introduction of tuning by mode-hopping bridges the gap between the coarse tuning of the OPO and the fine tuning of the pump laser. This allows access to any wavelength that lies within the phase-matched bandwidth (~0.5THz). This work has been published in *Optics Letters*.

Chapter 6 reports a DRO pumped by an ultra compact, frequency doubled, cw, microchip laser. The frequency selective properties of the DRO, as discussed in chapter 5, result in single frequency output even when using a multimode pump laser. Very compact, low threshold (typically 10mW), DROs of monolithic design have already been demonstrated. These very low threshold DROs, along with compact pump sources, provide the opportunity of developing very compact sources of tunable coherent light. The work on the microchip-laser pumped OPO was completed in collaboration with Richard Conroy at the University of St. Andrews and published in *Optics Letters*.

Chapter 7 reports a difference frequency generation experiment using the new nonlinear optical material periodically poled $KTiOPO_4$ (PPKTP). While KTP cut for type-II birefringent phase-matching is relatively insensitive to temperature, quasi-phase-matched KTP shows a useful degree of temperature tuning. An output power of 12μW around 1.6μm was generated by difference-frequency mixing the outputs of a frequency doubled Nd:YLF laser at 523nm (240mW) and a tunable Ti:sapphire laser near 760nm (340mW). The temperature tuning rate is consistent with the theoretical predictions based on Sellmeier and $\frac{\partial n}{\partial T}$ data. These theoretical predictions have been extended to assess the suitability of PPKTP as a nonlinear optical material for practical applications. The work on difference frequency generation was completed in collaboration with Graham Turnbull at the University of St. Andrews and published in *Applied Physics B*.

Chapter 8 reports a cw, single-frequency, DRO based on PPKTP. This OPO has been specifically designed as a single-frequency source operating around 1.65μm for spectroscopic applications. A maximum output power of 10mW at 1.65μm was obtained for a pump power of ~200mW at 523nm. The practicality of the OPO is demonstrated by recording the transmission spectrum of methane near 1649nm. This chapter discusses the importance of the mismatch in the free spectral ranges, ΔFSR, in terms of easily stabilising the OPO to obtain operation on a single pair of signal and idler modes. This work has been accepted for publication in *Optics Letters*.

Contents

1 Introduction

1.1 OPOs as sources of tunable light

Lasers have long been regarded as sources of high intensity, coherent, and highly directional radiation operating at well defined wavelengths. The highly monochromatic nature of laser radiation results from the presence of discrete energy levels within the atoms or molecules in the laser medium. For many laser applications the exact wavelength of the radiation is not important but there are a few applications, e.g. spectroscopy, that require a well defined range of wavelengths. Spectroscopy, in particular, requires the laser to be tuned to a particular frequency and then tuned through a resonance. There already exists a number of techniques to provide tunable sources of laser radiation using gain media with broadened energy bands. Two examples of such laser media are organic dyes and titanium doped sapphire. Although such tunable lasers are often pumped by conventional laser sources, this is simply to optically excite the lasing transition and the degree of coherence of the pump source has little bearing on the output of the tunable laser itself.

There exists a number of nonlinear techniques for frequency shifting the radiation of a laser beam. It was not until the advent of the laser that nonlinear techniques such as harmonic generation, sum frequency mixing and optical parametric generation [1] could be investigated. Unlike traditional lasers which use a high intensity noncoherent pump source, nonlinear techniques maintain the coherence of the

original pump laser. Optical parametric generation is a process where a pump photon, propagating in a nonlinear optical material, is converted into two new photons termed the signal and the idler.

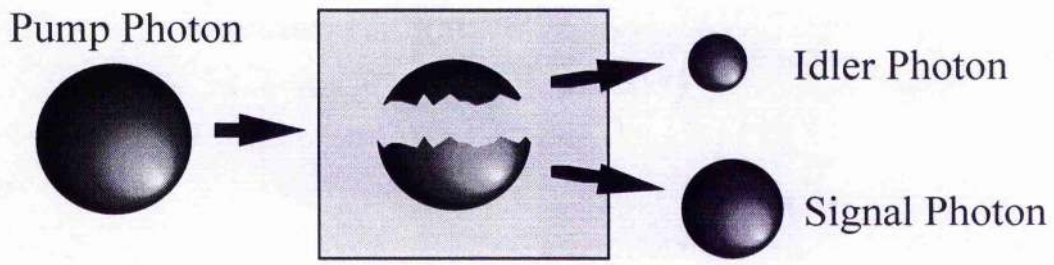

Figure 1.1 *Considering the nonlinear interaction in terms of photons the parametric down conversion process can be thought of as a pump photon being split into two new photons, signal and idler, within the nonlinear optical crystal such that the photon energies is conserved. By convention, the lower energy photon is called the idler.*

This process takes place such that the photon energy conservation relation is obeyed. The resulting pair of frequencies is determined by the momentum conservation relation which maintains the relative phase between the pump, signal, and idler. The momentum conservation relation, or more commonly the phase-matching condition, requires that the sum of the wave-vectors of the generated photons equals the wave-vector of the pump photon. Many pairs of signal and idler frequencies, obeying the energy conservation relation, can satisfy the phase matching condition and hence

provides a source of tunability. The phase-matching condition can be altered (as described below and in chapter 2) to provide coarse frequency tuning.

The signal and idler fields are generated simultaneously and are coherent and collinear with the pump beam itself. Within bulk nonlinear optical materials, phase-matching can be achieved by altering the refractive indices experienced by the signal and idler fields. This can be achieved by changing either the orientation or temperature of the nonlinear material and thus forms the basis of coarse tunability of the coherent light beams.

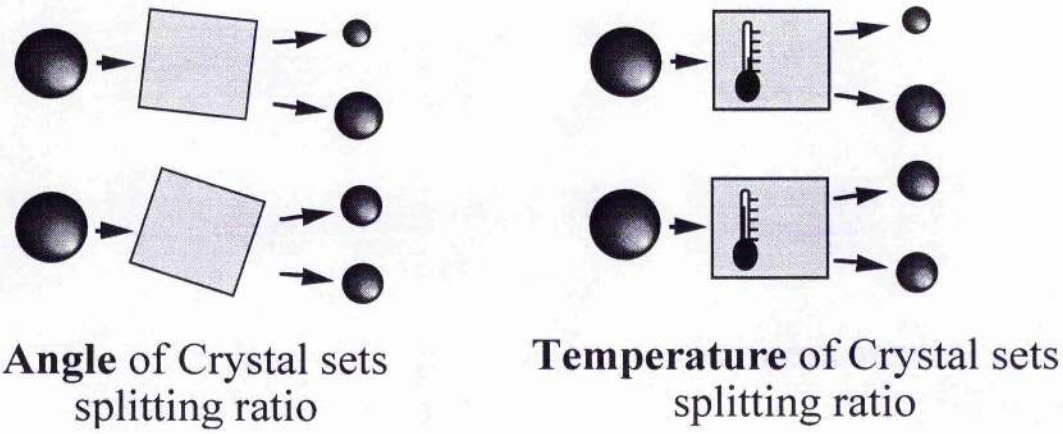

Figure 1.2 *Momentum conservation results in preferred signal and idler frequencies. The two most common methods of controlling the ratio of the signal and idler frequencies is to change the angle of incidence of the pump or temperature of the nonlinear crystal.*

The limitation of this coarse tuning is usually determined by the optical transparency of the nonlinear material. More recently there has been much interest in engineered (poled) nonlinear optical materials having a periodic domain structure. Phase-matching is achieved by choosing an appropriate period of the domain structure and is commonly referred to as Quasi-Phase-Matching (QPM). The domain period determines the frequencies of the signal and idler fields. The introduction of these new improved nonlinear optical materials not only provides greater conversion efficiency but also allows access to new spectral regions.

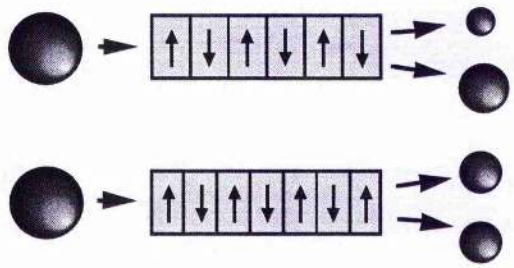

Period of Nonlinear Coefficient sets splitting ratio

Figure 1.3 *In the case of the new poled nonlinear materials the ratio of the signal and idler frequencies is determined by the period of the nonlinear domains.*

These nonlinear materials are commonly placed within an optical resonator to form a device known as an optical parametric oscillator (OPO). When the pump field intensity, fed into the resonator, reaches a critical value, referred to as the pump power threshold, parametric gain causes steady state oscillation to be set up at either

the signal or idler frequency, or at both these frequencies. This is determined by the nature of the mirror coatings at the signal and idler frequencies. The pump source must also be coherent, unlike the non-coherent sources used to pump conventional lasers.

The two main configurations for OPOs are pulsed or continuous wave (cw). OPOs configured as short-pulsed devices are now widely accepted as sources of tunable coherent radiation with many applications including, spectroscopy and quantum optics. However, due to threshold constraints and stability requirements, cw OPOs have still to achieve the same level of acceptance.

1.2 A brief history of the development of cw OPOs

The first demonstration of an OPO was by Giordmaine and Miller, in 1965, [2] and used a high peak power pulsed laser, wavelength 0.529μm, as the pump source. Tunable optical parametric oscillation was observed in lithium niobate ($LiNbO_3$) in the wavelength range 0.97 to 1.15μm. This pulsed device was followed by the first report of a cw OPO by Smith *et al.* in 1968 [3]. In order to reduce the pump power threshold to a level compatible to the majority of available laser sources this OPO was configured as a doubly resonant oscillator (both signal and idler fields resonant). The doubly resonant OPO (DRO) was based on barium sodium niobate ($Ba_2NaNb_5O_{15}$) and was pumped using a frequency doubled Nd:YAG laser. Parametric oscillation was observed over the wavelength range between 0.98μm and 1.06μm. However, this initial cw device revealed undesirable tuning characteristics

which was largely due to the competition between the longitudinal modes of the pump laser.

Attention then turned to singly resonant parametric oscillators (SROs). These were not constrained to having two discrete frequencies resonating within the same cavity and hence provided tunable radiation that was stable in amplitude and frequency. Due to only having one frequency resonant in the OPO cavity, the pump power threshold for SROs was generally too high for convenient cw pump sources and hence most of the earlier devices were pulsed. However, high-power Nd:YAG pump lasers [4], resonant pump enhancement [5], and more recently, periodically poled lithium niobate [6] have enabled cw SRO systems to be operated. Since the mid 1980's there has been a steady flow of new nonlinear optical materials with higher laser damage thresholds, wider optical transparencies, and relatively large nonlinear coefficients.

The first demonstration of a pump-enhanced SRO [5] combined the advantages of the SRO with relatively low pump powers. The required pump power density was achieved by resonating the pump and one of the generated fields. This OPO was based on lithium triborate (LiB_3O_5) and pumped by a single-frequency argon-ion laser. The OPO operated with a 1 watt threshold at 514.5nm and produced 500mW, non resonant wave, for a pump power of 3.4W.

Since their initial demonstration, the development of cw OPOs, in particular, lagged behind that of other sources of widely tunable radiation. The constraints of either maintaining two discrete frequencies simultaneously on resonance within DROs or

the high thresholds associated with SROs, have prevented the widespread use of cw OPOs. However, advances in pump laser sources [7] and efficient nonlinear parametric materials [7, 8], achieving ever increasing efficiencies, has allowed many different types of cw OPOs to be investigated. High pump power thresholds have long been regarded as the limiting factor in the design of cw OPOs. However, a cw, singly resonant, intracavity, OPO has been demonstrated [9]. This is based on a singly resonant potassium titanyl phosphate (KTP) OPO located directly within the cavity of a Ti:sapphire laser to exploit the high circulating power levels. This produced a maximum output power of 0.4W and displayed long-term amplitude-stable operation.

Smooth continuous frequency tuning of a cw DRO, pumped by a fixed frequency pump laser, was achieved by resonating the nondegenerate signal and idler fields in different optical cavities. This device known as a dual-cavity OPO [10] allowed continuous tuning through independent control of the signal and idler cavity lengths. A smooth tuning range of ~0.4GHz was achieved for the signal around 500nm, limited by the width of the pump resonance. Smooth frequency tuning of a single cavity DRO was demonstrated by Henderson *et. al.* [11]. The extra constraint of the double resonance condition was overcome by using a cavity length servo system to maintain a constant output power and operation on a single mode-pair. Smooth tuning of the output frequencies over ~5GHz was achieved by simultaneously tuning the pump laser and controlling the cavity length.

In the 1990's QPM using engineered nonlinear materials, in particular periodically poled lithium niobate (PPLN), has resulted in a large increase in the development of cw OPOs [6, 12]. QPM permits access to the highest nonlinear coefficient of the material (e.g. d_{33} in lithium niobate) hence resulting in greater efficiencies. The greater efficiencies of these new materials relaxes the pump power requirements of cw OPOs and hence gives more flexibility in the choice of pump lasers. SROs based on PPLN, having pump power thresholds of a few watts, have recently been demonstrated [6]. The pump power threshold can be reduced further by enhancing the pump field within the OPO cavity. A pump enhanced SRO based on PPLN has recently been demonstrated by Schneider et al. [13]. This device was pumped by a single-frequency miniature Nd:YAG ring laser and operated with a threshold of 260mW and a smooth tuning range of 2GHz. The increased flexibility of periodically poled materials has allowed the development of nonlinear devices using novel grating designs such as the cw PPLN OPO, using a fan-out grating design, demonstrated by Powers et al. [14].

The new nonlinear optical materials that have recently aided the development of cw SROs have also generated a renewed interest in cw DROs. For these materials the predicted pump power thresholds are within the range of available cw diode lasers and thus provides the opportunity of developing very compact and efficient sources of tunable radiation. A cw DRO based on PPLN and directly pumped by a commercial 978-nm cw diode laser has been demonstrated by Myers et al. [15].

Flux-grown KTP has also been successfully poled [16]. Periodically poled KTP (PPKTP) has the advantages of a high photorefractive damage threshold and low susceptibility to thermal lensing. PPKTP has recently been demonstrated in a near degenerate cw OPO [17]. This OPO operated near room temperature and was pumped by a frequency doubled Nd:YAG laser. Chapter 8 describes a cw OPO based on PPKTP that has been designed as a spectroscopic source for methane transitions near 1649nm.

The high efficiency and compactness of diode-pumped lasers, along with their excellent frequency stability, make them ideal for frequency conversion in cw OPOs. OPOs have the capacity to reproduce the spectral and spatial quality of their pump source. Therefore, the generation of narrow-linewidth radiation from an OPO is greatly eased by the use of a narrow-linewidth pump source. A renewed interest in cw OPOs has been accompanied by proposals to incorporate them within specific experiments for investigation into a variety of research areas: e.g. squeezed states of light [18], optical frequency division [19], [20], and high-resolution laser spectroscopy [21].

1.3 References

[1] J. A. Armstrong, N. Bloembergen, J. Ducuing and P. S. Pershan, *Phys. Rev.* **127**, 6, 1918 (1962).

[2] J. A. Giordmaine and R. C. Miller, *Phys. Rev. Lett.* **14**, 24, 973 (1965).

[3] R. G. Smith, J. E. Geusic, H. J. Levinstein, J. J. Rubin, S. Singh and V. Uitert, *Appl. Phys. Lett.* **12**, 9, 308 (1968).

[4] S. T. Yang, R. C. Eckardt and R. L. Byer, *Optics Lett.* **18**, 12, 971 (1993).

[5] G. Robertson, M. J. Padgett and M. H. Dunn, *Optics Lett.* **19**, 21, 1735 (1994).

[6] W. R. Bosenberg, A. Drobshoff, J. I. Alexander, L. E. Myers and R. L. Byer, *Optics Lett.* **21**, 10, 713 (1996).

[7] C. D. Nabors, R. C. Eckardt, W. J. Kozlovsky and R. L. Byer, *Optics Lett.* **14**, 20, 1134 (1989).

[8] F. G. Colville, A. J. Henderson, M. J. Padgett, J. Zhang and M. H. Dunn, *Optics Lett.* **18**, 3, 205 (1993).

[9] F. G. Colville, M. H. Dunn and M. Ebrahimzadeh, *Optics Lett.* **22**, 2, 75 (1997).

[10] F. G. Colville, M. J. Padgett and M. H. Dunn, *Appl. Phys. Lett.* **64**, 12, 1490 (1994).

[11] A. J. Henderson, M. J. Padgett, J. Zhang, W. Sibbett and M. H. Dunn, *Optics Lett.*, **20**, 9, 1029 (1995).

[12] L. E. Myers and W. R. Bosenberg, *IEEE J. Quant. Elect.*, **33**, 10, 1663 (1997).

[13] K. Schneider, P. Kramper, S. Schiller and J. Mlynek, *Optics Lett.* **22**, 17, 1293 (1997).

[14] P. E. Powers, Thomas J. Kulp and S. E. Bisson, *Optics Lett.* **23**, 3, 159 (1998).

[15] L. E. Myers, R. C. Eckardt, M. M. Fejer, R. L. Byer, W. R. Bosenberg and J. W. Pierce, *J. Opt. Soc. Am. B* **12**, 11, 2102 (1995).

[16] H. Karlsson and F. Laurell, *Appl. Phys. Lett.* **71**, 24, 3474 (1997).

[17] A. Garashi, A. Arie, A. Skliar and G. Rosenman, *Optics Lett.*, **23**, 22, 1739 (1998).

[18] S. Reynaud, C. Fabre and E. Giacobino, *J. Opt. Soc. Am. B* **4**, 10, 1520 (1987).

[19] N. C. Wong, *Optics Lett.* **15**, 1129 (1990).

[20] N. C. Wong, *Optics Lett.* **17**, 1155 (1992).

[21] E. S. Polzik, J. Carri and H. J. Kimble, *Appl. Phys.* **B55**, 279 (1992).

2 Theoretical background

2.1 Optical parametric generation

The optical parametric down-conversion process involves an input pump wave, propagating in a nonlinear optical material with frequency ν_p, being converted into two output waves, termed the signal and idler, at frequencies ν_s and ν_i respectively. This process takes place such that the energy conservation relation is obeyed i.e.

$$\nu_p = \nu_s + \nu_i . \qquad [2.1]$$

The parametric down conversion process can also be described as a pump photon breaking down into two lower energy photons. For a given pump frequency, there is a continuous choice of signal and idler frequencies which satisfy the condition of energy conservation. However, the specific pair of frequencies are determined by the momentum conservation, or phase-matching condition, which is described by the wave-vector mis-match Δk. Efficient parametric down-conversion requires that

$$\Delta k = k_p - k_s - k_i = \frac{2\pi}{c}(n_p\nu_p - n_s\nu_s - n_i\nu_i) = 0, \qquad [2.2]$$

where n_p, n_s, and n_i are the refractive indices of the pump, signal, and idler fields. k_p, k_s, and k_i are the corresponding wave-vector magnitudes. For perfect phase-matching the relative phase between the waves is maintained.

Anisotropic optical materials exhibit birefringence, refractive index dependent on the polarisation state of the light and direction of propagation. The most common method of satisfying the phase-matching condition is to make use of this birefringence to compensate for material dispersion. Within the transparency range of optical materials, dispersion results in the increase in refractive index with increasing frequency. This causes the relative phase of the pump, signal, and idler fields to change with propagation and thus sets a limit on the length of crystal that can be used. The phase-matching condition becomes more difficult to maintain as the crystal becomes longer. The effect of imperfect phase-matching on the efficiency of the nonlinear process is given by

$$efficiency \propto l^2 \mathrm{sinc}^2\left(\frac{\Delta k l}{2}\right). \qquad [2.3]$$

This proportionality is related to the function H_m, as defined in Boyd & Kleinman [1], and follows a sinc^2 relationship when plotted as a function of phase mismatch.

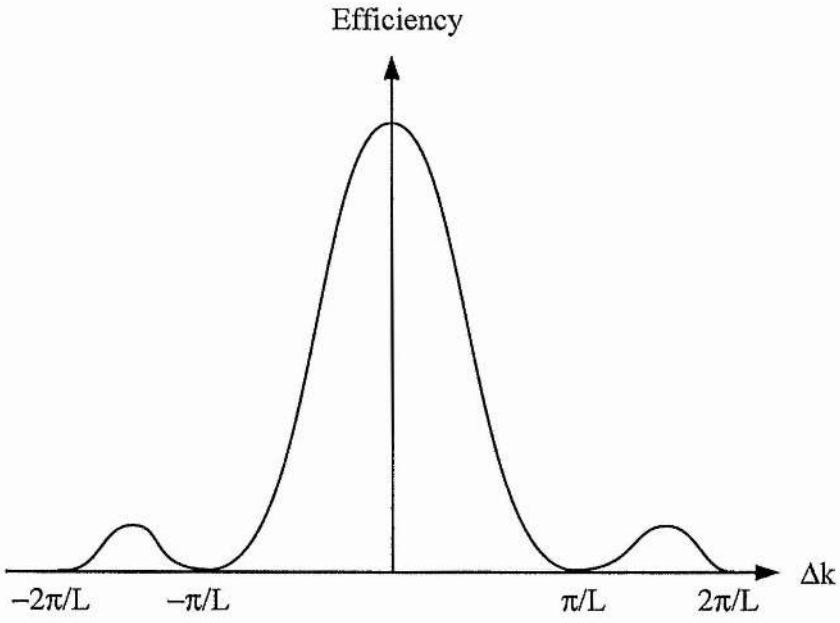

Figure 2.1 *The efficiency of the parametric down-conversion process for a given phase mismatch, Δk, follows a* sinc^2 *relationship.*

Useful parametric gain exists for $|\Delta k| \leq \frac{\pi}{l}$, where l is the length of the nonlinear material [2].

In an anisotropic medium the phase-matching is often controlled by altering the orientation or temperature of the crystal. This is referred to as birefringent phase-matching which is described in section 2.5.

2.2 The nonlinear interaction

When an electric field is applied to a dielectric material, the material becomes polarised. The resulting polarisation depends on the strength of the electric field and the dielectric susceptibility. In most cases where the applied electric field << intra-atomic field the induced polarisation, P, is linear and can be expressed as

$$P = \chi_s \varepsilon_o E, \qquad [2.4]$$

where ε_o is the permittivity of free space and χ_s is the linear (or 1st order) dielectric susceptibility.

For crystalline materials the relationship between P & E can be described as a tensor:-

$$\begin{bmatrix} P_x \\ P_y \\ P_z \end{bmatrix} = \varepsilon_o \begin{bmatrix} \chi_{1,1} & \chi_{1,2} & \chi_{1,3} \\ \chi_{2,1} & \chi_{2,2} & \chi_{2,3} \\ \chi_{3,1} & \chi_{3,2} & \chi_{3,3} \end{bmatrix} \begin{bmatrix} E_x \\ E_y \\ E_z \end{bmatrix}. \qquad [2.5]$$

For intense fields associated with lasers the electric field strength is comparable to the intra-atomic field. The polarisation can no longer be described by the linear relation of eqn. [2.4] and must be treated as a power series

$$P = \varepsilon_o(\chi_s^{(1)}E + \chi_s^{(2)}E^2 + \chi_s^{(3)}E^3 + \dots), \qquad [2.6]$$

where $\chi_s^{(1)}$, $\chi_s^{(2)}$, $\chi_s^{(3)}$ are the 1st, 2nd, and 3rd order susceptibilities respectively.

The relationship between E and P can be separated into its linear and nonlinear parts.

$$P = \varepsilon_o \chi_s^{(1)} E + P^{NL}. \qquad [2.7]$$

The higher order terms in the polarisation can couple together fields of different frequencies and polarisations. In particular, the second-order susceptibility $\chi_s^{(2)}$ tensor is responsible for second-harmonic generation, sum & difference-frequency generation, and parametric generation. The components of the tensor $\chi_s^{(2)}$ can be expressed in terms of the nonlinear coefficient d such that $\chi_s^{(2)} = 2d$.

The nonlinear polarisation in any particular direction can be related to the incident fields in the x, y, and z directions by the tensor d such that

$$\begin{bmatrix} P_x(\omega_3) \\ P_y(\omega_3) \\ P_z(\omega_3) \end{bmatrix} = 2\varepsilon_0 \begin{bmatrix} d_{11} & d_{12} & d_{13} & d_{14} & d_{15} & d_{16} \\ d_{21} & d_{22} & d_{23} & d_{24} & d_{25} & d_{26} \\ d_{31} & d_{32} & d_{33} & d_{34} & d_{35} & d_{36} \end{bmatrix} \begin{bmatrix} E_x(\omega_1)E_x(\omega_2) \\ E_y(\omega_1)E_y(\omega_2) \\ E_z(\omega_1)E_z(\omega_2) \\ E_y(\omega_1)E_z(\omega_2) + E_z(\omega_1)E_y(\omega_2) \\ E_x(\omega_1)E_z(\omega_2) + E_z(\omega_1)E_x(\omega_2) \\ E_x(\omega_1)E_y(\omega_2) + E_y(\omega_1)E_x(\omega_2) \end{bmatrix}, \qquad [2.8]$$

where $\omega_3 = \omega_1 + \omega_2$.

For a chosen propagation direction and set of polarisations, the nonlinear polarisations can be written in the form [1, 3].

$$P^{NL}(\nu_p) = \varepsilon_o 2d : E(\nu_s)E(\nu_i), \qquad [2.9(a)]$$

$$P^{NL}(\nu_s) = \varepsilon_o 2d : E^*(\nu_i)E(\nu_p), \qquad [2.9(b)]$$

$$P^{NL}(\nu_i) = \varepsilon_o 2d : E^*(\nu_s)E(\nu_p). \qquad [2.9(c)]$$

In general, the tensor representation of d can be dropped and replaced by a single scalar quantity called the effective nonlinear coefficient d_{eff}. d_{eff} is the net response of the nonlinearity and is calculated from d with reference to the interaction geometry. Examples of d_{eff} for phase-matching in KTP are given in section 2.5.

The polarisations described by equations 2.9 can be included in Maxwell's equations, applying the paraxial wave approximation ($\frac{k\partial E}{\partial z} >> \frac{\partial^2 E}{\partial z^2}$ ref. 3), to give the following set of coupled differential equations [4]

$$\frac{dE_p}{dz} + \alpha_p E_p = i\kappa_p \cdot E_i E_s e^{-i\Delta k \cdot z}, \qquad [2.10(a)]$$

$$\frac{dE_s}{dz} + \alpha_s E_s = i\kappa_s \cdot E_p E_i^* e^{i\Delta k \cdot z}, \qquad [2.10(b)]$$

$$\frac{dE_i}{dz} + \alpha_i E_i = i\kappa_i \cdot E_p E_s^* e^{i\Delta k \cdot z}, \qquad [2.10(c)]$$

where $\alpha_i = \mu_o \sigma_i \frac{c}{2}$ is the field absorption coefficient and $\kappa_i = \frac{\omega_i d_{eff} \varepsilon_o}{n_i c}$ is the interaction coefficient.

2.3 Optimum focussing for nonlinear interactions

In order to increase the nonlinear efficiency the interacting beams are focused in the nonlinear medium. In practice the pump signal and idler fields are linearly polarised fundamental Gaussian beams. The expression of the fields defined along a propagation direction z can be expressed as

$$E_j(z,r,t) = E_j(z)\exp\left(\frac{-r^2}{W_{0_j}^2}\right)\exp\left[i\left(2\pi\nu_j t - k_j z\right)\right], \qquad [2.11]$$

where the radial dependence, r, has a Gaussian shape characterised by the beam waist W_{0_j}. The incident Gaussian beam is characterised by the confocal parameter $z_0(=\pi W_0^2 n/\lambda)$ which is the distance from the waist in which the beam area is doubled. Higher nonlinear efficiencies can be achieved by reducing the value of W_0 until the confocal parameter, z_0, becomes comparable to the length of the crystal. A focussing parameter, ξ, can be defined as

$$\xi = \frac{l}{z_0}, \qquad [2.12]$$

where l is the length of the crystal.

The optimum focussing parameter for parametric generation can be obtained using the analysis given by Boyd and Kleinman [1]. Here, the parametric generation power is represented by the function $h_m(B,\xi)$, where B is a double-refraction parameter.

Parametric generation is maximum in the absence of double refraction (B=0). Figure 2.2 shows that h_m reaches a maximum for a focussing parameter of $\xi = 2.8$.

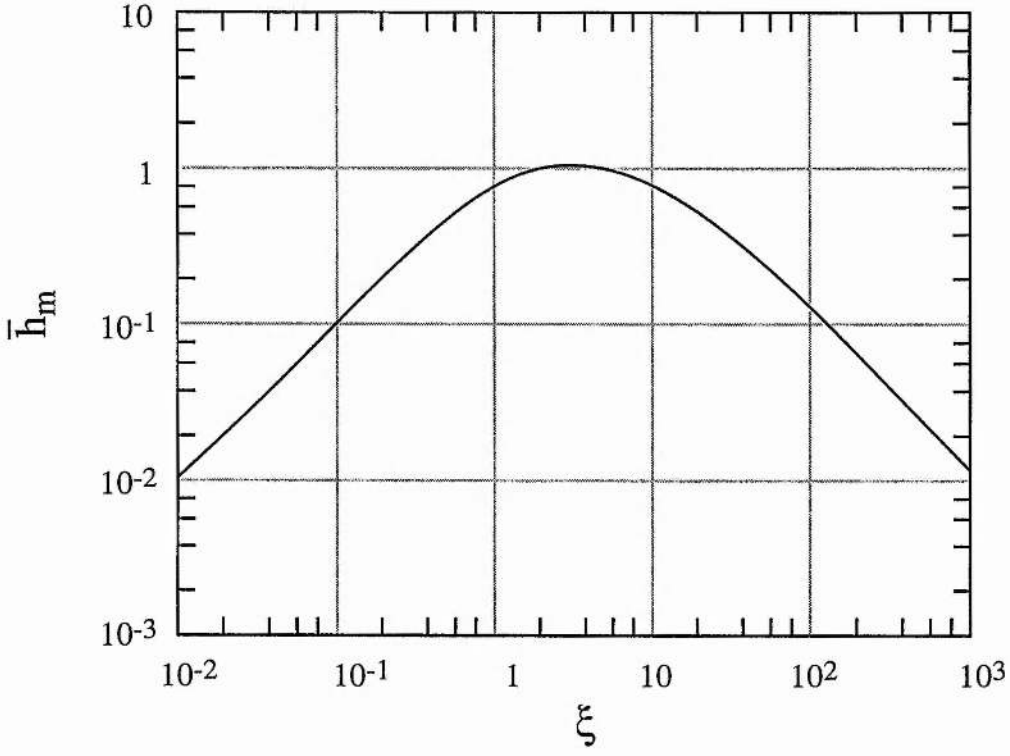

Figure 2.2 *Parametric generated power, represented by h_m as defined in Boyd & Kleinman, as a function of focussing parameter ξ in the absence of double refraction. Here, the maximum parametric generation is achieved for a focussing parameter $\xi = 2.8$.*

A more common approach is to focus the beam until $z_0 = l/2$ and is referred to as confocal focusing. Here, the beams are approximately collimated over the length of

the crystal and thus beam diffraction has less of an effect on the overlap of the three interacting waves.

2.4 The coupled amplitude equations

It is useful to describe the propagation of the pump, signal, and idler fields through the nonlinear medium as a set of coupled amplitude equations. Equations [2.10] can be integrated by developing the expression of the fields in powers of z [5] to give

$$\alpha_p(l) = \alpha_p(0) - 2\chi^*\alpha_s(0)\alpha_i(0), \qquad [2.13(a)]$$

$$\alpha_s(l) = \alpha_s(0) + 2\chi\alpha_p(0)\alpha_i^*(0), \qquad [2.13(b)]$$

$$\alpha_i(l) = \alpha_i(0) + 2\chi\alpha_p(0)\alpha_s^*(0), \qquad [2.13(c)]$$

where $|\alpha_j|^2$ represents the number of incident photons per unit time in the mode, χ is a coupling coefficient which describes the nonlinear interaction and is given by

$$\chi = \sqrt{\frac{|d_{eff}|^2 \pi^2 l v_P^3}{2\varepsilon_o c^4 n^2} h v_p}, \qquad [2.14]$$

where l is the length of the nonlinear crystal, v_P is the frequency of the pump field, and d_{eff} is the effective nonlinear optical coefficient. The above equation assumes perfect phase-matching and confocal focusing.

A more general expression for the nonlinear coupling coefficient χ (assuming confocal focusing) is given by

$$|\chi|^2 = |d_{eff}|^2 \frac{\pi^2 l \nu_p^3 (1-\delta^2)^2 \operatorname{sinc}^2\left[\frac{\Delta k l}{2}\right]}{2\varepsilon_o c^4 n_p^2} (h\nu_p), \qquad [2.15]$$

where δ is a measure of how far from degeneracy the signal and idler fields are phase-matched. This is given by

$$\delta = \frac{2\nu_s - \nu_p}{\nu_p} = \frac{\nu_p - 2\nu_i}{\nu_p}. \qquad [2.16]$$

The coupled equations 2.13 are useful in the work detailed in chapter 4 where the time evolving output of a doubly resonant optical parametric oscillator is modelled.

2.5 Birefringent phase-matching

As discussed in section 2.1 one method of satisfying the phase-matching condition is to make use of birefringence to compensate for material dispersion. In anisotropic materials the phase-matching condition can be altered by changing the orientation or temperature of the crystal. This provides a means of tuning the output frequencies.

In uniaxial nonlinear crystals, in which the highest degree of rotational symmetry is applied to only a single axis, the two eigen-polarisations associated with any general propagation direction are denoted ordinary and extraordinary polarisations. The corresponding indices of refraction are n_o and n_e respectively. The axis of symmetry is chosen as the z-axis, also referred to as the optic axis, such that $n_x = n_y = n_o$, and $n_z = n_e$

$$\frac{x^2}{n_o^2} + \frac{y^2}{n_o^2} + \frac{z^2}{n_e^2} = 1. \qquad [2.17]$$

The ordinary wave is polarised such that the refractive index n_o is independent of the direction of propagation. The extraordinary wave is polarised in the plane containing the optic axis and the propagation direction and has a refractive index n_e which is direction dependent. The dependence of the extraordinary wave on the angle θ between the propagation direction and the crystal optic axis is given by

$$\frac{1}{n_e^2(\theta)} = \frac{\cos^2(\theta)}{n_o^2} + \frac{\sin^2(\theta)}{n_e^2}. \qquad [2.18]$$

The refractive index of the ordinary or extraordinary waves increases with frequency. Therefore, within bulk nonlinear crystals, it is impossible to satisfy the phase-matching condition for pump and generated waves of the same type. However, it is possible to phase match two waves of different types, ordinary and extraordinary, by temperature or angle tuning. Phase matching can be characterised into two groups,

type-I or type-II, depending on the relative polarisation states of the three fields (detailed in table 2.1 below).

	$E(\omega_1)$ and $E(\omega_2)$	$E(\omega_3)$
TYPE-I	Parallel polarisations	Orthogonally polarised with respect to $E(\omega_1)$ and $E(\omega_2)$
TYPE-II	Orthogonal polarisations	Parallel polarisation with respect to $E(\omega_1)$ or $E(\omega_2)$

Table 2.1 *Comparison of TYPE-I and TYPE-II phase-matching.* $\omega_3 = \omega_1 + \omega_2$.

In the case of the biaxial nonlinear crystal potassium titanyl phosphate ($KTiOPO_4$, KTP), which forms the basis of the experimental configurations detailed in this thesis, the indices of refraction allow both type-I and type-II phase-matching. The values of the second order nonlinear tensor d can be used to calculate the d_{eff}. In KTP, the expressions for d_{eff} are [6]

$$d_{eff}(\text{Type}-\text{I}) = \frac{1}{2}(d_{15} - d_{24})\sin 2\theta \sin 2\phi, \qquad [2.19]$$

$$d_{eff}(\text{Type}-\text{II}) = (d_{24} - d_{15})\sin 2\theta \sin 2\phi - (d_{15}\sin^2\phi + d_{24}\cos^2\phi)\sin\theta, \qquad [2.20]$$

where θ is the angle relative to the z axis, and ϕ is the angle in the x-y plane relative to the x axis. d_{eff} is much smaller for type-I than for type-II, so for efficient interactions type-II is preferred.

One possible method of birefringent phase matching is to set the orientation of the crystal such that either the type-I or type-II condition is satisfied. However, due to the elliptical nature of the variation of n_e with angle, the o-ray and e-ray become separated as they propagate through the crystal. This process, referred to as Poynting vector walk-off, means that the overlap of the pump, signal, and idler beams can only be maintained over a short distance into the crystal, hence imposing an upper limit on the length of crystal that can be used. The special case where $\theta = 90^o$ is referred to as non critical phase-matching. In this case the e-ray propagates perpendicularly to the optic axis. This means that there is no walk off between the o-ray and the e-ray and hence an increase in efficiency of the nonlinear interaction. The dependence of Δk on angular misalignment is smaller and hence temperature tuning is commonly used to achieve non critical phase matching. Phase matching at an angle θ other than 0° or 90° is termed critical phase matching.

2.6 Quasi-phase-matching

An alternative technique to birefringent phase matching (BPM) is Quasi-Phase-Matching (QPM) where the relative phase of the interacting fields is corrected at regular intervals using a structural periodicity built into the nonlinear medium [3, 7, 8]. Due to normal dispersion in the material, the pump, signal, and idler waves travel at different phase velocities. The relative phase of the three waves is important since this determines the sign of power flow between the pump and generated waves. Therefore the continuous phase slip between these waves leads to an alternation in the direction of power flow as indicated in trace (A) in figure 2.3 below. The distance over which the relative phase of the waves changes by π is called the coherence length ℓ_c which is typically a few microns.

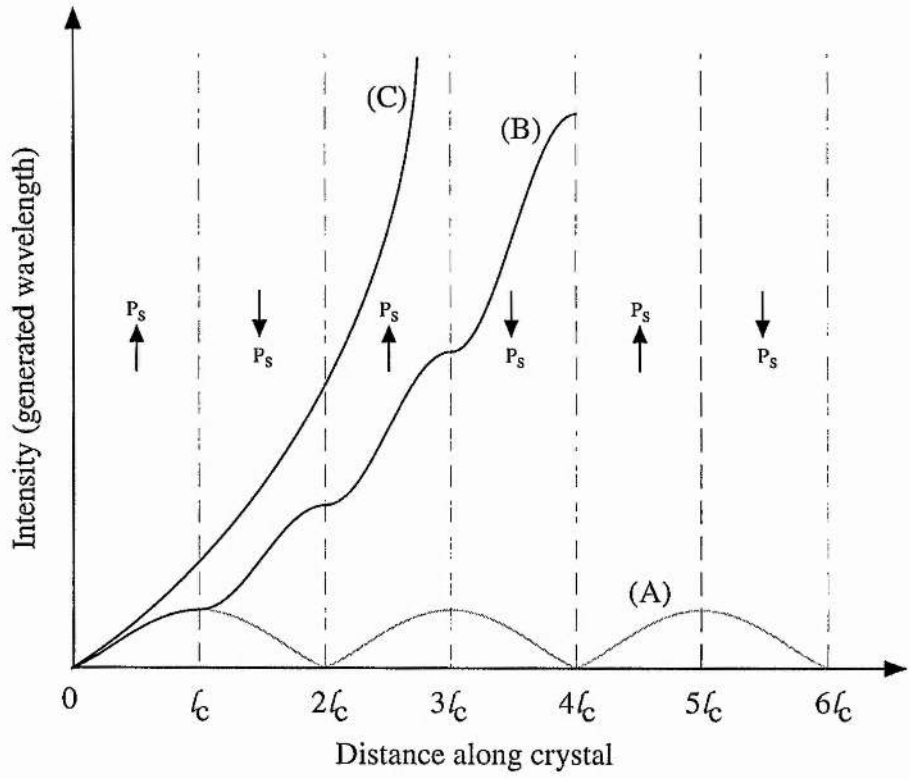

Figure 2.3 *The effect of QPM on the conversion efficiency of parametric generation. A: nonphase-matched interaction. B: first order QPM by reversing the sign of P_s every coherence length ℓ_c. C: perfect phase-matching in bulk material. ℓ_c, coherence length.*

Continuous growth of the signal and idler fields requires the repeated inversion of the relative phase between the waves after an odd number of coherence lengths. This can be achieved by modulating the sign of the nonlinear coefficient (each reversal termed a "domain") which maintains the proper phase-relationship for the growth of the generated wavelengths. The highest conversion efficiency is obtained when the sign of the nonlinear coefficient is reversed every coherence length and is referred to as first order QPM (indicated in trace B in figure 2.3).

The theory of QPM is discussed in detail by M. Fejer [8] and L. Myers [9] and is summarised below. The equations relating to QPM are similar to those of BPM with a few simple substitutions.

For QPM the effective nonlinear coefficient is given by

$$d_Q = d_{eff} G_m, \qquad [2.21]$$

where d_{eff} is the same as for the single-domain bulk material and G_m is the Fourier coefficient for the periodic modulation. The Fourier coefficient is given by

$$G_m = \frac{2}{m\pi} \sin(m\pi D). \qquad [2.22]$$

$D = l_d / \Lambda$ is the duty cycle where l_d is the length of a reversed domain and Λ is the domain period. The optimum value of duty cycle depends on the QPM order m ($D_{opt.}$=50% for m=1). The effective nonlinear coefficient for QPM is largest for a first order process with a 50% duty cycle. In this case the nonlinear coefficient is given by

$$d_Q = \frac{2}{\pi} d_{eff}. \qquad [2.23]$$

The wave-vector mismatch for QPM is now given by

$$\Delta k_Q = k_p - k_s - k_i - k_m, \qquad [2.24]$$

where k_m is the mth order grating wave-vector which is given by

$$k_m = \frac{2\pi m}{\Lambda}. \qquad [2.25]$$

Therefore, perfect first order QPM is achieved when

$$\Delta k_Q = k_p - k_s - k_i - \frac{2\pi}{\Lambda} = 0. \qquad [2.26]$$

For ideal periodic structures, QPM can only be achieved for mth orders where m is an odd number [8].

QPM is commonly implemented in ferroelectric crystals by periodic reversal of the spontaneous polarisation P_s. Changing the sign of P_s, corresponding to changing the sign of the nonlinear coefficient, is achieved by momentarily applying an electric field using lithographically defined electrodes [10, 11]. Such crystals are said to be "periodically poled" with a domain (grating) period.

QPM allows longer crystals to be used and has the added advantage that the interacting waves can be chosen to access the largest nonlinear coefficient (e.g. d_{33} in $LiNbO_3$, $KTiOPO_4$, $RbTiOAsO_4$). With an appropriate choice of grating essentially

any wavelength combination within the transparency range of the nonlinear material can be phase-matched in a noncritical geometry. QPM allows phase-matching at arbitrary temperatures with no walk-off and extends the utility of existing materials. To date the most readily available QPM material is Periodically Poled Lithium Niobate (PPLN) although there is an increasing interest in the new material Periodically Poled Potassium Titanyl Phosphate (PPKTP) [12]. These poled crystals, sometimes referred to as "chips", can be fabricated with a selection of grating periods [13] and novel grating designs [14, 15, 16].

2.6.1 Quasi-phase-matching tolerances

In periodically poled materials the efficiency is reduced for departures from the ideal grating structure. The effects of period and duty cycle errors on the conversion efficiency have been analysed by Fejer *et al.* [8]. The point where the power conversion efficiency is halved can be used to calculate the tolerances of these errors.

Constant errors in the domain period, where the periodicity of the domains is otherwise perfect, cause a shift in the phase-matching curve from the desired operating point. This lowers the efficiency at the desired operating point. Equation 29 in ref. 8 gives the tolerance for the period to be

$$\frac{\delta\Lambda}{\Lambda} = \frac{1.77}{Nm}, \qquad [2.27]$$

where $\delta\Lambda$ is the period error, $N = L/ml_c$ is the number of domains in the sample of length L, l_c is the coherence length. For m=1 and N=1000 the tolerance for the period is ~0.2%.

Random errors in the domain period cause a broadening of the phase-matching curve due to a normal distribution of errors with standard deviation σ_l. Equation 76 in ref. 8 gives the tolerance on the mean square error to be

$$\frac{\sigma_l}{l_c} < \frac{0.72}{\sqrt{N}}. \qquad [2.28]$$

For N=1000 the tolerance for random period errors is ~2%.

Departures from the desired domain duty cycle, usually 50/50, reduce the parametric gain but do not affect the bandwidth. Equation 69 in ref. 8 gives the tolerance on the rms error to be

$$\frac{\sigma_l}{l_c} < \frac{\sqrt{2\ln 2}}{\pi}. \qquad [2.29]$$

The tolerance for duty cycle errors is therefore ~38%. Sensitivity to duty cycle errors is very small, with rms errors as large as $l_c/3$ resulting in < 50% reduction in efficiency.

Equation 41 in ref. 8 gives the FWHM angular acceptance for a noncritical QPM interaction

$$\delta\nu = 2\sqrt{1.772\frac{n_2}{n_1}\frac{l_c}{L}\cos\nu}, \qquad [2.30]$$

where ν is the angle of the fundamental wave vector to the z axis. Here the bandwidth depends inversely on the square root of the device length L and is comparable to that of a noncritical BPM interaction.

In summary, efficient QPM is very sensitive to both constant and random period errors while being much more tolerant to errors in the duty cycle. However, with electric-field poling (used in PPLN, PPRTA and PPKTP), where the periodicity is precisely determined by a lithographically defined electrode, period errors have not been a serious issue.

A nonlinear optical crystal can be placed inside an optically resonating cavity to form an OPO, resulting in oscillation at either, or both, the signal and idler frequencies. The nature of the oscillation is determined by the levels of feedback provided by the cavity mirrors at the signal and idler frequencies. The optically resonating cavity is usually external to the pump source but can also be formed within the resonator of the pump source [17].

2.7 Doubly resonant oscillators

In order to reduce the pump power threshold to a level compatible with modest pump sources and the majority of nonlinear materials, OPOs can be configured as doubly resonant oscillators (DROs) in which both the signal and idler fields are simultaneously resonant in the cavity [18].

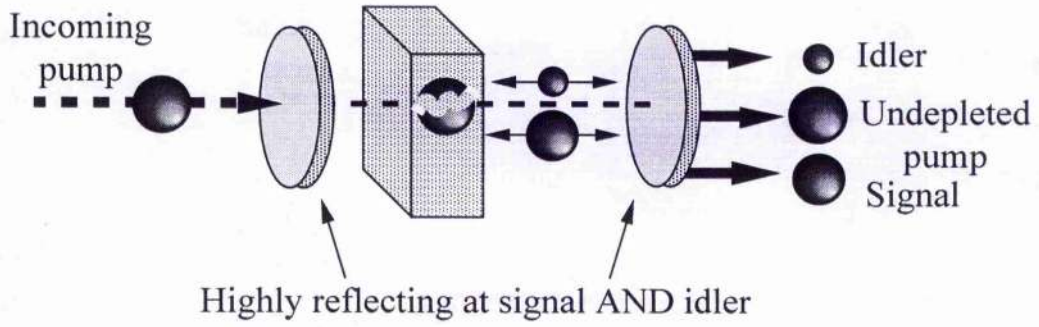

Figure 2.4 *Doubly Resonant Oscillators (DROs) have the advantage of very low pump power thresholds, typically 10s of milliwatts or less. However the conditions for the simultaneous resonance of signal and idler are not satisfied for any arbitrary selection of cavity length, pump frequency, and phase matching.*

2.7.1 Pump power thresholds for DROs

An important consideration in the design of OPOs is the pump power threshold which is proportional to the product of the losses at the pump, signal, and idler fields. The powers of the three fields are related to the number of incident photons per unit time in the mode by

$$P_i = |\alpha_i|^2 (h\nu_i). \qquad [2.31]$$

Oscillation can only occur when the round-trip gain exceeds the losses. The threshold analysis for a linear cavity OPO, as used in the experimental configurations detailed in this thesis, is similar to that for a ring cavity, with the exception of a modification of the nonlinear coupling coefficient. Starting from the analysis of the ring cavity outlined in Debuisschert et al. [5] the pump intensity required to reach threshold is given by

$$\left|\alpha_p^{in}\right|^2_{threshold} = \frac{\gamma_p'^2 \gamma_s' \gamma_i'}{8|\chi|^2 \gamma_p}(1+\Delta^2)(1+\Delta_p^2), \qquad [2.32]$$

where γ_j is the transmission coefficient, γ_j' is defined by $\gamma_j' = \gamma_j + \mu_j = \frac{\pi}{F_j}$, where μ_j is the spurious energy loss coefficient, and $\Delta_j = \frac{2\Delta\nu_j F_j}{FSR_j}$ is the relative detuning of wave from perfect resonance.

This can also be written as

$$\left|\alpha_p^{in}\right|^2_{threshold} = \frac{\pi^2}{4|\chi|^2 F_s F_i}\left(1+\Delta^2\right)\frac{\pi^2}{2\gamma_p F_p^2}\left(1+\Delta_p^2\right) \qquad [2.33]$$

or

$$\left|\alpha_p^{in}\right|^2_{threshold} = \frac{\pi^2}{4|\chi|^2 F_s F_i}\left[1+\left(\frac{2\Delta\nu F_s F_i}{FSR_i F_s + FSR_i F_s}\right)^2\right]\frac{1}{Enh_p}\left[1+\left(\frac{2\Delta\nu_p F_p}{FSR_p}\right)^2\right], \quad [2.34]$$

where $Enh_p = \frac{2\gamma_p F_p^2}{\pi^2}$ is the maximum enhancement of the pump field inside the cavity, F_j is the finesse, and FSR_j is the free spectral range.

Therefore, in the case of a ring cavity DRO with pump enhancement, the pump intensity required to reach threshold is minimum for zero detuning from exact resonance and is given by

$$\left|\alpha_p^{in}\right|^2_{threshold} = \frac{\pi^2}{4|\chi|^2 F_s F_i Enh_p}. \quad [2.35]$$

The discussion for the ring cavity given in ref. 5 is valid for the case of the linear cavity provided that the coupling coefficient χ is replaced by

$$\chi' = \chi\left[1+\exp(i\Delta kl - i\theta')\right], \quad [2.36]$$

where θ' is the accumulated cavity round-trip phase shift for the three waves. This is due to the fact that standing waves, and not travelling waves, must be matched for optimum coupling in the crystal. Phase matching now depends on the mirror phase shifts, which determine the relative position of nodes and antinodes of the three interacting waves and the value of their overlap.

For the case of a linear cavity DRO with pump enhancement it can be shown that the minimum pump intensity required to reach threshold is given by [5]

$$\left|\alpha_p^{in}\right|^2_{threshold} = \frac{\pi^2}{16\kappa^2 l^2 F_s F_i Enh_p}. \qquad [2.37]$$

The pump power threshold can now be written in the form

$$P_{threshold} = K\frac{\pi^2}{4F_s F_i Enh_p}. \qquad [2.38]$$

where $K = \dfrac{n_p^2 \varepsilon_o c^4}{2\pi^2 L_{crystal}\left|d_{eff}\right|^2\left(1-\delta^2\right)^2 \nu_p^3}$.

Using a similar analysis for the case of a single pass pump field the pump power threshold can be written as

$$P_{threshold} = K\frac{\pi^2}{F_s F_i}. \qquad [2.39]$$

DROs can have thresholds at the mW level. A major disadvantage of DROs is that they are over constrained by requiring four conditions to be satisfied simultaneously (summarised in table 2.2 below).

Energy conservation,	$\nu_s + \nu_i = \nu_p$
Phase matching,	$k_s + k_i = k_p$
Cavity resonance for the signal field,	$m\frac{\lambda_s}{2} = L$
Cavity resonance for the idler field.	$m\frac{\lambda_i}{2} = L$

Table 2.2 *Requirements for operation of a DRO*

Therefore, operation can only occur at discrete cavity lengths where the signal and idler frequencies satisfy the above constraints. This introduces complications in the tuning of these devices [18, 19], resulting in the occurrence of mode and cluster hops [19, 20].

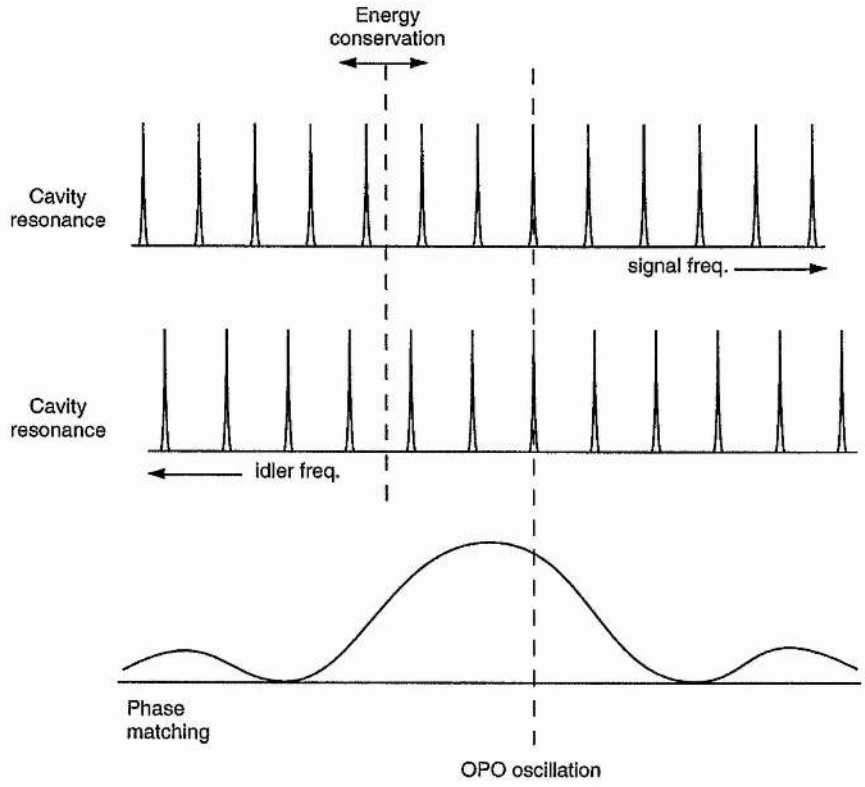

Figure 2.5 *Relationship between the signal and idler resonance frequencies, conservation of energy, and phase-matching condition on a DRO. Axes for signal and idler modes are plotted in opposite directions. Any vertical line satisfies the conservation of energy relation. A signal-idler mode-pair that has both resonances centred on a vertical line satisfies the simultaneous resonance condition.*

Figure 2.5. shows how the various constraints are related in a DRO. The phase-matching condition is adequately satisfied for a range of signal and idler frequencies and the selectivity is imposed by the requirement for simultaneous resonance of the signal and idler fields. The resonance conditions for the signal and idler fields are

$$\nu_s = \frac{m_s c}{2\left(L_s + (n_s - 1)l\right)}, \qquad [2.40(a)]$$

$$\nu_i = \frac{m_i c}{2\left(L_i + (n_i - 1)l\right)}, \qquad [2.40(b)]$$

where m_s and m_i are the longitudinal mode numbers of the signal and idler fields respectively, n_s and n_i are the refractive indices of the signal and idler within the nonlinear material, L_s and L_i are the signal and idler cavity lengths, and l is the length of the nonlinear crystal.

Small changes in either the cavity length or the pump frequency may lead to the OPO output switching from one mode pair to another. This switch can either be to an adjacent mode-pair (called a mode-hop) or over many mode-pairs (called a cluster-hop) [19].

For a fixed frequency pump source, a change in the length of the cavity by $\Delta L_{s,i}$ causes a change in the resonant frequency of the signal or idler field by

$$\Delta\nu_s = \frac{-\Delta L_s \nu_s}{L_s + (n_s - 1)l}, \qquad [2.41(a)]$$

$$\Delta\nu_i = \frac{-\Delta L_i \nu_i}{L_i + (n_i - 1)l}. \qquad [2.41(b)]$$

Or expressed in terms of the free spectral range $FSR_{s,i}$ of the signal or idler cavity

$$\Delta\nu_s \approx \frac{-2\Delta L_s \nu_s FSR_s}{c}, \qquad [2.42(a)]$$

$$\Delta\nu_i \approx \frac{-2\Delta L_i \nu_i FSR_i}{c}. \qquad [2.42(b)]$$

It is useful to consider the maximum detuning allowed while maintaining oscillation on a single signal and idler mode pair. From figure 2.6 below it can be seen that this maximum detuning $\Delta\nu_{\max}$ is approximately

$$\Delta\nu_{\max} = \Delta\nu_s + \Delta\nu_i \leq \frac{FSR_s}{2F_s} + \frac{FSR_i}{2F_i}, \qquad [2.43]$$

where $\Delta\nu_s$ and $\Delta\nu_i$ are the half-width at half-maximum of the signal and idler resonance.

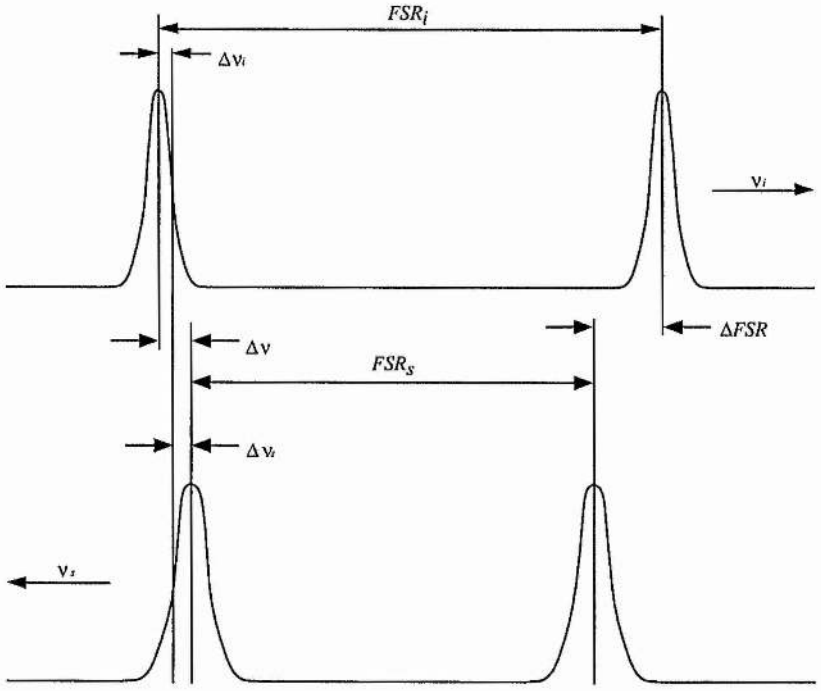

Figure 2.6. *Requirement for simultaneous resonance of signal and idler fields for a DRO. The diagram shows the maximum detuning allowed if the oscillation frequencies are to remain within the FWHM of the cavity resonances.*

Eqn. (2.43) is related to the third term of the pump power threshold equation derived in Eckardt et al. [19]. For a DRO the pump power threshold is

$$P_{th} \propto \left(\frac{1}{\mathrm{sinc}^2(\Delta kl/2)}\right)\left(\frac{\pi^2}{F_i F_s}\right)\left(1+\left(\frac{2(\Delta\nu_s+\Delta\nu_i)F_s F_i}{F_i FSR_s + F_s FSR_i}\right)^2\right). \qquad [2.44]$$

The first term is related to the increase in the threshold for detuning from perfect phase-matching. The second term is related to the reduction in the threshold when the OPO is configured to be doubly resonant. The third term is related to Eqn. (2.43)

and corresponds to the detuning in pump frequency or cavity length that doubles the threshold of operation for the particular mode-pair. This detuning is an indication of the range over which the OPO can operate on a single mode-pair. Using equations (2.42) to express the detuning as a change in cavity length, the maximum cavity length detuning, $\Delta L_{\max}$, that can be tolerated for the OPO is to remain operational on a single mode-pair can be written as

$$\left| 4\left(\frac{\Delta L_{\max} FSR_s}{\lambda_s} + \frac{\Delta L_{\max} FSR_i}{\lambda_i} \right) \right| < \frac{FSR_s}{F_s} + \frac{FSR_i}{F_i}. \qquad [2.45]$$

This gives the cavity length stability, ΔL_{stab}, required to maintain the output to a single mode-pair to be [20]

$$\Delta L_{stab} < \frac{\lambda_p}{4}\left(\frac{1}{F_s} + \frac{1}{F_i} \right), \qquad [2.46]$$

For the case of a single-cavity OPO, where it can be assumed that $\Delta L_s = \Delta L_i = \Delta L$ and $FSR_s \approx FSR_i \approx FSR$, the pump frequency stability requirement to maintain the output to a single mode-pair is

$$\Delta \nu_{p-stab} < \frac{FSR}{2}\left(\frac{1}{F_s} + \frac{1}{F_i} \right) \qquad [2.47]$$

Equating equations (2.46) and (2.47) gives the relationship between ΔL and $\Delta\nu_p$ to be

$$\Delta\nu_p \approx -2\Delta L\left(\frac{FSR}{\lambda_p}\right). \qquad [2.48]$$

When either pump frequency or cavity length is changed, the above equation gives the required tuning of the other parameter in order to maintain the simultaneous resonance of the signal and idler fields.

2.7.2 Stability requirements for single mode-pair operation of DROs

The cavity length and pump frequency stability requirements for DROs, with regard to obtaining single mode-pair output, have been discussed by Henderson et al. [20]. The level of cavity length or pump frequency detuning required to cause a hop to an adjacent pair of signal and idler modes (mode-hop) is dictated by the mismatch in the free spectral ranges, ΔFSR. Providing that the original mode-pair is exactly on resonance, tuning the cavity mode frequencies by ΔFSR is sufficient for a mode-hop to occur.

$$\Delta FSR \approx \frac{2(\Delta L_s \nu_s FSR_s + \Delta L_i \nu_i FSR_i)}{c} \qquad [2.49]$$

For an OPO in which the signal and idler fields are resonant in a single cavity, the change in cavity length required to achieve a mode-hop is given by [20]

$$\Delta L_{hop} \approx \frac{\Delta FSR}{2\ FSR}\lambda_p, \qquad [2.50]$$

where λ_p is the pump wavelength. This can also be written as

$$\Delta L_{hop} = \frac{c}{2\,\nu_p}\frac{|n_s - n_i|l}{(L + (\overline{n} - 1)l)}, \qquad [2.51]$$

where $\overline{n}$ is the average refractive index for signal and idler.

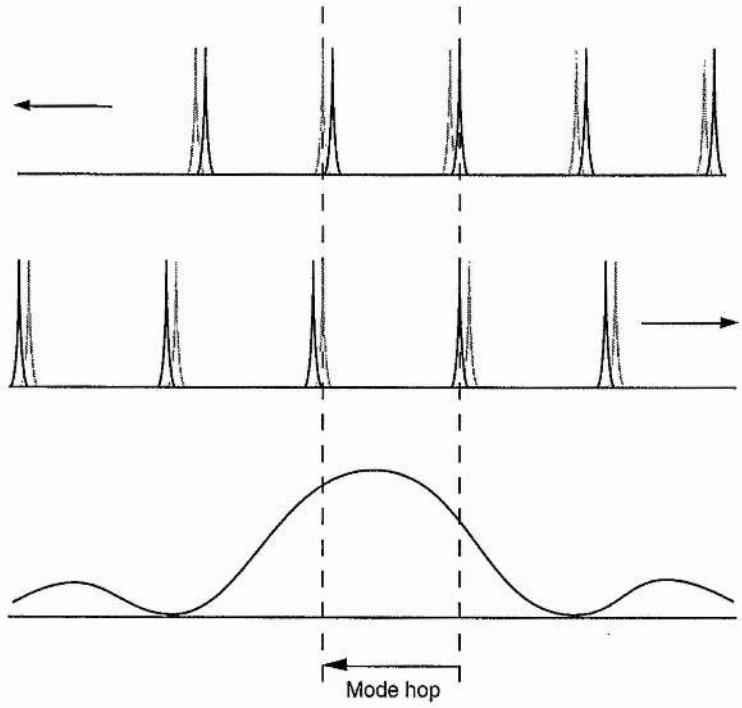

Figure 2.7. *The change in cavity length required for a mode hop. A small change in cavity length will cause the mode frequencies to shift along the axes.*

Mode-hops can also occur due to pump frequency detuning. The pump frequency detuning required to cause a mode-hop is given by

$$\Delta\nu_{p-hop} = \Delta FSR \qquad [2.52]$$

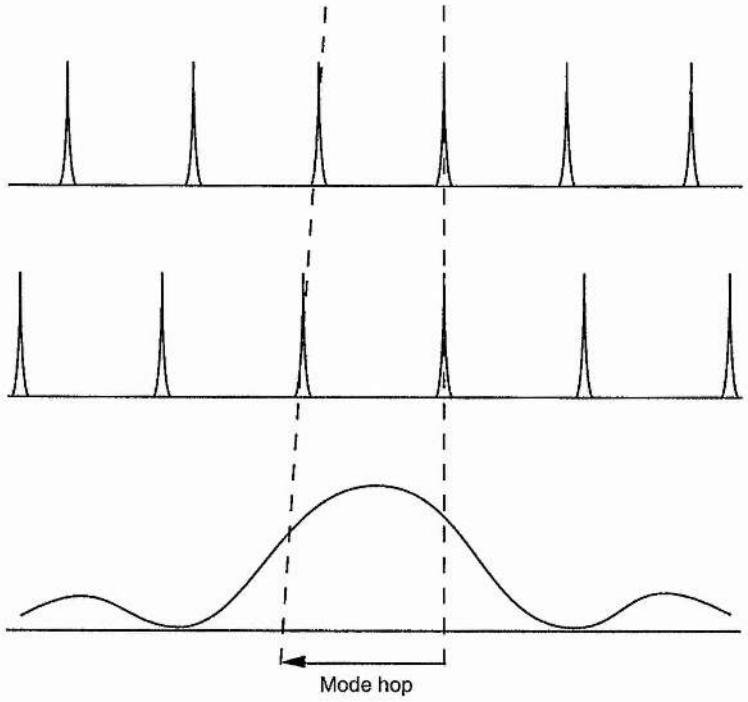

Figure 2.8. *The change in pump frequency required for a mode hop. For a change in pump frequency the frequencies of the signal and idler resonance peaks remain fixed on the axes while the axes themselves shift relative to each other.*

When ΔFSR is large, detuning the cavity length results in discrete output peaks, corresponding to individual pairs of signal and idler modes. This discrete nature of the output arises when particular mode-pairs are detuned off resonance before the

next adjacent mode-pair reaches threshold (see figure 2.9 below). This gives a clear feature upon which to lock the output of the OPO and ensure single-frequency operation. The requirement for easily stabilised operation on a single mode-pair is therefore

$$\Delta L_{hop} > \Delta L_{stab} \qquad [2.53]$$

Previously Henderson et al. [20] demonstrated single mode-pair operation of a CW-DRO based on a bulk KTP crystal configured for near-degenerate, type-II, critical phase-matching. Type-II phase-matching results in a large ΔFSR even for operation near frequency degeneracy.

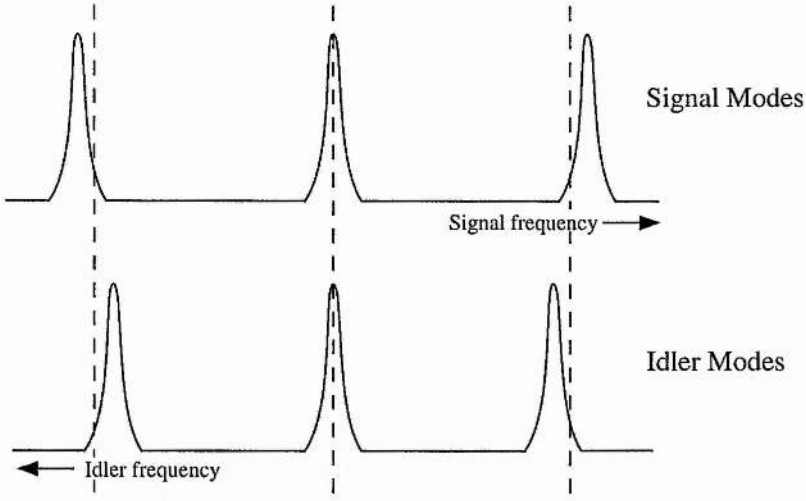

Figure 2.9 *In general for type-II phase-matching near degeneracy* $\Delta L_{hop} > \Delta L_{stab}$. *Scanning the cavity length results in discrete output peaks arising when particular mode-pairs are detuned off resonance before the next adjacent mode-pair reaches threshold.*

For type-I phase-matching near degeneracy, where ΔFSR is small, $\Delta L_{hop} < \Delta L_{stab}$. Therefore, detuning of the cavity length causes hops between different pairs of signal and idler modes while remaining above threshold (see figure 2.10). In this case it is more difficult to hold the output to a single mode-pair.

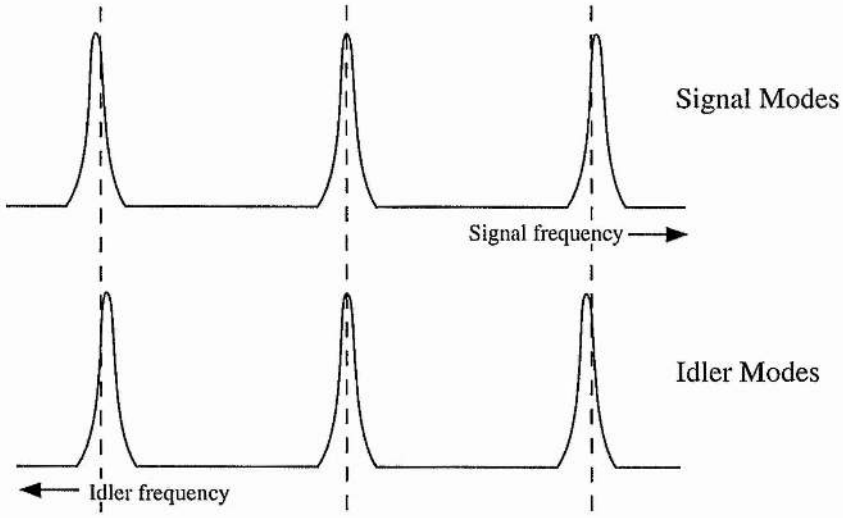

Figure 2.10 *In general for type-I phase-matching near degeneracy* $\Delta L_{hop} < \Delta L_{stab}$. *Scanning the cavity length causes hops between different mode-pairs while remaining above threshold.*

Chapter 8 details a DRO in which the signal and idler waves have the same linear polarisation. Operation of the DRO away from frequency degeneracy was essential in obtaining the necessary ΔFSR to satisfy equation 2.53.

2.8 The singly resonant oscillator (SRO)

OPOs can be configured as singly resonant oscillators (SROs) in which only one of the signal or idler fields is resonant in the cavity. Owing to the elimination of the simultaneous resonance of two discrete frequencies within the same cavity, SROs provide tunable light that is stable in amplitude and frequency.

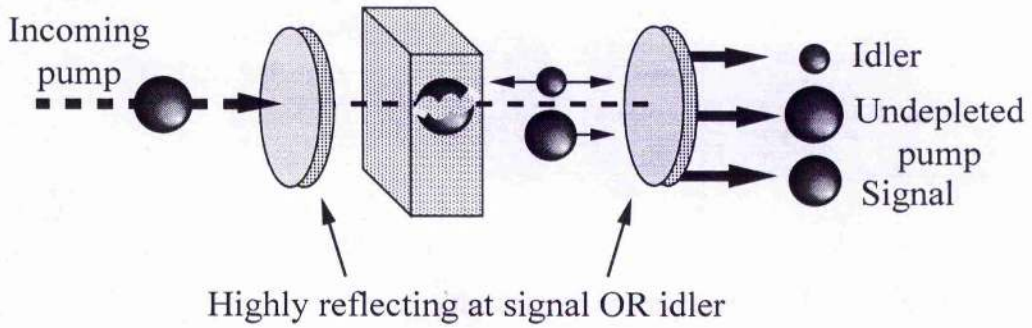

Figure 2.11 *Singly Resonant Oscillators (SROs) are devices that are relatively easy to control but require relatively high pump powers to reach threshold.*

2.8.1 Pump power thresholds for SROs

Resonating only one field in the cavity increases the pump power requirements for SROs. For the case of a single pass pump, the pump intensity required to reach threshold is given by

$$\left|\alpha_p^{in}\right|^2_{threshold} = \frac{\pi^2}{4\kappa^2 l^2 F_i} \times \frac{1}{\mathrm{sinc}^2\left(\frac{\Delta kl}{2}\right)}. \qquad [2.54]$$

This corresponds to a minimum pump power threshold of

$$P_{threshold} = K\frac{\pi}{F_i}, \qquad [2.55]$$

where $K = \dfrac{n_p^2 \varepsilon_o c^4}{2\pi^2 L_{crystal}\left|d_{eff}\right|^2\left(1-\delta^2\right)^2 \nu_p^3}$ and is typically at the watt level.

Similarly for the case of pump enhancement, the pump power threshold is given by

$$P_{threshold} = K\frac{\pi}{2F_i Enh_p}. \qquad [2.56]$$

Pump enhanced SROs have thresholds that are typically 100's mW.

The required stability in cavity length is the same as in a conventional laser and is given by

$$\Delta L_{stab} \approx \pm\frac{\lambda_{res}}{4}. \qquad [2.57]$$

Similarly the required stability in pump frequency is given by

$$\Delta\upsilon_{stab} \approx \pm FSR \frac{\lambda_{res}}{\lambda_{nonres}}. \qquad [2.58]$$

This results in the oscillation of the resonant wave at a frequency corresponding to the cavity mode which lies closest to the optimum phase-matching condition (figure 2.12 below).

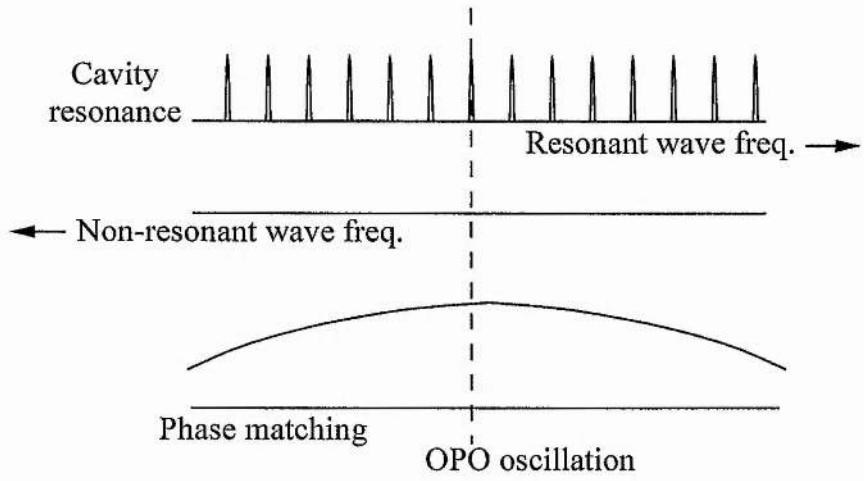

Figure 2.12 *In the case of the singly resonant OPO, operation is on the resonant mode that lies nearest to the optimum phase-matching condition.*

The frequency of the field which is non-resonant is dictated by the energy conservation relation (Eqn. 2.1). This results in the relatively straight forward control of the OPO frequencies. Changing the phase matching provides coarse tuning while the simultaneous change of phase matching and cavity length provides

fine tuning of the output frequencies. However, in the absence of intracavity tuning elements, SROs have a limited fine tuning range compared to that of DROs. This is discussed further in chapter 5.

A major disadvantage of SROs is that their high pump power thresholds place restrictions on the choice of pump sources. One method of reducing the pump power required to reach threshold in an SRO is to resonate the pump field in addition to one of the generated fields (figure 2.13 below). This is referred to as pump enhancement and was first demonstrated by Robertson et al. [21].

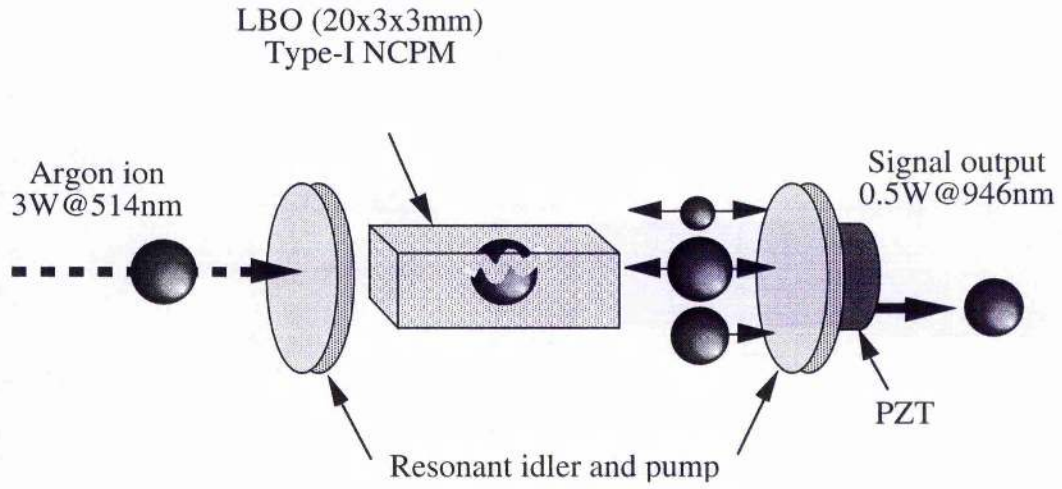

Figure 2.13 *Continuous wave SRO with pump enhancement.*

However, pump enhancement does not reduce the pump power threshold of SROs to that of true DROs (signal and idler resonant).

2.9 Continuous frequency tuning of DROs

For applications such as high-resolution spectroscopy, the output frequency of the OPO must be set to a spectral region of interest and then continuously tuned over that region. The standard cw DRO employs a single cavity which is resonant for both signal and idler fields. However, single cavity DROs using a fixed pump source cannot maintain the simultaneous resonance of a signal and idler mode pair while tuning continuously. This is due to the fact that, from the conservation of energy relation, the change in idler frequency is of the same magnitude, but opposite in sign, to the change in signal frequency.

One method of continuously tuning in DROs with fixed frequency pump sources is to resonate the signal and idler frequencies in different optical cavities. This device is known as a dual-cavity OPO [22, 23] and allows continuous tuning through independent control of the signal and idler cavity lengths. Figure 2.14 below shows a dual-cavity, doubly resonant, optical parametric oscillator as demonstrated by Colville *et al.* [23].

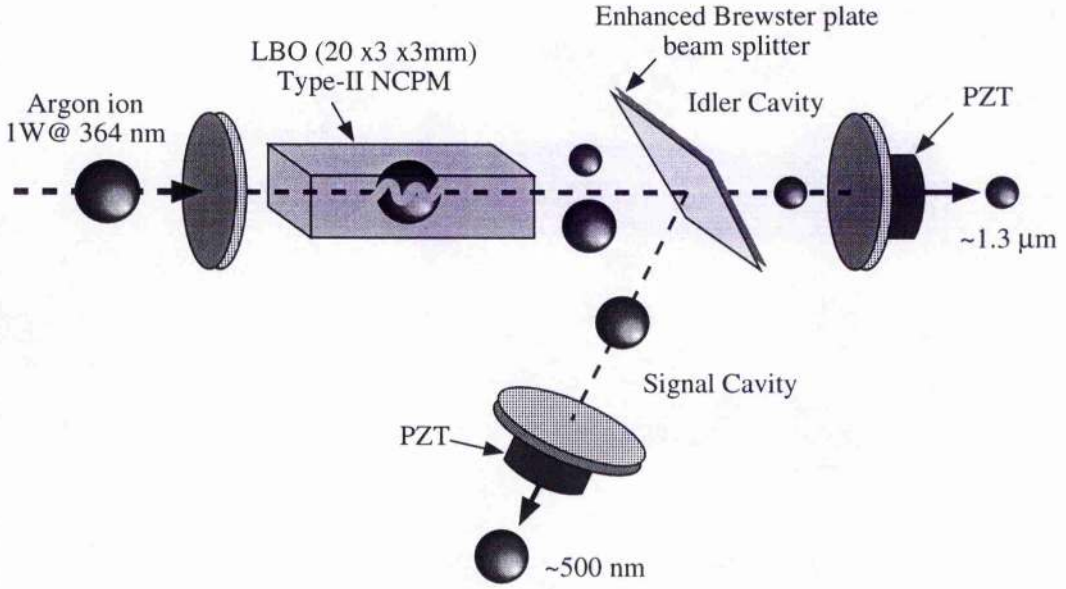

Figure 2.14 *Schematic diagram of a dual-cavity, doubly resonant, optical parametric oscillator. For type II phase-matching, the signal and idler fields are orthogonally polarised and can therefore be separated using a Brewster-angled beam splitter.*

The two factors that are critical for the operation of this dual-cavity OPO are type-II phase matching and non-degenerate frequencies. Type-II phase matching, providing orthogonal polarisations of the signal and idler fields, allows decoupling using a polarising beam splitter whereas non-degeneracy allows effective dichroic-coating separation. In dual cavity devices the low pump power threshold associated with standard DROs is maintained. Smooth tuning of the signal and idler outputs is achieved by smoothly scanning the idler cavity while servo controlling the signal cavity.

A dual cavity DRO based on KTP has previously been demonstrated with a smooth tuning range of the signal and idler frequencies over ~900MHz [24]. However, residual pump resonances and polariser leakage at the nonideal beam splitter are the main factors limiting the smooth tuning range.

Single frequency, and continuous wave, operation can be achieved within a single cavity DRO by controlling either the cavity length or the pump frequency. Equation 2.48 gives the relationship between cavity length and pump frequency. Therefore, servo controlling the cavity length corrects for both cavity length and pump frequency fluctuations, hence maintaining a constant output power, holding the OPO output to a single pair of signal and idler modes [20].

Schematic of a simple cavity length servo, using a 'side of fringe' locking technique, for a single cavity DRO. The output signal and idler power of the DRO OPO is monitored using a standard photodiode which is compared with a voltage reference. Any deviation from the desired constant output power results in an error signal which is integrated and amplified to control the length of the OPO cavity thus maintaining the double resonance condition.

Figure 2.15

When using a tunable pump source, to pump a single cavity DRO, the signal and idler frequencies can be tuned in the same sense. Such a pump source has been used to pump a single cavity DRO based on KTP [25] (figure 2.16 below). The orientation of the nonlinear crystal provides coarse tuning about frequency degeneracy (900-1100nm). The resonance of the signal and idler frequencies is maintained by a simple cavity length servo system while the pump frequency is smoothly tuned over ~10GHz. It is the simultaneous control of the two parameters, cavity length and pump frequency, that allows the smooth tuning of the OPO output. For continuous tuning of the pump frequency over ~10GHz, the near degenerate signal and idler frequencies each tune over ~5GHz. The smooth tuning range of the OPO output is limited to the smooth tuning range of the pump laser.

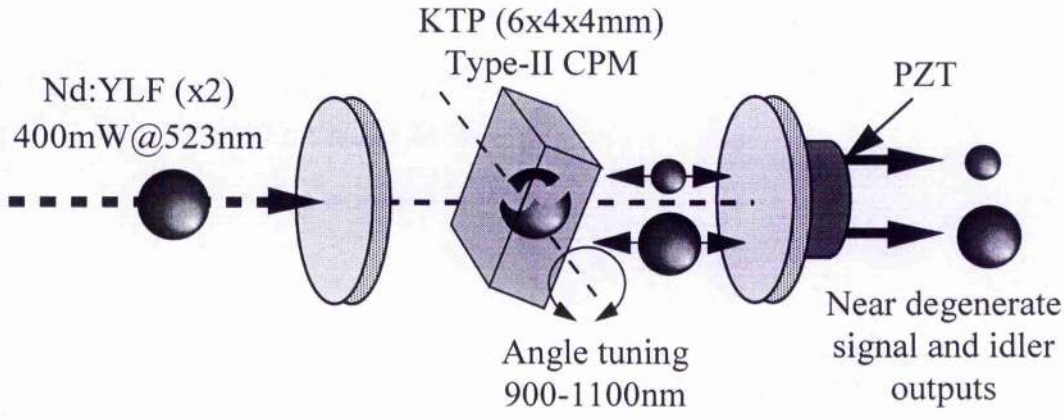

Figure 2.16 *Single cavity DRO-OPO with smoothly tunable output. Angle tuning of KTP crystal gives coarse tuning. Servo control of cavity length maintains operation on a single pair of signal and idler modes. Simultaneous tuning of pump frequency and cavity length gives continuous tuning of OPO output.*

2.10 Summary and conclusions

SROs are much more tolerant to perturbations in cavity length and pump frequency than DROs. However, once cw operation is achieved through stabilisation of the cavity length, the DRO has the advantages of simple design and modest pump power requirements. Cavity length servo systems not only correct for fluctuations in cavity length but also fluctuations in pump frequency. The mismatch in the FSRs for the signal and idler wavelengths is an important factor in the easy stabilisation of the DRO with regard to single-frequency operation. For a DRO the output frequencies can be smoothly tuned by simultaneously controlling the cavity length and pump frequency. The very low pump power threshold associated with DROs provides the opportunity of developing very compact sources of tunable light, such as the microchip laser pumped OPO detailed in chapter 6.

2.11 References

[1] G. D. Boyd and D. A. Kleinman, *Appl. Phys.* **39**, 8, 3597 (1968).

[2] A. Yariv and W. H. Louisell, *IEEE J. Quant. Elect.* **QE-2**, 9, 418 (1966).

[3] J. A. Armstrong, N. Bloembergen, J. Ducuing and P. S. Pershan, *Phys. Rev.* **127**, 6, 1918 (1962).

[4] A. Yariv, *"Quantum Electronics," 3rd ed., Wiley, New York* , (1989).

[5] T. Debuisschert, A. Sizmann, E. Giacobino and C. Fabre, *J. Opt. Soc. Am. B* **10**, 9, 1668 (1993).

[6] T. Y. Fan, C. E. Huang, B. Q. Hu, R. C. Eckardt, Y. X. Fan, R. L. Byer and R. S. Feigelson, *Appl. Optics* **26**, 12, 2390 (1987).

[7] P. A. Franken and J. F. Ward, *Rev. Mod. Phys.* **35**, 23 (1963)

[8] Martin M. Fejer, G. A. Magel, Dieter H. Jundt and R. L. Byer, *IEEE J. Quant. Elect.* **28**, 11, 2631 (1992).

[9] L. E. Myers, R. C. Eckardt, M. M. Fejer, R. L. Byer, W. R. Bosenberg and J. W. Pierce, *J. Opt. Soc. Am. B*, 12, 11, 2102 (1995).

[10] M. Yamada, N. Nada, M. Saitoh and K. Watanabe, *Appl. Phys. Lett.* **62**, 435 (1993).

[11] W. K. Burns, W. McElhanon and L. Goldberg, *IEEE Photon. Technol. Lett.* **6**, 252 (1994).

[12] H. Karlsson and F. Laurell, *Appl. Phys. Lett.* **71**, 24, 3474 (1997).

[13] L. E. Myers, R. C. Eckardt, M. M. Fejer and R. L. Byer, *Optics Letters* **21**, 8, 591 (1996).

[14] P. T. Nee and N. C. Wong, *Optics Lett.* **23**, 1, 46 (1998).

[15] P. E. Powers, Thomas J. Kulp and S. E. Bisson, *Optics Lett.* **23**, 3, 159 (1998).

[16] G. Imeshev, M. Prcotor and M. M. Fejer, *Optics Lett.* **23**, 9, 673 (1998).

[17] F. G. Colville, M. H. Dunn and M. Ebrahimzadeh, *Optics Lett.* **22**, 2, 75 (1997).

[18] D. Lee and N. C. Wong, *J. Opt. Soc. Am. B* **10**, 9, 1659 (1993).

[19] R. C. Eckardt, C. D. Nabors, W. J. Kozlovsky and R. L. Byer, *J. Opt. Soc. Am. B* **8**, 3, 646 (1991).

[20] A. J. Henderson, M. J. Padgett, F. G. Colville, J. Zhang and M. H. Dunn, *Optics Comm.* **119**, 256 (1995).

[21] G. Robertson, M. J. Padgett and M. H. Dunn, *Optics Lett.* **19**, 21, 1735 (1994).

[22] N. C. Wong, *Phys. Rev. A* **45**, 5, 3176 (1992).

[23] F. G. Colville, M. J. Padgett and M. H. Dunn, *Appl. Phys. Lett* **64**, 12, 1490 (1994).

[24] D. Lee and N. C. Wong, *Appl. Phys. B* **66**, 133 (1998).

[25] A. J. Henderson, M. J. Padgett, J. Zhang, W. Sibbett and M. H. Dunn, *Optics Lett.* **20**, 9, 1029 (1995).

3 A continuous wave, continuously tunable, single frequency, doubly resonant OPO

3.1 Introduction

This chapter describes the operation of a single cavity, near-degenerate, OPO based on the nonlinear material Potassium Titanyl Phosphate (KTP). The OPO is based on a configuration similar to that reported earlier by Henderson et al.[1] and forms the basis of the main experimental work within this thesis.

The pump source for the OPO is an all-solid-state, diode-laser-pumped, frequency doubled laser capable of generating ~1 watt, TEM_{00}, single longitudinal mode output at 523nm for 10 watts of diode pump power. Figure 3.1 shows the configuration of the pump laser and OPO. A single laser-diode (operating at 798nm) is used to end-pump an Nd:YLF slab. The mirrors M1, M2, and the coating on the end face of the Nd:YLF slab are arranged to form a folded cavity. Frequency-doubling is achieved using a 6mm long, hydrothermal grown, KTP crystal, cut for type-II phase-matching. The crystal is oriented such that the fundamental wave propagates with its polarisation at 45 degrees to the crystal axes. The fundamental wave at 1047nm (as opposed to 1053nm) is selected using a Brewster plate and this in combination with the KTP acting as a birefringent filter results in single frequency output for the second harmonic. Collimation of the output beam is achieved using a 150mm focal length lens. Back reflections from the OPO are prevented from feeding back into the pump laser by a Faraday isolator which provides >30dB attenuation.

The OPO is configured as a single cavity device of length ~1cm with the mirrors being highly reflecting at both the signal and idler wavelengths, thus forming a doubly resonant oscillator. The pump beam is mode-matched into the OPO cavity by a single lens of focal length 150mm. The corresponding beam waist in the OPO is ~30μm. The OPO is based on a 6mm long, flux grown, KTP crystal cut for near-degenerate, type-II, critical phase-matching ($\theta = 90^\circ$, $\phi = 37^\circ$). The KTP crystal is AR coated at both the pump wavelength (523nm) and the generated wavelengths (1047nm).

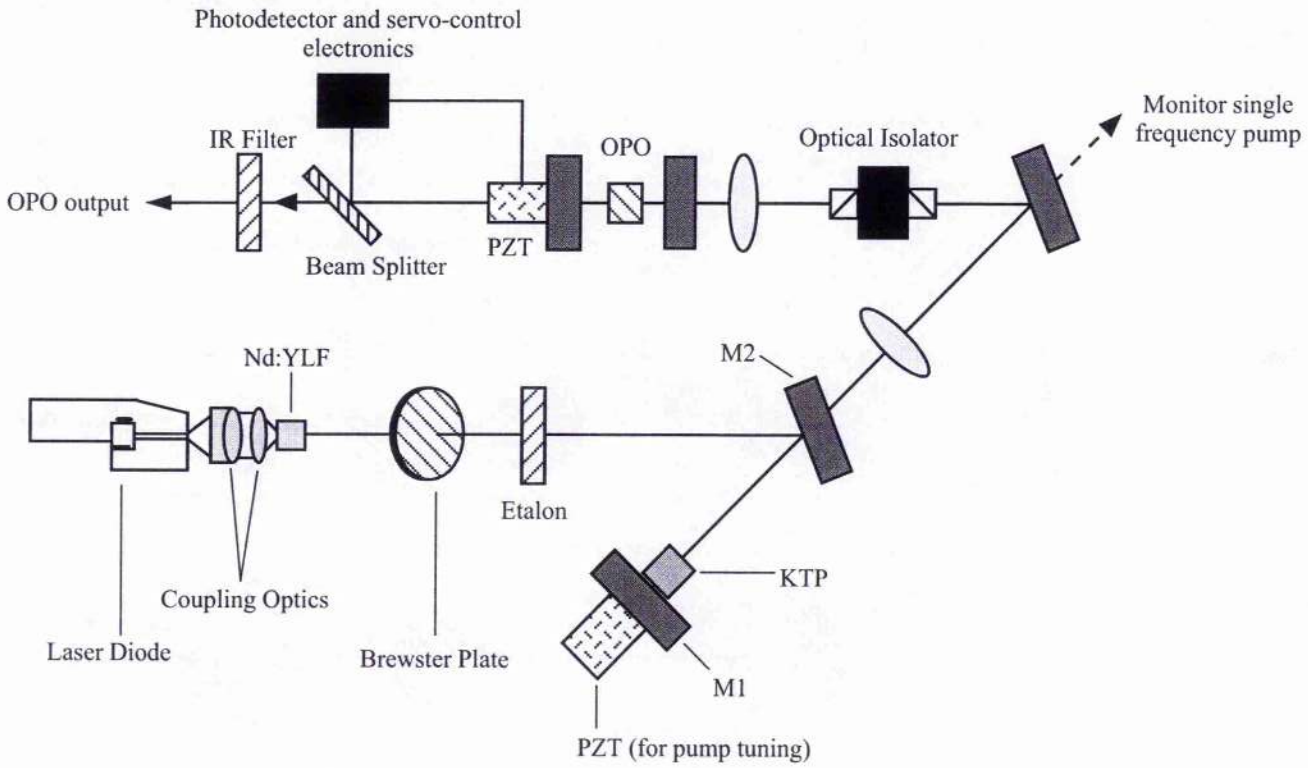

Figure 3.1 Configuration of the all-solid-state, frequency doubled, pump laser and KTP OPO.

Chapter 2 discusses the conditions that have to be satisfied in order to operate a DRO. Four conditions have to be satisfied simultaneously; energy-conservation, phase-matching, and cavity resonances for the signal and idler waves. From ref. 1 the calculated stability requirements for the OPO are $\Delta L_{hop} = 9.7\text{nm}$; $\Delta\nu_{p-hop} = 405\text{MHz}$; $\Delta L_{stab} = 0.4\text{nm}$; $\Delta\nu_{p-stab} = 18\text{MHz}$.

In a previous configuration, the OPO mirrors had an additional 50% reflectivity at the pump wavelength. This resulted in an enhancement of the pump field reducing the pump power threshold and providing a means of aligning the cavity. However, enhancement of the pump field places further constraints on the DRO, affecting its stability and tuning behaviour, and was later removed by using mirrors that were highly transmitting at the pump wavelength.

Configuring the OPO for type-II phase-matching provides orthogonally-polarised signal and idler fields. This gives a greater refractive index mis-match than for type-I phase-matching. This finite difference in FSRs at degeneracy is an advantage with regard to obtaining single signal and idler mode-pair output for near-degenerate operation. The mismatch in the FSRs is related to the cavity length/pump frequency detuning required to cause a mode-hop and is significantly greater for type-II phase-matching than for type-I. A previous comparison of two near-degenerate OPOs, one based on LBO (type-I noncritical phase-matching), the other based on KTP (type-II critical phase-matching), [1] showed the type-II phase-matched OPO to be at least 4 times more tolerant of both cavity length and pump frequency perturbation with regards to stable, single frequency, operation.

3.2 Experimental observations of a KTP OPO (type-II phase-matching)

The OPO operated with a minimum pump power threshold of 30mW and the output frequencies could be tuned (at room temperature) from 1020 to 1070nm by angle tuning the KTP crystal over 4°. This tuning range is limited by the increasing reflection loss from the crystal surfaces away from normal incidence. A tuning range of 950-1150nm is possible with appropriately cut crystals.

The KTP OPO was assessed by scanning the cavity length over μm ranges and monitoring the OPO output on a standard photodiode. The output of the OPO was characterised by discrete output peaks of equal width (see Figure 3.2). This shows that the OPO is over-constrained and does not reach threshold for any arbitrary cavity length.

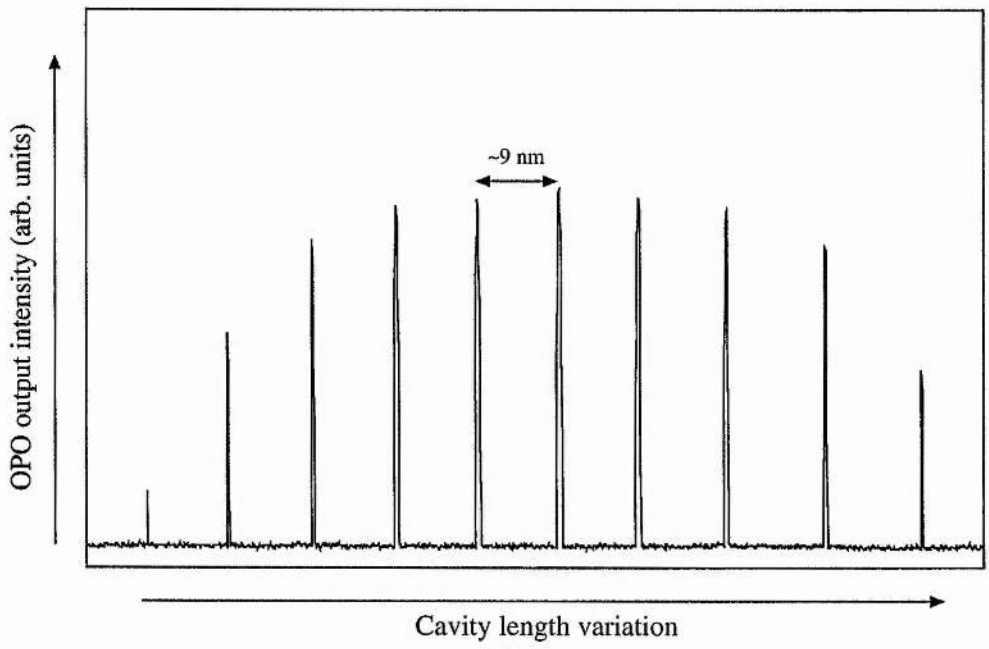

Figure 3.2 *Experimentally observed mode-hops when scanning the cavity length of the OPO.*

In order to keep the cavity in resonance for the signal and idler fields simultaneously, a locking system which maintains a constant cavity length is required. From equation (7) in ref. 1 it can be shown that the required stability in cavity length is ~0.5nm and in pump frequency ~20MHz. Equation (9) in ref. 1 gives the relationship between cavity length and pump frequency. Servo control of the OPO cavity corrects for both cavity length and pump frequency fluctuations. In this experiment the cavity length is servo controlled to maintain a constant output power, holding the OPO output to a single pair of signal and idler modes.

When locking conventional lasers it is common practice to induce a small periodic modulation to the cavity length and compare this modulation to the change in output

power, monitored by a photodiode. A phase sensitive detector generates an error signal proportional to the differential of the output power w.r.t the displacement from the locking position. This approach works well for output powers that follow Gaussian or Lorentzian profiles with cavity length. However, in DROs the output power is characterised by a profile which has steep sides due to the nature of the double resonance condition. The shapes of these profiles are detailed in chapter 4. Using a modulation technique to lock a DRO results in a nonlinear error signal which limits the effectiveness of the servo system. It was found that a servo system using a side-of-fringe locking technique was an effective method of stabilising the DRO achieving amplitude stabilisation of a single signal and idler mode-pair.

The error signal is obtained by slightly detuning the OPO from optimum power and then monitoring the output power on a standard photodiode. The output of this photodiode is subtracted from a voltage reference to give an error signal having information on both the amount of cavity length correction and the sign of correction that is required for stabilising the DRO. A circuit diagram for generating the error signal is shown in appendix C.

The generated error signal is then integrated and a correction is applied to the cavity length using a piezoelectric transducer driven by a high voltage amplifier. The frequency response of the servo system was limited by the high voltage amplifier which had a –3dB cut-off frequency of ~1kHz. This was sufficient to lock the DRO having a residual intensity modulation of ~5%. Figure 3.3 shows the block-diagram of the overall servo system.

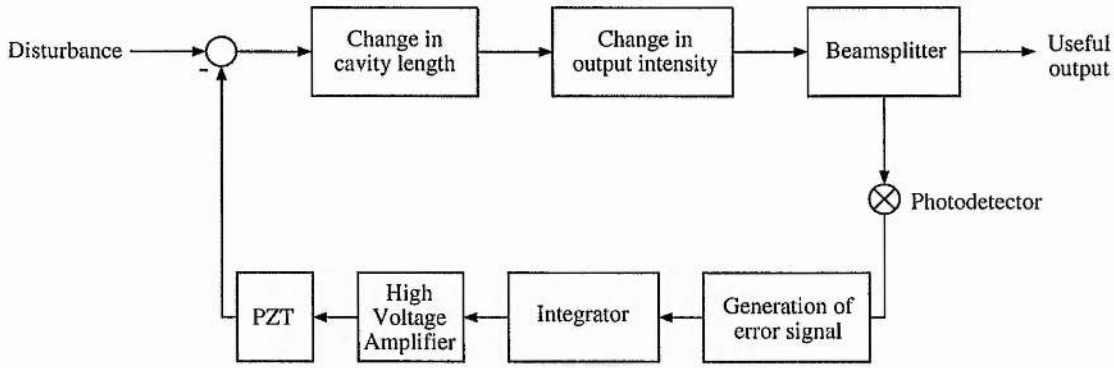

Figure 3.3 *Block diagram of cavity length servo system for OPO. The output intensity is monitored on a standard photodiode and a correction signal is applied via a piezoelectric transducer. A beamsplitter provides a signal for the servo loop. PZT; piezoelectric translator.*

The power output coupler of the DRO was 0.5% for both the signal and idler frequencies. A 50% beamsplitter was used for monitoring the output power and providing a signal for the cavity length servo control. This configuration provided ~5 mW of useful output power, for both signal and idler, for an input pump power of 200 mW. Figure 3.4 shows the output intensity of the OPO when the cavity length is servo controlled.

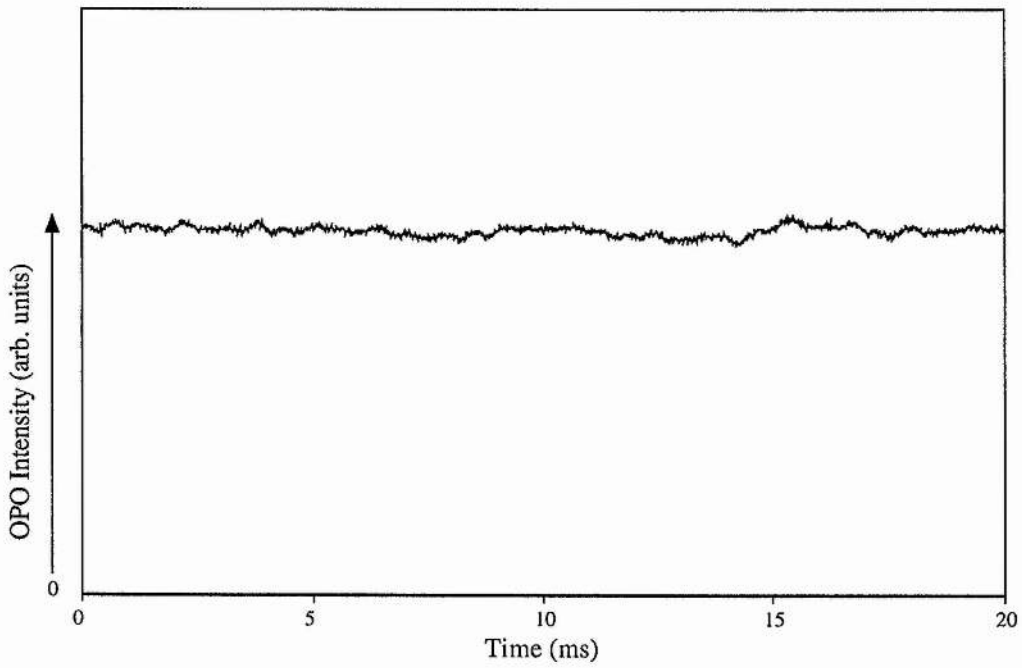

Figure 3.4 *Output intensity as a function of time for the locked OPO as monitored on a standard photodiode. The residual intensity modulation is typically ~5% at kHz frequencies, traceable to the frequency noise of the pump laser.*

Although the servo system corrects for both changes in cavity length and pump frequency, each affect the outputs of the OPO differently. The exact frequencies of the signal and idler fields are determined by the pump frequency whereas perturbations in the cavity length result in the detuning of the cavity mode resonances away from the generated frequencies. The detuning of the cavity mode resonance leads to a decrease in conversion efficiency. Therefore, for a DRO, fluctuations in cavity length lead to fluctuations in intensity not frequency. Hence a DRO has a linewidth inherently that of its pump source.

Figure 3.5 below shows the single frequency output of the OPO, when the cavity length is servo controlled, for a single frequency pump input.

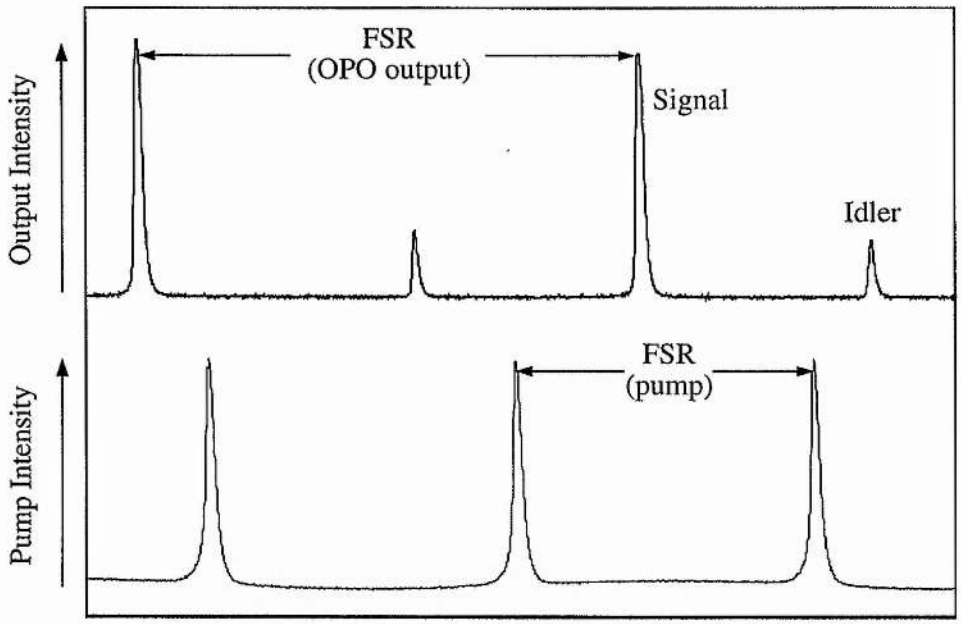

Figure 3.5 *The output of the OPO when pumped by a single longitudinal-mode pump laser consists of a single pair of signal and idler modes. The output was observed with a Fabry-Perot interferometer. FSR, free spectral range.*

3.3 Smooth/continuous frequency tuning

As discussed in chapter 2 the smooth tuning of a single cavity DRO requires the simultaneous control of two parameters, namely pump frequency and cavity length. Therefore, smoothly tuning the OPO pump source while simultaneously servo controlling the cavity length results in the smooth tuning of the OPO output frequencies. Pump-tuned single cavity cw OPOs have previously been demonstrated [2, 3].

Once the OPO was stabilised, operating on a single signal and idler mode-pair, the pump laser was tuned through ~10GHz by piezoelectric control of its cavity length. This 10GHz of smooth tuning resulted in the smooth tuning, without mode-hops of both the signal and idler over ~5GHz. Chapter 5 and ref. [4] shows that this smooth tuning range is limited only by the smooth tuning range of the pump laser.

3.4 Summary and conclusions

To summarise, this chapter details the operation of a single cavity, cw, doubly resonant OPO based on KTP. The OPO was stabilised using a simple cavity length servo system, resulting in single mode-pair operation and continuous output power. Tuning the pump source over 10GHz, while servo controlling the cavity length, resulted in the smooth tuning of the OPO output frequencies over 5GHz without mode-hops. These observations are consistent with those reported by Henderson et al. [3]. This configuration forms the basis of the main experimental work within this thesis.

3.5 References

[1] A. J. Henderson, M. J. Padgett, F. G. Colville, J. Zhang and M. H. Dunn, *Optics Comm.* **119**, 256 (1995).

[2] E. S. Polzik, H. Mabuchi, and H. J. Kimble, in *Conference on Lasers and Electro-Optics, Vol. 11 of 1993 OSA Technical Digest Series (Optical Society of America, Washington, D. C., 1993)*, paper CThK6, p. 434.

[3] A. J. Henderson, M. J. Padgett, J. Zhang, W. Sibbett and M. H. Dunn, *Optics Lett.* **20**, 9, 1029 (1995).

[4] G. M. Gibson, M. H. Dunn and M. J. Padgett, *Optics Lett.* **23**, 1, 40 (1998).

4 Dynamic behaviour of a doubly resonant optical parametric oscillator

4.1 Introduction

As discussed earlier in chapter 3, for the case of a DRO, changes in cavity length or pump frequency, by a few nm or MHz respectively, results in the OPO switching on and off as adjacent pairs of signal and idler modes come into and out of simultaneous resonance. This phenomenon is more commonly referred to as mode hopping and can be studied experimentally by scanning the cavity length of the OPO [1, 2]. Discrete output peaks are observed, each of which correspond to a simultaneous resonance of the signal and idler fields.

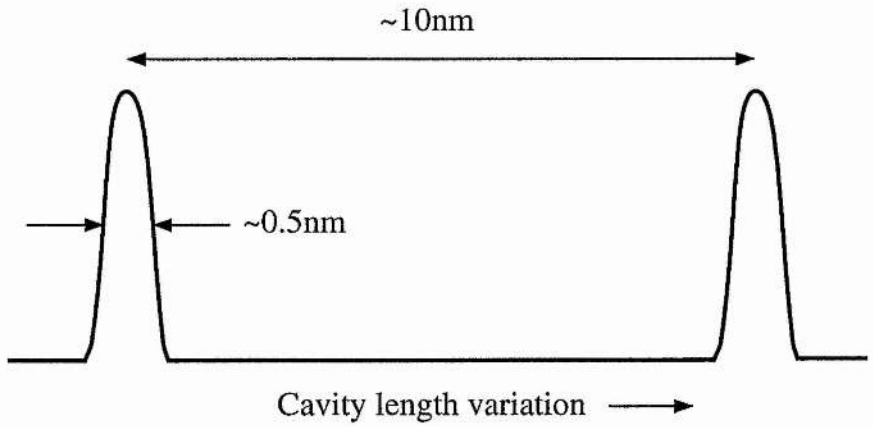

Figure 4.1 *Discrete output peaks observed when scanning a DRO cavity. The spacing of the peaks corresponds to the FSR of the OPO cavity*

It is observed that, as the scan rate increases, these output peaks show a step in intensity on their leading edge (as shown in figure 4.2 below). This step change (or build-up time) may have an important effect on the stabilisation of DROs since they become more difficult to stabilise as the rate of change in intensity with cavity length increases.

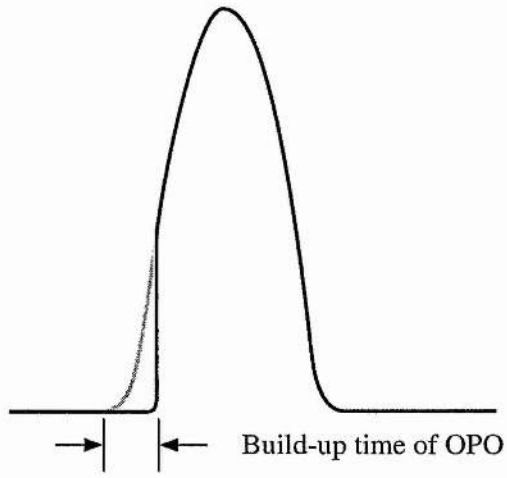

Figure 4.2 *Diagram showing the build-up time for an OPO (typically ~μs). This effect becomes more significant as the scanning rate is increased.*

A computer model was developed to establish the origin of this effect and understand the implications it has on the servo control of the OPO output. Important questions that arise are: What OPO parameters affect this build-up time? and, what parameters result in a build-up time large enough to prevent the OPO from reaching threshold?

Previously, Richy *et al.* [3] considered the build-up time for a DRO cavity held on resonance while the pump power was swept through the threshold value. This chapter describes a general model for calculating the time evolving output of a DRO and applies it specifically to the case where the pump power is held constant and the cavity is tuned on and off simultaneous resonance. The model is shown to be in excellent agreement with experimental observations.

4.2 Modelling the dynamic behaviour of a DRO

Modelling the output of a DRO is achieved by calculating the build-up of the signal and idler fields from the spontaneous parametric fluorescence [4]. Similar to the method used by Debuisschert *et al.* [5] the model uses three coupled equations to describe the amplitudes of the signal, idler, and pump fields after the N^{th} round trip in the cavity.

$$\alpha_p(N+1) = \alpha_p(N)e^{i\phi_p}r_{p,1}r_{p,2}\gamma_p - 4\chi\alpha_s(N)\alpha_i(N)e^{i\phi_p}r_{p,1}r_{p,2}\gamma_p + t_{p,1}\alpha_{p_{incident}},$$

$$\alpha_s(N+1) = \alpha_s(N)e^{i\phi_s}r_{s,1}r_{s,2}\gamma_s + 4\chi\alpha_p(N)\alpha_i^*(N)e^{i\phi_s}r_{s,1}r_{s,2}\gamma_s,$$

$$\alpha_i(N+1) = \alpha_i(N)e^{i\phi_i}r_{i,1}r_{i,2}\gamma_i + 4\chi\alpha_p(N)\alpha_s^*(N)e^{i\phi_i}r_{i,1}r_{i,2}\gamma_i, \qquad [4.1]$$

where $|\alpha_j|^2$ represents the number of incident photons per unit time in the mode, $r_{p_{1,2}}$, $r_{s_{1,2}}$, $r_{i_{1,2}}$ are the amplitude reflectivity coefficients for the pump, signal, and idler fields at the input and output mirrors respectively,

$\gamma = \sqrt{1 - \text{power loss per round trip}}$, t_{P_1} is the amplitude transmission coefficient, at the pump wavelength, for the input mirror, ϕ represents the relative phase between fields, zero when all three fields are resonant within the cavity, and is related to the detuning in cavity length, ΔL, and wavelength, λ, by $\phi_j = 4\pi\Delta L_j / \lambda_j$, and χ is the coupling coefficient.

Debuisschert *et al.* solve these equations analytically for the steady state solutions, deriving expressions for the pump power threshold. However, in this case the dynamic behaviour is modelled by numerically evaluating the three fields as a function of time.

The coupled equations shown above (eqns. 4.1) are not used directly to model the dynamic behaviour of a DRO. Instead the forward and backward travelling fields are treated separately to account for the pump field depletion as it propagates through the crystal (a schematic diagram of the OPO cavity is shown in figure 4.3).

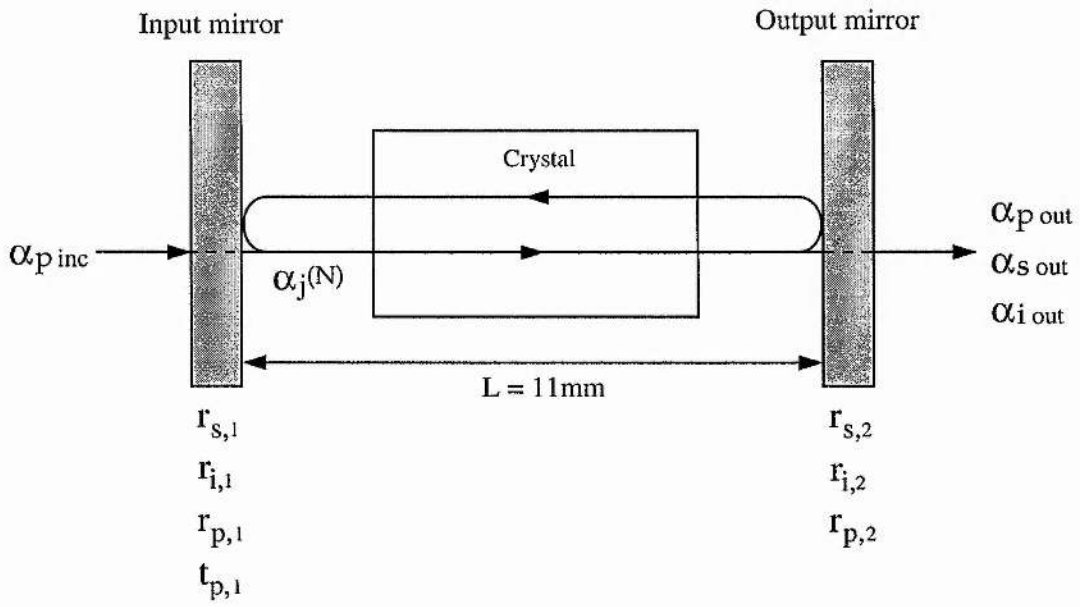

Figure 4.3 *Schematic diagram of OPO cavity.* $\alpha_j(N)$ *represents the circulating pump, signal, and idler fields after the Nth round trip in the cavity.* $\alpha_{p_{inc}}$ *represents the pump field incident on the OPO cavity.*

The equations, as used in the model, can be derived by starting with the coupled equations for the pump, signal, and idler fields propagating through the nonlinear medium [5].

$$\begin{aligned} \alpha_p(l) &= \alpha_p(0) - 2\chi^*\alpha_s(0)\alpha_i(0), \\ \alpha_s(l) &= \alpha_s(0) + 2\chi\alpha_p(0)\alpha_i^*(0), \\ \alpha_i(l) &= \alpha_i(0) + 2\chi\alpha_p(0)\alpha_s^*(0) \end{aligned} \qquad [4.2]$$

where l is the length of the nonlinear crystal.

Considering the case of a nonlinear crystal within an optical resonating cavity, taking into account the relative phase between fields and including the effect of losses at the crystal surfaces, the coupled equations describing the three fields, as they complete one half of the cavity round trip time, can be written as

$$\begin{aligned}
\alpha_p(L) &= \alpha_p(0) r_p \gamma_p e^{i\phi_p} - 2\chi \alpha_s(0)\alpha_i(0) r_p \gamma_p e^{i\phi_p}, \\
\alpha_s(L) &= \alpha_s(0) r_s \gamma_s e^{i\phi_s} + 2\chi \alpha_p(0)\alpha_i^*(0) r_s \gamma_s e^{i\phi_s}, \\
\alpha_i(L) &= \alpha_i(0) r_i \gamma_i e^{i\phi_i} + 2\chi \alpha_p(0)\alpha_s^*(0) r_i \gamma_i e^{i\phi_i},
\end{aligned} \qquad [4.3]$$

where L is the cavity length. It should be noted that ϕ now represents the relative phase between fields after a single pass, i.e. half round trip of cavity.

From figure 4.3 the equations can be written as two separate sets of coupled equations describing the forward and backward travelling fields in the cavity.

In the forward direction:

$$\begin{aligned}
\alpha_{p_+}(n) &= \alpha_{p_-}(n-1) e^{i\phi_p} r_{p_2} \gamma_p - 2\chi \alpha_{s_-}(n-1)\alpha_{i_-}(n-1) e^{i\phi_p} r_{p_2} \gamma_p, \\
\alpha_{s_+}(n) &= \alpha_{s_-}(n-1) e^{i\phi_s} r_{s_2} \gamma_s + 2\chi \alpha_{p_-}(n-1)\alpha_{i_-}^*(n-1) e^{i\phi_s} r_{s_2} \gamma_s, \\
\alpha_{i_+}(n) &= \alpha_{i_-}(n-1) e^{i\phi_i} r_{i_2} \gamma_i + 2\chi \alpha_{p_-}(n-1)\alpha_{s_-}^*(n-1) e^{i\phi_i} r_{i_2} \gamma_i,
\end{aligned} \qquad [4.4]$$

In the backward direction:

$$\alpha_{p_-}(n+1) = \alpha_{p_+}(n)e^{i\phi_p} r_{p_1}\gamma_p - 2\chi\alpha_{s_+}(n)\alpha_{i_+}(n)e^{i\phi_p} r_{p_1}\gamma_p + t_{p_1}\alpha_{p_{inc}},$$

$$\alpha_{s_-}(n+1) = \alpha_{s_+}(n)e^{i\phi_s} r_{s_1}\gamma_s + 2\chi\alpha_{p_+}(n)\alpha^*_{i_+}(n)e^{i\phi_s} r_{s_1}\gamma_s, \qquad [4.5]$$

$$\alpha_{i_-}(n+1) = \alpha_{i_+}(n)e^{i\phi_i} r_{i_1}\gamma_i + 2\chi\alpha_{p_+}(n)\alpha^*_{s_+}(n)e^{i\phi_i} r_{i_1}\gamma_i,$$

where each increment of n represents a single pass through the cavity.

The above sets of coupled equations (4.4–4.5) for the forward and backward travelling fields can now be used directly to model the build up of the signal and idler fields.

A first approach to accounting for the pump depletion as it propagates through the nonlinear crystal was to consider the forward and backward travelling fields separately. However, the above sets of equations (4.4–4.5) still assumes that the pump field is constant over a single pass of the nonlinear crystal. To more accurately account for the pump depletion within one pass of the crystal, the model calculates the complex field amplitudes at ten positions along the length of the crystal (a flow diagram of the modeling program is shown in figure 4.4). To model the output power over a period of several micro-seconds typically requires a few 10's of millions of iterations, easily achieved on a desktop computer running for a few minutes.

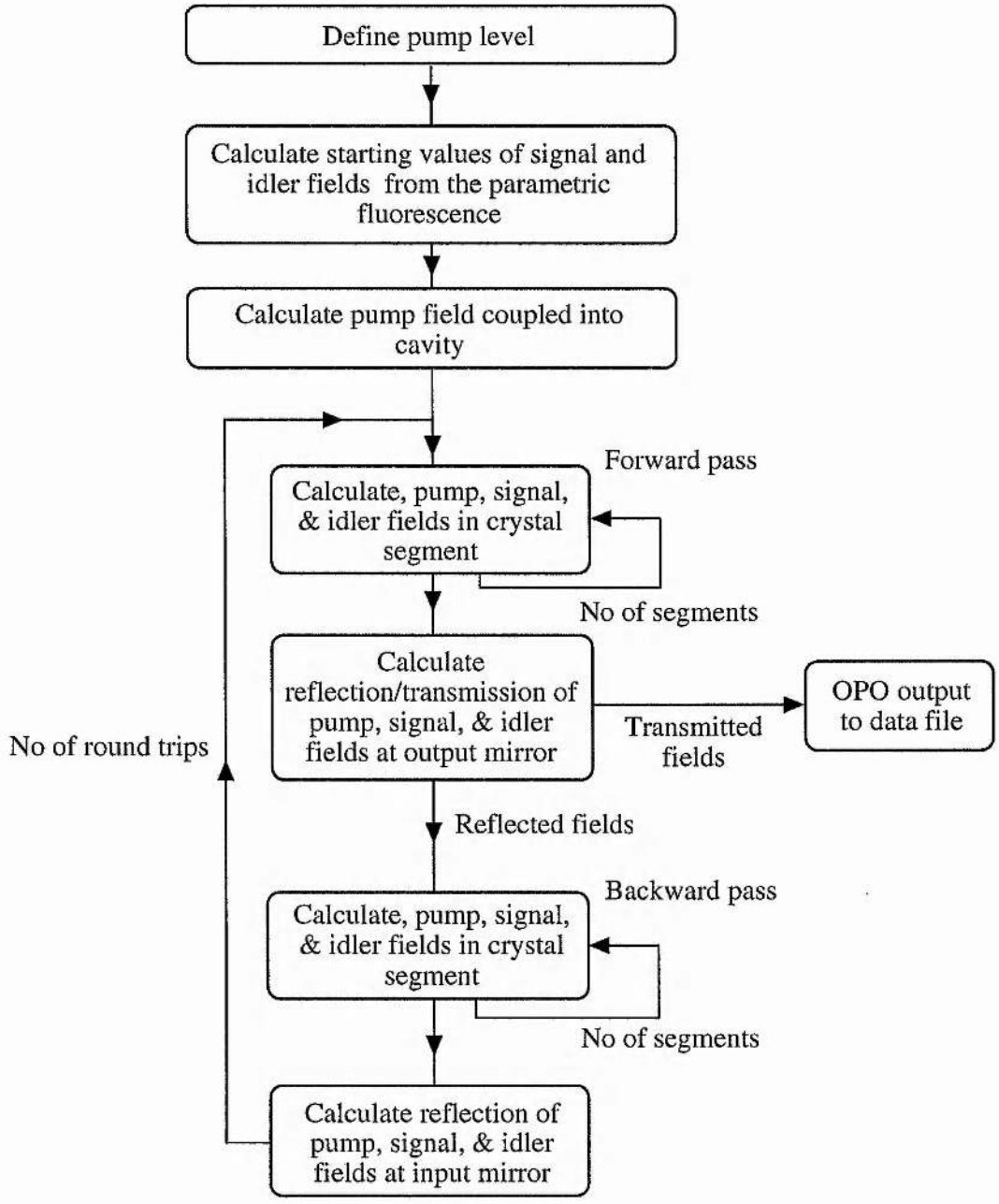

Figure 4.4 *Flow diagram of modelling program. Mirror and crystal losses, input fields, time varying detuning and the strength of the nonlinear interaction are all taken into account.*

A key parameter in the behaviour of the model is the choice of the starting values of the signal and idler fields. These were calculated by considering the level of spontaneous parametric fluorescence arising from the pump field [4, 6].

It has been established that even in the absence of any inputs, a nonlinear optical material irradiated by a pump, frequency ν_p, will spontaneously emit radiation at frequencies ν_s and ν_i such that the conservation of energy is obeyed. This effect has been predicted quantum mechanically but not classically [7, 8, 9]. However, it can be treated classically by considering the zero-point energy of the electromagnetic modes as providing an effective input field with an intensity equivalent to one photon per mode.

The starting values of the signal and idler fields were calculated by considering the parametric fluorescence within a single cavity mode. The spontaneously emitted power P_{sp} in an incremental frequency range $d\nu$ per signal mode is given by [4]

$$P_{sp} = \frac{4\pi^2 d_{eff}^2 hl}{n_s n_i n_p \varepsilon_o^3 \lambda_s^2 \lambda_i^2} P_p d\nu \qquad [4.6]$$

where h is Planck's constant, and l is the crystal length. The term $d\nu$ denotes the bandwidth of a single cavity mode and is given by

$$d\nu = \frac{FSR}{F} \qquad [4.7]$$

Since the FSR is inversely proportional to the cavity length L, increasing L results in a decrease in the spontaneously emitted power.

The parametric fluorescence power within any single cavity mode is approximately five orders of magnitude lower than the total fluorescence power across the full phase-matched bandwidth of KTP. As an example, for a pump power of 70mW, the parametric fluorescence power within any single cavity mode within the experimental configuration detailed below is $\sim 6 \times 10^{-16}$W. This value was used to derive the initial amplitude of the signal and the idler fields. However, it was found that changing the starting amplitudes of the signal and idler fields by 2 orders of magnitude resulted in only a 10% change in the build-up time of the modeled OPO output.

4.3 Experimental configuration

The experimental configuration used for this work is shown in figure 4.5. The OPO is based on a 6mm long KTP crystal, cut for near-degenerate, type-II, critical phase-matching. The plane front mirror of the resonating cavity is coated for high reflectivity at signal and idler wavelengths (99.8%) and 50% for the pump wavelength. The rear mirror has a radius of curvature of 10mm and is 99.5% reflective for the signal and idler wavelengths and 50% reflecting for the pump wavelength. The crystal was anti-reflection coated for the pump and output wavelengths, and mounted on a galvanometer to allow angle-tuning. The rear mirror was mounted on a piezoelectric transducer (PZT) to allow scanning of the cavity

length. The threshold pump power for this OPO configuration was found to be 30mW.

The pump source for the OPO is an all-solid-state, diode pumped, intracavity frequency-doubled Nd:YLF laser [10] which is capable of providing ~1W of green (523nm) single mode light. The output from the pump laser is mode-matched into the OPO cavity by a single 150mm focal length lens which gives a beam waist of ~30μm. The pump laser is isolated from back reflections from the OPO by a Faraday isolator which provides >30 dB attenuation.

As the cavity length is scanned, photodiodes allow both the transmitted pump and OPO output intensities to be recorded as a function of cavity length.

Configuration for the doubly-resonant OPO using KTP as the nonlinear material.

Figure 4.5

4.4 Comparison of experimental and modelled results

The observed output of the OPO was recorded for different scan rates of cavity length (see figure 4.7 –figure 4.9). It can be seen from the results that there is a sharp rise in intensity on the leading edges of each of the output pulses. This sharp rise in output power becomes more obvious as the scan rate is increased. In each case, the asymmetry in the pulses corresponds to a build-up time of the OPO of approximately one microsecond.

The graphs (figure 4.7 –figure 4.9) show that excellent agreement is obtained between the experimental observations and the numerical predictions. To allow direct comparison between the different scan rates these results were obtained for a simultaneous resonance of the signal and idler fields close to the centre of the broad resonance of the pump field (figure 4.6). However, equally good agreement was observed for all cases, irrespective of the detuning of the pump field off resonance. Further confirmation as to the accuracy of our numerical modelling was obtained with reference to the transmitted pump intensity as a function of cavity length, where excellent agreement between modelling and observation was again observed.

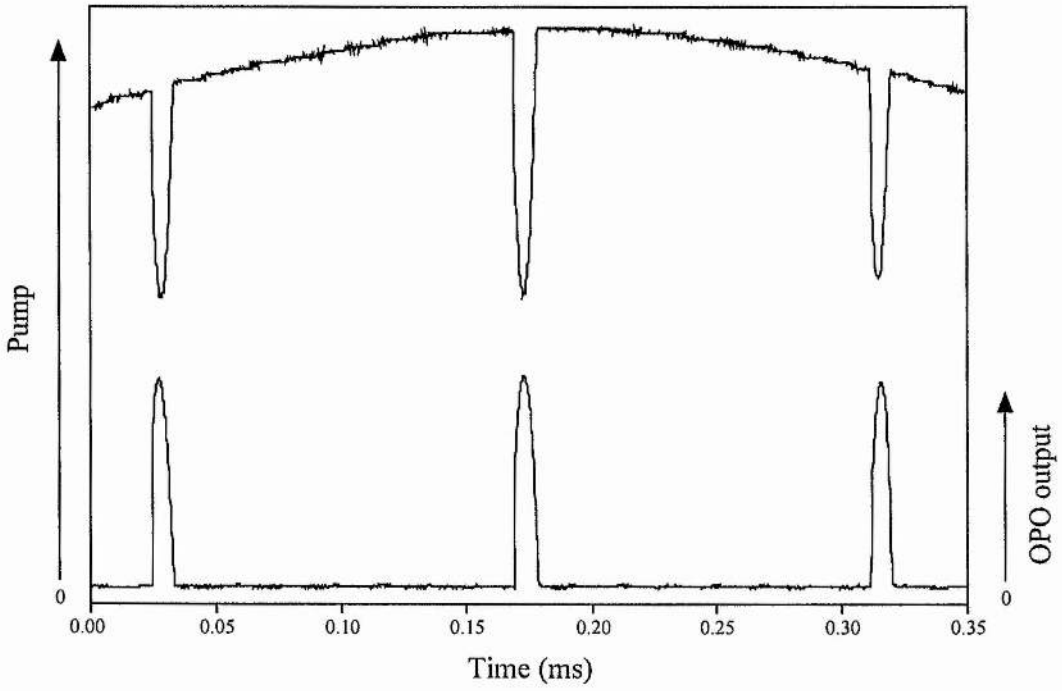

Figure 4.6 *Pump and OPO output intensities monitored when scanning cavity.*

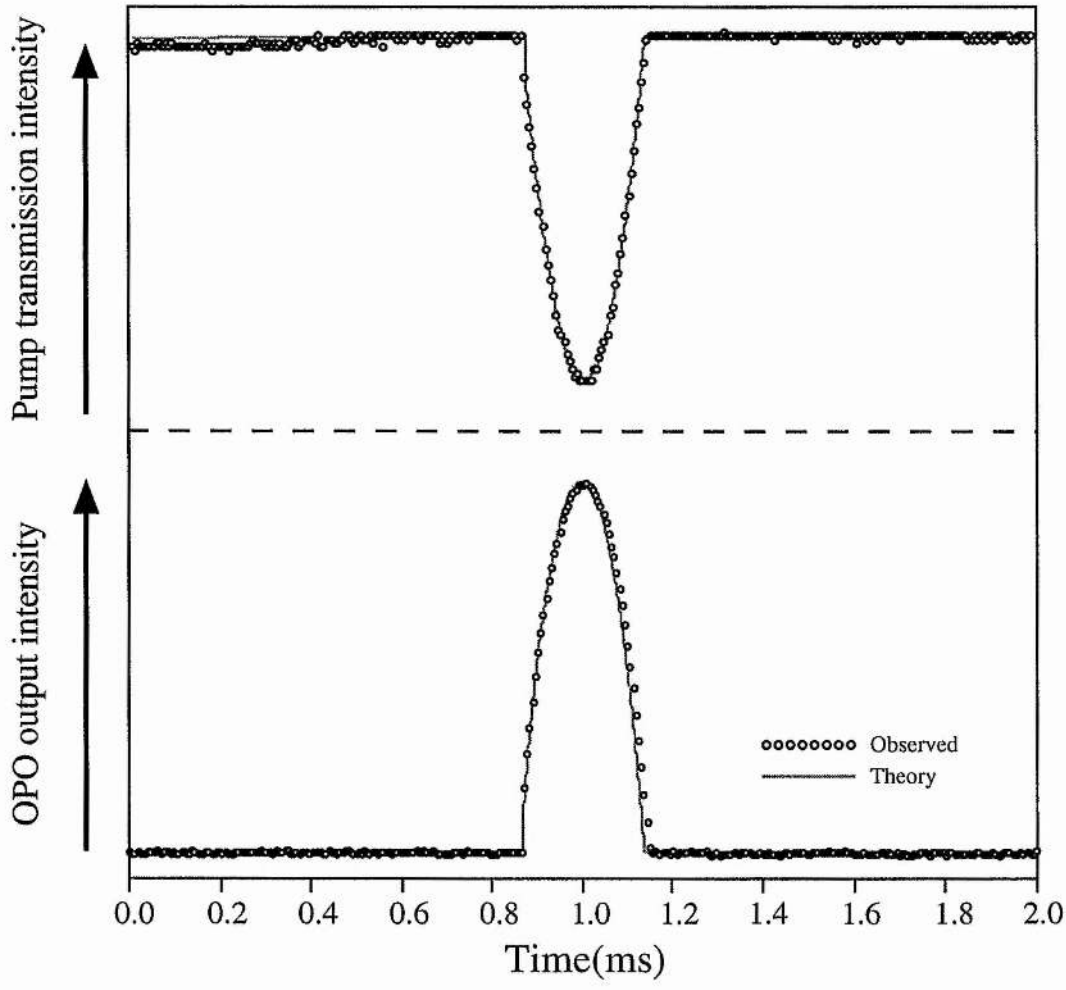

Figure 4.7 *Comparison of modelled and experimental results for slow scanning rate (1.6μm /sec). The modelled results are represented as a continuous trace and the experimental results are represented as discrete points.*

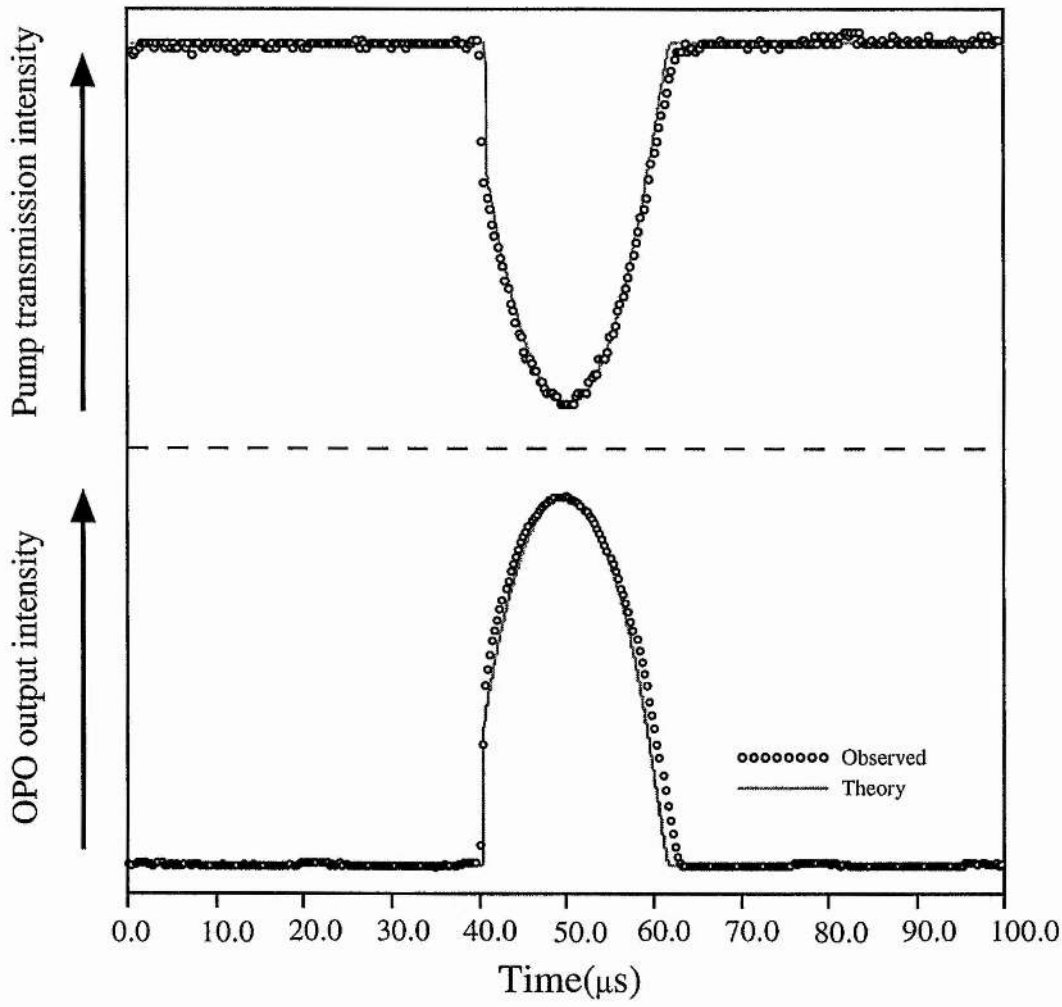

Figure 4.8 *Comparison of modelled and experimental results for medium scanning rate (20.6μm /sec). The modelled results are represented as a continuous trace and the experimental results are represented as discrete points.*

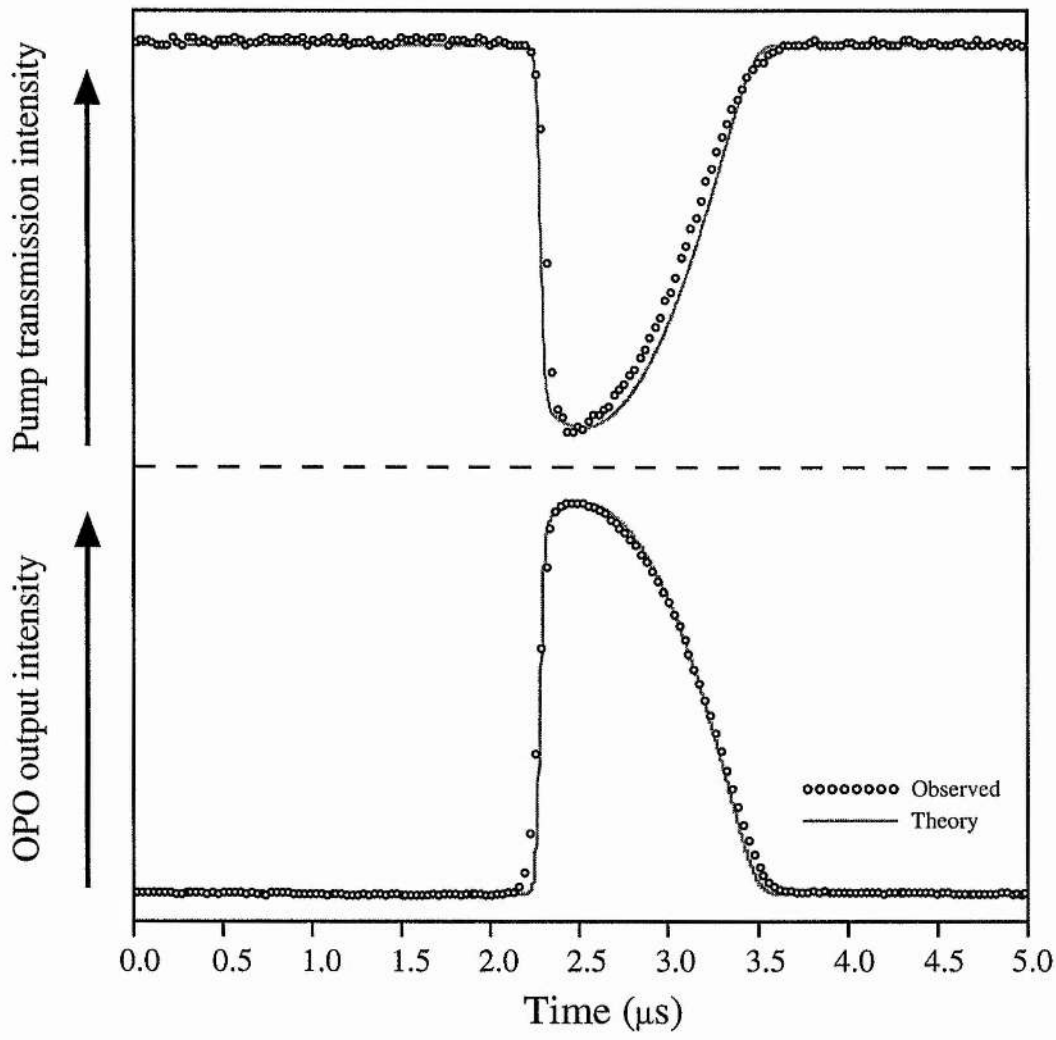

Figure 4.9 *Comparison of modelled and experimental results for fast scanning rate (278.5μm /sec). The modelled results are represented as a continuous trace and the experimental results are represented as discrete points.*

When the OPO is operating stably above threshold, a change in cavity length causes a change in the output level of the OPO. The time taken for the output to reach equilibrium after a step change in the cavity length is a measure of the response time of the OPO (see figure 4.10 below). The response time is found to be comparable to the build-up time of the OPO and effectively sets an upper bandwidth limit to any servo system for frequency or intensity stabilisation of the OPO output.

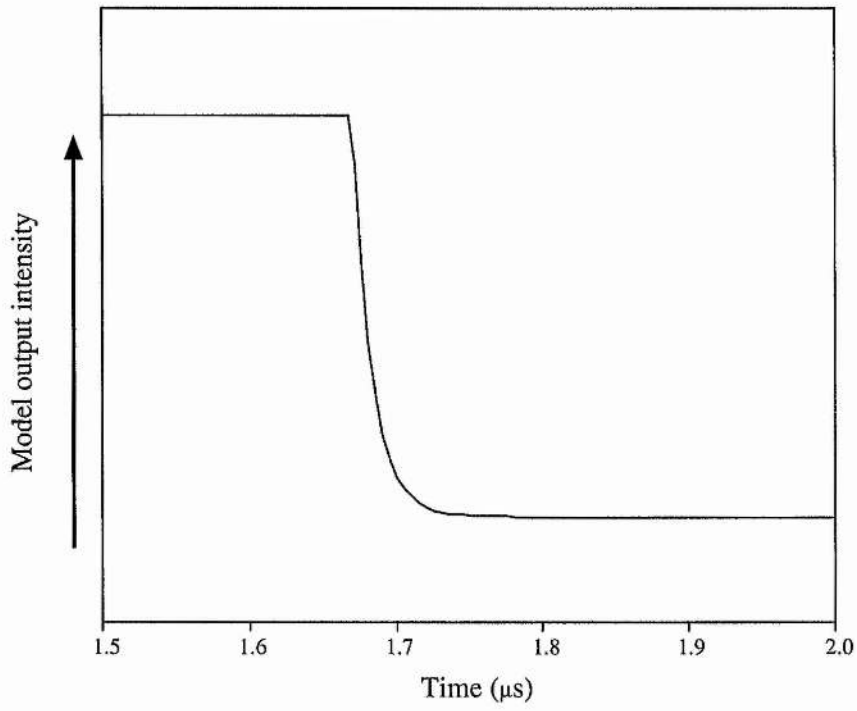

Figure 4.10 *Modelled OPO response to an instantaneous, but small, change in the cavity length. Change in cavity length is ~0.5nm. The graph shows that the OPO reaches its new steady state output power in approx. one tenth of a microsecond.*

The validity of the computer model is established by its excellent agreement with experimental observations. The model was used to explore how the dynamic behaviour of the DRO is influenced by the various design parameters. Starting with design specifications corresponding to the system detailed in the previous section, the roles of cavity length, pump level, cavity Finesse and the strength of the nonlinear interaction were investigated. To ensure a representative comparison for changing the various parameters, the model was used to find the cavity scan rate which reduced the time averaged output power of the OPO by half.

Figure 4.11 below shows a graph of the critical scan rate, as a function of cavity length for various Finesses for the signal and idler fields, with a pumping level 1.75 times threshold. It should be noted that the beam waist diameter is the same for each cavity length.

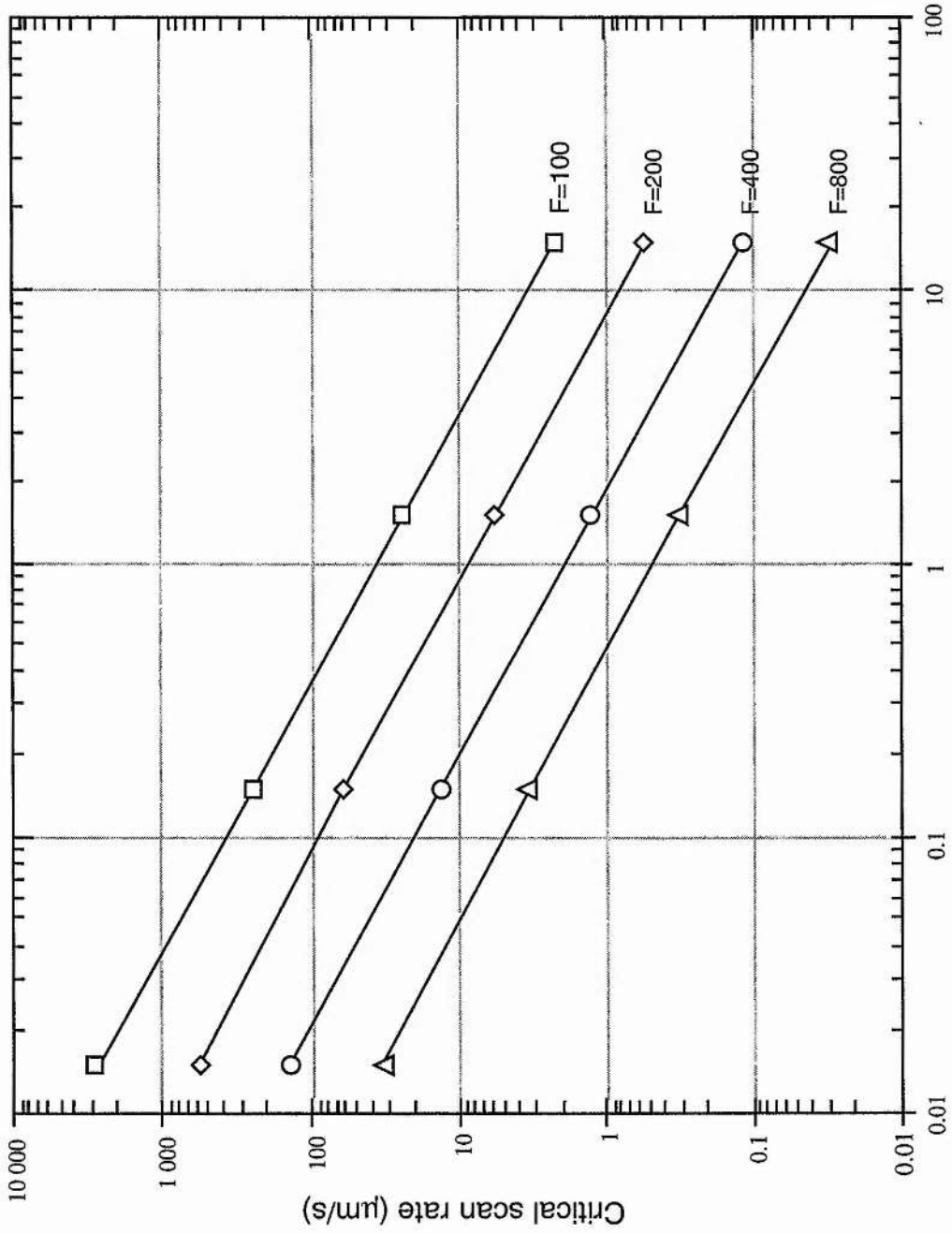

Critical scan rate as a function of cavity length for various Finesses for the signal and idler fields.

Figure 4.11

For long, high-Finesse cavities, residual mechanical noise leading to continual fluctuations in cavity length may effectively prevent the OPO from reaching threshold. This suggests that the use of long cavity DRO's, e.g. for the detection of gravity waves [11], may require sophisticated cavity stabilisation techniques in order to initiate the OPO output. For a constant pumping factor above threshold, the critical scan rate is inversely proportional to the cavity length and inversely proportional to the square of the cavity finesse but independent of the magnitude of the nonlinearity. This is to be expected since the nonlinear gain within the OPO is proportional to both the nonlinearity itself and the intensity of the pump, which for a constant pump factor scales inversely with the nonlinearity.

Pumping further above threshold results in a shorter build-up time for the OPO output. Pumping twice as hard above threshold, approximately halves the build-up time of the OPO.

4.5 Summary and conclusions

A numerical model that describes the dynamic behaviour of a DRO has been developed. As the cavity is scanned in and out of simultaneous resonance of the signal and idler fields, the model correctly predicts the delayed switch on of the OPO output after threshold is achieved. The modelled results are in excellent agreement with the experimental observations and can totally be accounted for in terms of the build-up time from the parametric fluorescence which arises from the background pumping level.

From the computer model it is established that, for a constant pumping factor above threshold, the scan-rate which reduces the time averaged output power of the DRO OPO by half is inversely proportional to the length of the optical cavity, inversely proportional to the square of the cavity finesse and independent of the nonlinear coefficient. For long cavities with high Finesse for the signal and idler fields, mechanical instabilities in cavity length may prevent the OPO from reaching threshold.

4.6 References

[1] D. Lee and N. C. Wong, *J. Opt. Soc. Am. B* **10**, 9, 1659 (1993).

[2] R. C. Eckardt, C. D. Nabors, W. J. Kozlovsky and R. L. Byer, *J. Opt. Soc. Am. B* **8**, 3, 646 (1991).

[3] C. Richy, K. I. Petsas, E. Giacobino, C. Fabre and L. Lugiato, *J. Opt. Soc. Am. B* **12**, 3, 456 (1995).

[4] S. E. Harris, M. K. Oshman and R. L. Byer, *Phys. Rev. Lett.* **18**, 18, 732 (1967).

[5] T. Debuisschert, A. Sizmann, E. Giacobino and C. Fabre, *J. Opt. Soc. Am. B* **10**, 9, 1668 (1993).

[6] A. Yariv, *"Quantum Electronics," 3rd ed., Wiley, New York*, (1989).

[7] W. H. Louisell, A. Yariv and A. E. Siegman, *Phys. Rev.* **124**, 1646 (1961).

[8] J. P. Gordon, W. H. Louisell and L. R. Walker, *Phys. Rev.* **129**, 481 (1963).

[9] W. G. Wagner and R. W. Hellwarth, *Phys. Rev.* **133**, A915 (1964).

[10] A. J. Henderson, M. J. Padgett, J. Zhang, W. Sibbett and M. H. Dunn, *Optics Lett.* **20**, 9, 1029 (1995).

[11] N. C. Wong, *Phys. Rev. A* **45**, 5, 3176 (1992).

5 The application of a continuously-tunable, cw, optical parametric oscillator for high resolution spectroscopy.

5.1 Introduction

For many years OPOs configured as short pulsed devices have been widely accepted as sources of tunable coherent light. However, despite their first demonstration in the 1960s, [1, 2] cw OPOs have still to achieve the same level of acceptance. In the case of the DRO the extremely stringent conditions for maintaining the double resonance has given DROs the reputation of being devices that are difficult to control and with undesirable tuning characteristics. In this chapter it is shown that when the DRO is successfully stabilised by means of a cavity length servo system the above restriction becomes a significant advantage, making the DRO strongly frequency selective. This frequency selective property allows the output frequencies to be tuned over the phase-matched bandwidth, typically 0.5THz, without the need for intracavity frequency selective components. This configuration provides the unique combination of pump power thresholds of 10's of milliwatts and continuous tuning ranges of 10's of GHz.

Advances in pump lasers [3] and the improved efficiency of new non-linear materials [3, 4] has allowed various other designs of CW OPOs to be investigated. Dual cavity designs were proposed [5] and implemented [6] which eases the requirement for simultaneous resonance of the signal and idler frequencies. However, to date, they have only delivered limited tuning ranges of less than 1GHz [6, 7]. Similarly,

birefringence within the non-linear material itself allows limited independent tuning of the signal and idler cavity modes [8].

With very high pump powers or highly efficient non-linear materials it is possible to design a cw OPO for which threshold can be achieved with feedback for only one or other of the signal and idler fields. These singly resonant oscillators (SROs) are much simpler to tune since only one field is resonant in the OPO cavity. However, a cw SRO reported in 1993 [9], based on KTP, still had a pump power threshold well in excess of 1watt. Introducing feedback at the pump frequency [10, 11] or mounting the OPO intracavity [12] allows the threshold of an SRO to be reduced, but not to the same extent as in a true DRO (signal & idler resonant).

More recently, there has been much interest in materials for highly efficient quasi-phase-matched frequency conversion. The recent demonstrations of cw operation from SROs based on periodically poled lithium niobate (PPLN) represent a significant step in the development of devices suitable for high-resolution laser spectroscopy [13, 11]. However, despite their reduced pump power threshold (still $\approx$ 1 Watt), problems do exist in regard to producing single-frequency tunable output. Particularly when pumped in the visible region of the spectrum, photo-refractive damage [14], extremely rapid temperature tuning [15] and thermal lensing [16] make the design and operation of a reliable device difficult. To date, the maximum reported smooth tuning of the output frequency from a PPLN device has only been 2GHz [11]. Consequently, it may be that in many applications an OPO based on a bulk crystal, configured as a DRO with some method for tuning the output frequencies may represent the optimum design choice.

5.2 Frequency selective properties of a stabilised DRO

Several authors have discussed the tuning behaviour of DRO OPOs [8, 17]. Once oscillating on a particular pair of signal and idler modes a small change in cavity length or pump frequency of a few nanometers or megahertz respectively leads to the OPO output switching to different modes. For a DRO formed within a high Finesse cavity, the condition for simultaneous resonance of the signal and idlers fields is extremely stringent. When $FSR_{average}/\Delta FSR$ for the signal and idler fields exceeds the cavity Finesse (as is usually the case for Type-II phase-matching), in general no simultaneous resonances fall within the phase-matched bandwidth of the device. This dictates that the cavity length of the OPO needs to be scanned to find a simultaneous resonance and then precisely controlled if the OPO is to be maintained above threshold. However, in terms of subsequent output tuning this restriction is a significant advantage since it ensures the OPO output will comprise of only a single pair of signal and idler modes. Tuning the pump source while servo controlling the cavity length of the OPO to maintain the simultaneous resonance ensures smooth tuning of the OPO output frequencies without mode-hops [18]. The spectral window over which the OPO can be scanned is limited by the tuning range of the pump laser. However, the subsequent selection of a neighbouring pair of signal and idler modes allows many such adjacent windows to be scanned, allowing a full spectrum to be accumulated.

In contrast, for an SRO, the frequency of the resonant wave is that of the cavity mode that lies closest to optimum phase-matching. In the absence of any intra-cavity tuning elements one might expect the tuning range to be limited to one *FSR* of the OPO cavity. It has more recently been proposed that, in practice, the back conversion inherent within the non-linear process may suppress competing modes leading to a tuning range that exceeds the *FSR* of the OPO cavity. However, to date, these so called "striction" effects have not been demonstrated experimentally and no cw SRO has been tuned in excess of 2GHz [11].

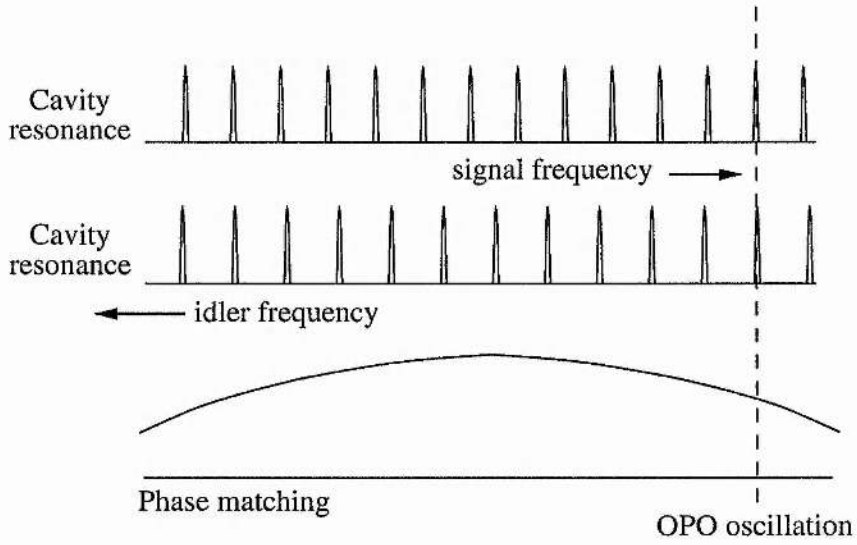

Figure 5.1 *DRO-OPO can be locked to any pair of signal and idler modes within the phase-matching bandwidth.*

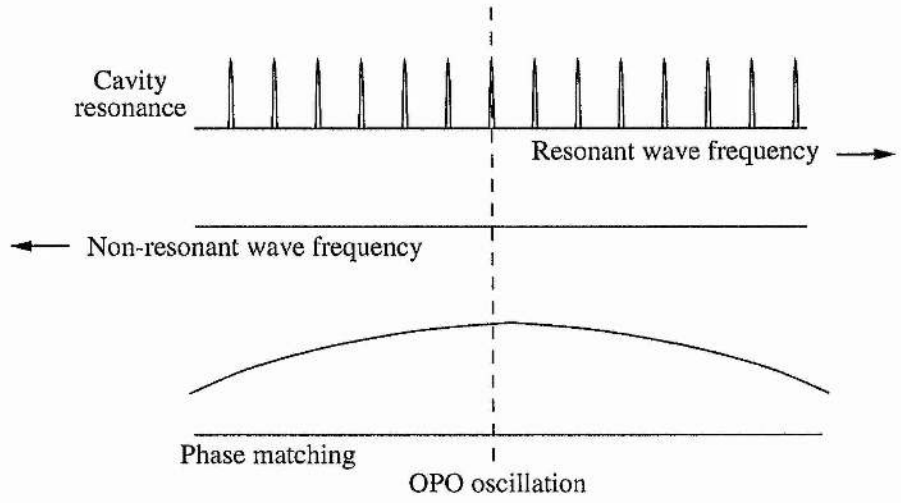

Figure 5.2 *SRO-OPO operates on the resonant mode closest to optimum phase-matching condition.*

5.3 Experimental configuration

The OPO used in this work is similar in design to one reported earlier [19] and is based on a 6mm long KTP crystal cut for near-degenerate, critical, type-II, phase matching for a pump wavelength of 523nm. The doubly resonant 10mm long cavity has a free spectral range (FSR) of approximately 9GHz and finesse for the signal and idler fields in excess of 200. The mirror curvatures are calculated to give a waist size of 40μm. The DRO configuration reduces the pump power threshold to only 30mW. Angle tuning the KTP crystal gives course tuning of the signal and idler outputs over approximately 100nm in the 1μm spectral region. Once the course tuning has been set to the spectral region of interest, a simple servo system controls the cavity length maintaining a constant output power and hence holding the oscillation to a specific pair of signal and idler cavity modes. Tuning the pump frequency and relying on the

servo system to maintain the OPO operating on the specific mode pair allows the signal and idler frequencies to be tuned smoothly.

The pump laser is an all-solid-state, frequency-doubled Nd:YLF laser with an output at 523nm of several 100's mW. The Nd:YLF crystal is coated to provide one of the mirrors of the standing wave cavity. The combination of spatial hole-burning in the gain medium, coupled with the KTP intra-cavity frequency doubling crystal acting as a birefringent filter ensures operation on a single longitudinal mode. In addition, by piezoelectric control of the cavity length the output frequency can be smoothly tuned over ~10GHz without the need for additional frequency selective components. (Figure 5.3 shows the configuration of the OPO and pump source).

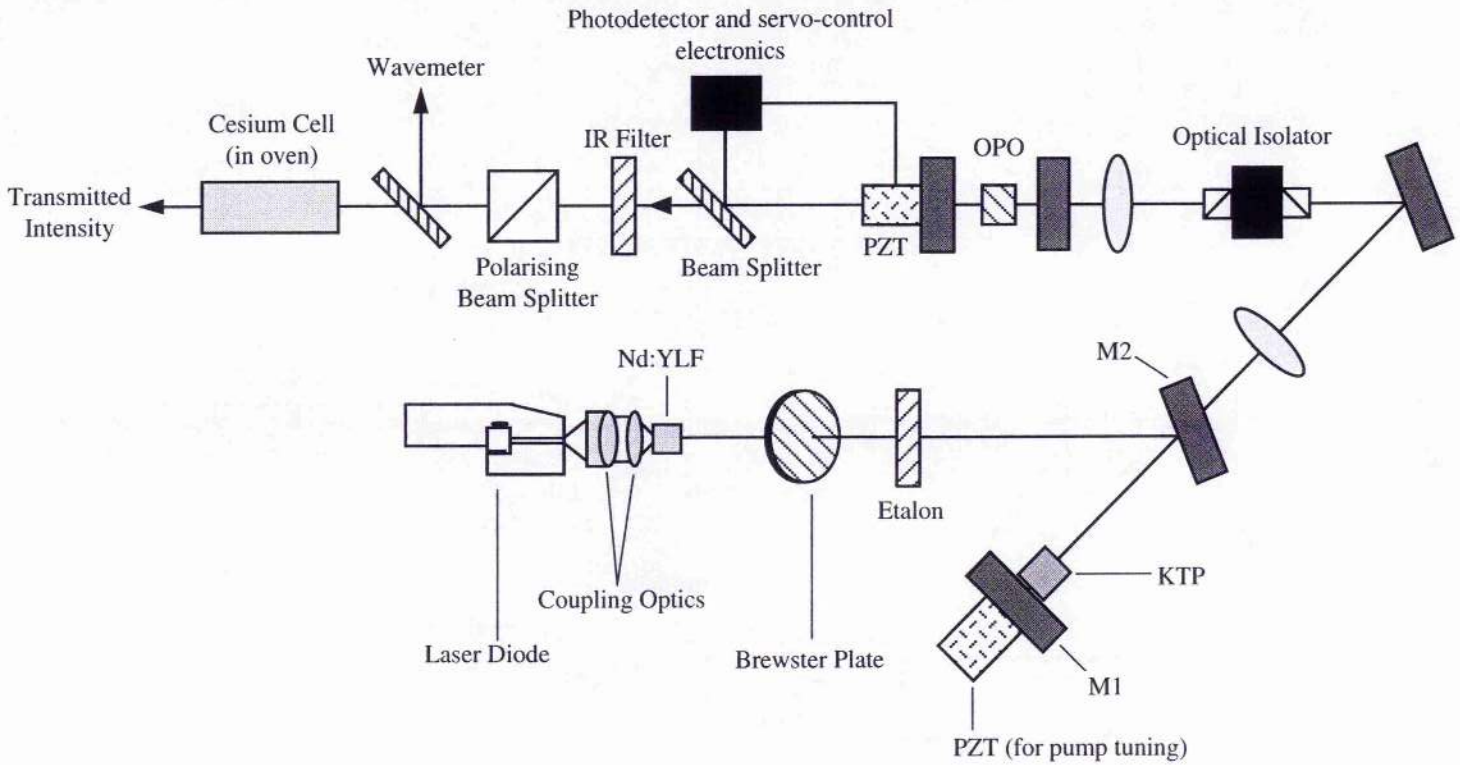

Figure 5.3

All solid state OPO. Smooth tuning of the pump laser, over ~10GHz, is achieved by piezoelectric control of its cavity length.

For near degenerate operation of the OPO the 10GHz of pump tuning yields 5GHz of tuning for both the signal and idler fields.

For a DRO the linewidth and frequency stability of both the signal and idler fields corresponds exactly to that of the pump source. By contrast for an SRO, the frequency of the resonant wave matches that of the cavity mode and any small changes in pump frequency are imposed on the non-resonant wave. Similarly, for a DRO perturbations in cavity length do not, to first order, perturb the signal and idler frequencies. Consequently, given a highly stable pump source a DRO guarantees that the high degree of spectral purity will be transferred to the OPO output.

Within the OPO configuration described above the phase-matched bandwidth corresponds to approximately 500 GHz. Servo control of the cavity length allows the OPO to be locked to any pair of signal and idler modes within this phase-matching bandwidth and tuning of the pump frequency results in tuning of the OPO without any evidence of further mode hopping. The nature of the servo control system is such that the cavity is always scanned in the same direction to find the next simultaneous resonance. This allows the OPO output frequencies to be tuned in steps equal to the FSR of the OPO cavity. Figure 5.4 shows the frequency of the signal field corresponding to the OPO being locked to successive pairs of signal and idler modes which fall within the phase-matched bandwidth.

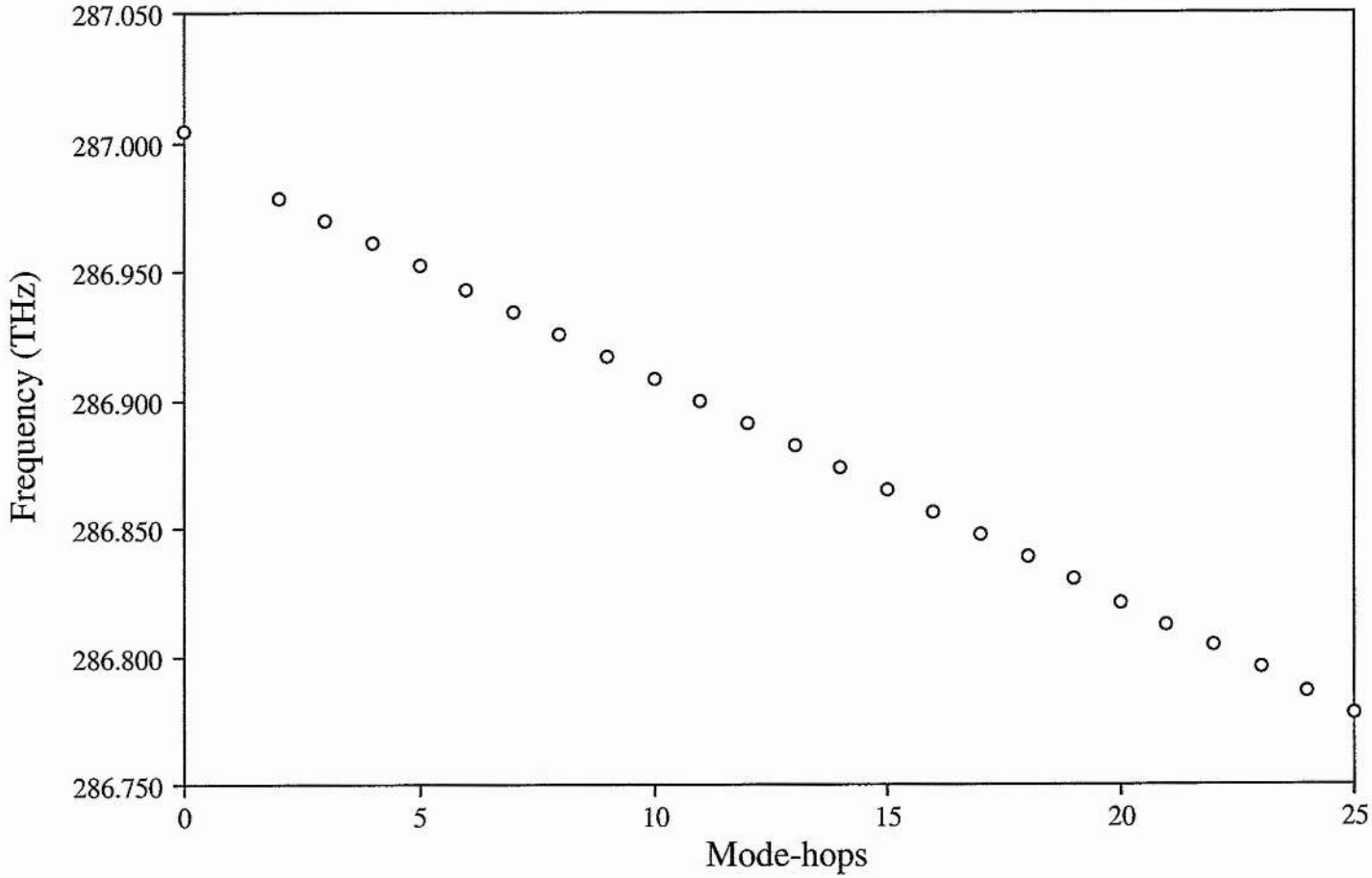

Figure 5.4

Frequency of the signal field corresponding to the OPO being locked to successive pairs of signal and idler modes which fall within the phase-matched bandwidth. Figure shows tuning over 220 GHz by 25 successive mode-hops. Successive mode-hops are achieved by applying small perturbations to the OPO cavity length.

To move from one pair of signal and idler modes to the next requires a cavity length change of ~8nm. With the servo lock on, it was found that a light tap applied to one of the mirrors was sufficient for the OPO to reliably hop from one mode-pair to an adjacent one. In this way, the signal frequency of the OPO was reliably tuned over 220GHz by 25 successive mode-hops. The smooth tuning range of the OPO can be centred on any of these mode pairs and is limited only by the smooth tuning range of the pump laser. This demonstrates that the OPO can be stabilised to any frequency within the phase-matched bandwidth without the need for additional intracavity frequency selective components. The elimination of intracavity components is a key advantage within a DRO since the pump power threshold is proportional to the square of the round trip losses. Continuous tuning across the phase-matched bandwidth can be achieved by smooth tuning the OPO over a range greater than the FSR. Recently mode-hop-free tuning of a suitable pump laser by 40GHz has been reported [20]. This would give approximately 20GHz of smooth tuning of the OPO output which is sufficient to bridge the gap between adjacent mode pairs of the OPO without the need for further adjustment. Given a pump source of increased tuning range the tuning range associated with any mode pair could be extended across the phase-matching bandwidth of the non-linear process.

The practicality of the OPO was demonstrated by recording the absorption spectrum of the cesium molecule (Cs_2) in the 1μm spectral region. A 75mm long cell containing cesium with a purity of 99.95% was heated to 320°C giving a vapour pressure of 3.1 mm Hg. This was sufficient to give ~60% absorption of the strongest lines. The pump frequency was scanned by applying a high voltage signal to the piezoelectric translator. A maximum pump frequency scanning range of

12GHz was achieved which resulted in a 6GHz scan of the OPO output frequency (see figure 5.5).

Figure 5.5 *Transmission spectrum of cesium vapour in the 1μm spectral region*

A tuning range of 4GHz of the OPO output frequency was reliably achieved by scanning the pump frequency over 8GHz. This 4GHz scan was centred at different locations within the phase-matching bandwidth by a combination of angle tuning and mode-hops. The repeatability of the system was demonstrated by overlapping adjacent regions of the absorption spectra of molecular cesium. The transmitted OPO power is recorded as a function of frequency using a photodiode (see Figure

5.6) and the location of each spectral region is set using a wavemeter based on a combination of Fizeau wedges and etalons (Burleigh 4500) [21].

Absorption spectra of cesium vapour at 1050 nm. Each spectrum covers a 4-GHz scanning range; the spectra overlap to form a continuous spectrum.

Figure 5.6

5.4 Summary and conclusions

A smoothly-tunable, single-frequency, cw, DRO has been demonstrated in the application of high-resolution spectroscopy. It was shown that the strong frequency selective nature of the DRO ensures operation on a single mode pair and allows the output to be tuned across the phase-matched bandwidth. Smooth tuning of the OPO output over a spectral window is achieved by smoothly tuning the pump source while simultaneously servo controlling the cavity length. The subsequent selection of a neighbouring pair of signal and idler modes allows many such adjacent windows to be scanned, allowing a full spectrum to be accumulated. The practicality of this approach was demonstrated by using the OPO system to record the transmission spectra of cesium vapour in the 1μm spectral region. The combination of low pump power threshold, single mode-pair operation, and simple OPO design provides the opportunity of developing compact tunable sources for spectroscopy.

5.5 References

[1] R. G. Smith, J. E. Geusic, H. J. Levinstein, J. J. Rubin, S. Singh and V.Uitert, *Appl. Phys. Lett.* **12**, 9, 308. (1968).

[2] R. L. Byer, M. K. Oshman, J. F. Young and S. E. Harris, *Appl. Phys. Lett.* **13**, 3, 109 (1968).

[3] C. D. Nabors, R. C. Eckardt, W. J. Kozlovsky and R. L. Byer, *Optics Lett.* **14**, 20, 1134 (1989).

[4] F. G. Colville, A. J. Henderson, M. J. Padgett, J. Zhang and M. H. Dunn, *Optics Lett.* **18**, 3, 205 (1993).

[5] N. C. Wong, *Phys. Rev. A* **45**, 5, 3176 (1992).

[6] F. G. Colville, M. J. Padgett and M. H. Dunn, *Appl. Phys. Lett* **64**, 12, 1490 (1994).

[7] D. Lee and N. C. Wong, *Conference on Lasers and Electro-Optics (CLEO) (OSA Technical Digest Series)* **8**, CWE5, 200 (1994).

[8] D. Lee and N. C. Wong, *J. Opt. Soc. Am. B* **10**, 9, 1659 (1993).

[9] S. T. Yang, R. C. Eckardt and R. L. Byer, *Optics Lett.* **18**, 12, 971 (1993).

[10] G. Robertson, M. J. Padgett and M. H. Dunn, *Optics Lett.* **19**, 21, 1735 (1994).

[11] K. Schneider, P. Kramper, S. Schiller and J. Mlynek, *Optics Lett.* **22**, 17, 1293 (1997).

[12] F. G. Colville, M. H. Dunn and M. Ebrahimzadeh, *Optics Lett.* **22**, 2, 75 (1997).

[13] W. R. Bosenberg, A. Drobshoff, J. I. Alexander, L. E. Myers and R. L. Byer, *Optics Lett.* **21**, 10, 713 (1996).

[14] L. E. Myers, R. C. Eckardt, M. M. Fejer, R. L. Byer, W. R. Bosenberg and J. W. Pierce, *J. Opt. Soc. Am. B* **12**, 11, 2102 (1995).

[15] G. J. Edwards and M. Lawrence, *Opt. Quant. Elect.* **16**, 373 (1983).

[16] G. A. Turnbull, T. J. Edwards, M. H. Dunn and M. Ebrahimzadeh, *Electron. Lett.* **33**, 21, 1817 (1997).

[17] R. C. Eckardt, C. D. Nabors, W. J. Kozlovsky and R. L. Byer, *J. Opt. Soc. Am. B* **8**, 3, 646 (1991).

[18] A. J. Henderson, M. J. Padgett, J. Zhang, W. Sibbett and M. H. Dunn, *Optics Lett.* **20**, 9, 1029 (1995).

[19] A. J. Henderson, M. J. Padgett, F. G. Colville, J. Zhang and M. H. Dunn, *Optics Comm.* **119**, 256 (1995).

[20] P. J. Hardman, W. A. Clarkson, K. I. Martin, S. D. Butterworth and D. C. Hanna, *Conference on Lasers and Electro-Optics (CLEO), OSA Technical Digest Series.* **11**, CFO3, 520 (1997).

[21] Burleigh, *Burleigh Instruments, Inc., Burleigh Park, Fishers, N.Y. 14453.*

6 Microchip laser pumped cw doubly resonant OPO

The work detailed in this chapter was carried out in collaboration with Richard Conroy and the Microchip Laser Group at the University of St. Andrews.

6.1 Introduction

Cw OPO's traditionally require high intensity pump sources that operate on a single transverse and longitudinal mode. However, such pump lasers are usually several 100's mm in length and incorporate intracavity elements to ensure single mode operation. This chapter describes the use an ultra-compact, frequency-doubled, microchip laser as the pump source for a cw OPO. Despite the multi-longitudinal mode output of the pump laser the frequency selectivity inherent in a DRO, as discussed in chapter 5, results in the output being held to a single-pair of signal and idler modes.

It has been shown previously that frequency doubled microchip lasers, based on a sandwich of Nd:YVO_4 and KTP, are efficient sources of green light [1]. Their compact size and inherent ability to operate in near single transverse and longitudinal modes make them ideal sources for low power applications for which laser diodes have insufficient mode quality. Passively Q-switched microchip lasers have been successfully used to pump a KTP DRO [2]. This chapter reports the first cw

operation of an OPO pumped by a frequency-doubled microchip laser. Single mode-pair operation of the OPO was achieved even when pumped by a multi-longitudinal mode laser.

6.2 Experimental configuration

The pump laser was composed of a sandwich of 3% doped Nd:YVO_4 (3x3x0.5mm) and KTP (5x5x2mm), with the external faces coated for high reflection (~99.97%) at 1064nm and transmissive at 532nm. This sandwich was mounted on a temperature-controlled mount and pumped by a 1.2W laser diode at 810nm. No attempt was made to double pass the pump. This set-up produced 92mW of power in a nearly single longitudinal, single transverse, mode, as much as 186mW of power in a single transverse mode, and as much as 220mW of power in a multi-transverse mode. Less than 10mW of residual 1064nm power was produced. The overall conversion efficiency from diode pump to green power was 40% of which 20% was produced in the forward direction. Figure 6.1 shows the configuration of the microchip laser.

There was no active locking of the frequency of the laser to maintain the frequency spectrum of the output, other than through temperature control of the mount. Back reflections from the OPO, resulting in intensity and frequency instabilities in the pump laser, were suppressed using an optical isolator. The frequency stability of the green laser was measured to be ~50MHz over several minutes with a short-term linewidth less than 300kHz. The intensity stability of the pump laser was better than

3% peak-to-peak. These stability measurements are believed to be determined by the small fluctuations in the diode pump power and changes in the environment surrounding the microchip. There was no significant "green noise" [3] observed. The frequency output of the microchip laser could be smoothly tuned by controlling the temperature of the thermoelectric mount.

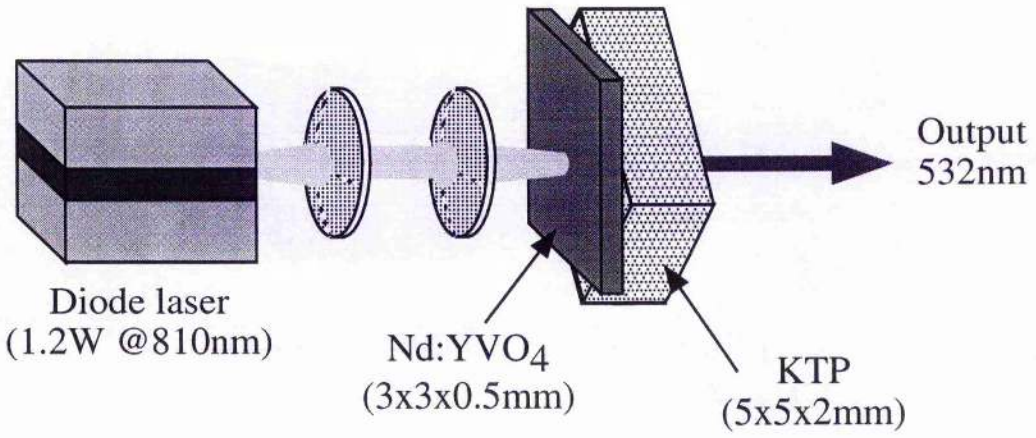

Figure 6.1 *Frequency Doubled Microchip Laser. Based on sandwich of Nd:YVO4 & KTP (External faces coated HR@1064nm and HT@532nm).*

Until recently, threshold considerations have meant that most cw OPO's have been configured as DRO's where both the signal and idler fields are resonated in the cavity. Even when using the latest nonlinear materials, singly resonant oscillators (SRO's) still require pump powers of many watts for efficient operation [4], reducing to ~1W for pump enhanced systems [5]. Such pump powers are well outside the

capabilities of a microchip laser. By contrast DRO's have been built with pump power thresholds of a few 10's mW [6] or lower [7, 8].

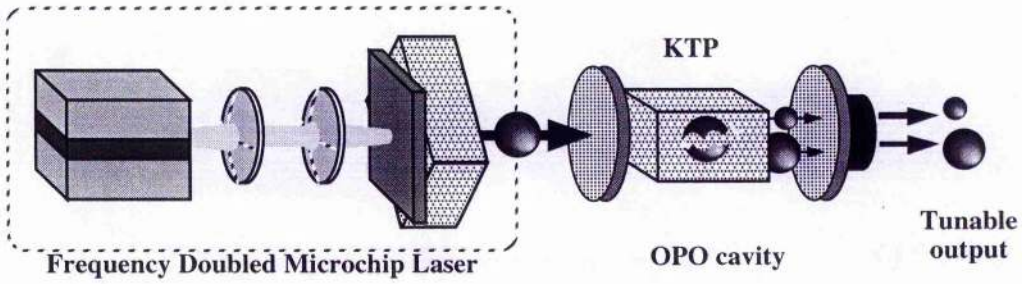

Figure 6.2 *Frequency Doubled Microchip Laser used as a pump source for a cw OPO.*

As discussed in chapter 5 the extremely stringent conditions for maintaining the double resonance in the DRO is an advantage in producing single mode-pair output. Once stabilised the DRO operates on a single mode-pair without intracavity frequency selective components [9]. This allows the demonstration of an OPO which has the combination of good frequency selection while maintaining a very low pump power threshold.

In this work the DRO was successfully stabilised by means of a cavity length servo system maintaining a constant output power and hence holding the OPO to a single signal and idler mode pair. Smooth tuning of the pump source while servo

controlling the cavity length, to maintain constant output power, resulted in the smooth tuning of the OPO output frequencies [10]. Figure 6.3 shows the experimental configuration of the pump laser and OPO.

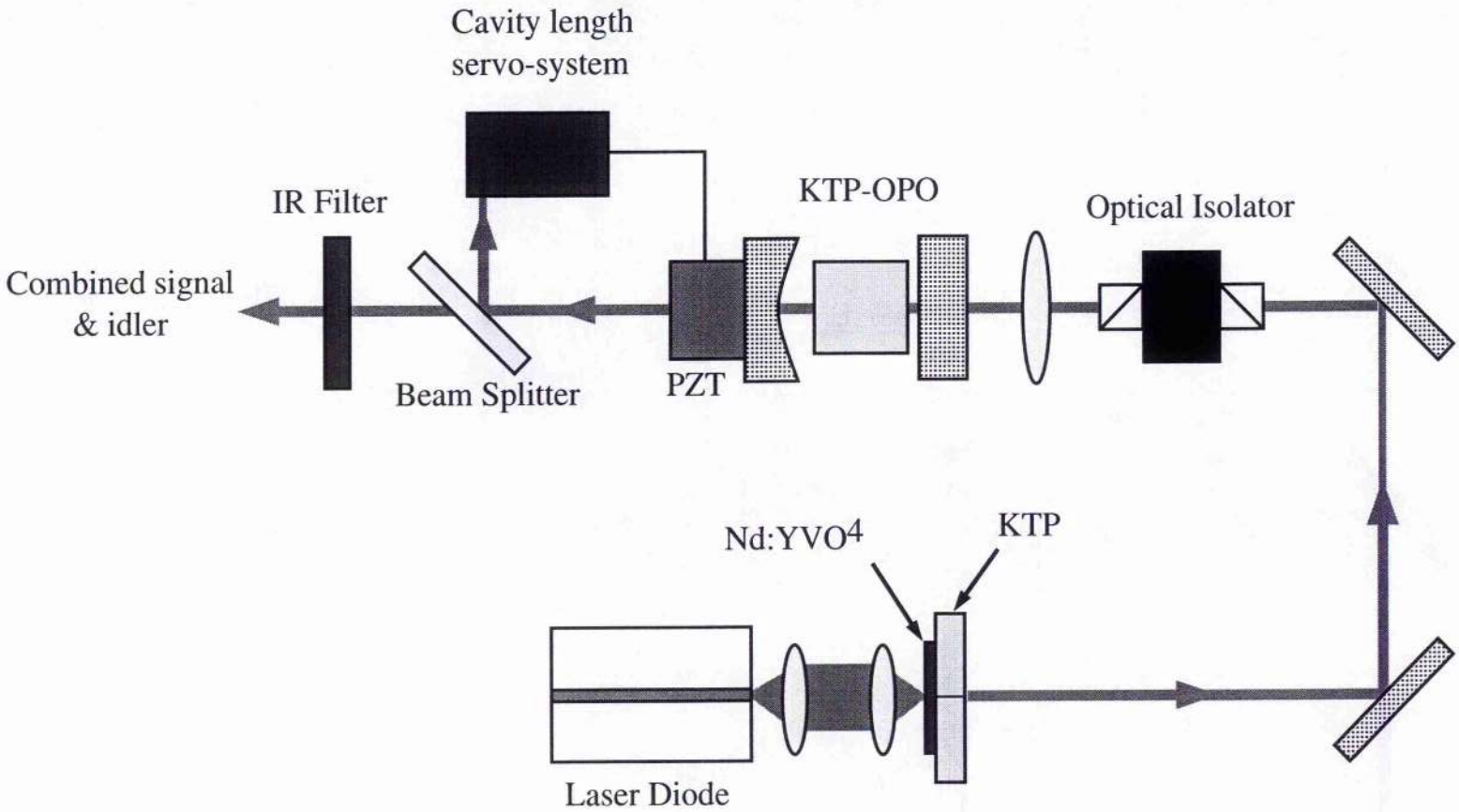

Figure 6.3

Experimental configuration of microchip pump source and doubly resonant OPO. A simple cavity length servo system holds the OPO on a single pair of signal and idler modes. This mode-pair was smoothly tuned over 1.7 GHz by temperature tuning the microchip laser while simultaneously servo controlling the cavity length.

The experimental configuration of the OPO used in this work was similar to that reported in ref. [6] and was based on a 6mm long KTP crystal cut for near-degenerate, critical, type-II, phase matching. The mirrors used were highly-reflecting at both the signal and idler wavelengths, thus forming a doubly resonant oscillator, and their curvatures calculated to give a beam waist of only 40μm at the centre of the crystal. The resulting threshold of our OPO varied between 35mW and 120mW depending on the number of longitudinal modes oscillating within the pump laser. In all cases, however, the strong frequency selectivity of our the DRO ensured that the output of the OPO was a single pair of signal and idler modes (figure 6.4). With the OPO stabilised in this way, a combined signal and idler output power of 10mW was obtained, with an intensity modulation of ~8% at kilohertz frequencies. By temperature tuning the pump laser, while servo controlling the cavity length of the OPO, the output frequencies were smoothly tuned over 1.7GHz. This was limited only by the tuning range of the pump laser. The doubly resonant nature of the DRO eliminates cavity length related frequency drifts [6] hence the linewidth of the OPO is expected to be that of the pump source (in this case, better than 300kHz).

Output of OPO consists of a single pair of signal and idler modes when pumped by a multi-longitudinal mode pump laser. Observed with a Fabry-Perot interferometer.

Figure 6.4

6.3 Summary and conclusions

In summary, a pump laser operating on several longitudinal modes was used to pump a doubly resonant OPO operating on a single pair of signal and idler modes. The OPO operated successfully with both single and multiple longitudinal mode pumping, only suffering an increase in threshold. An output power of 10mW was obtained and smooth tuning over 1.7GHz was possible by temperature tuning the pump laser. This demonstration of the first cw operation of a DRO pumped by a green microchip laser shows that the microchip laser is an attractive source for developing compact sources of widely-tunable, coherent light. The microchip laser may prove to be an ideal pump source for DROs based on the latest nonlinear materials, having an even further reduction in threshold. The microchip laser concept could possibly be extended to develop a microchip device incorporating both pump laser and OPO within a single composite chip. This offers the technological opportunity of forming an ultra compact OPO device. To date, the most compact cavity design reported for an entire OPO system is that reported by Conroy et.al. [11].

6.4 References

[1] R. S. Conroy, A. Kemp, N. MacKinnon and B. D. Sinclair, *Conference on Lasers and Electro-Optics (CLEO), OSA Technical Digest Series* **11**, CFO6, 521 (1997).

[2] J. J. Zayhowski, *IEEE Photonics Technology Letters* **9**, 7, 925 (1997).

[3] T. Baer, *J. Opt. Soc. Am. B* **3**, 9, 1175 (1986).

[4] W. R. Bosenberg, A. Drobshoff, J. I. Alexander, L. E. Myers and R. L. Byer, *Optics Lett.* **21**, 10, 713 (1996).

[5] K. Schneider, P. Kramper, S. Schiller and J. Mlynek, *Optics Lett.* **22**, 17, 1293 (1997).

[6] A. J. Henderson, M. J. Padgett, F. G. Colville, J. Zhang and M. H. Dunn, *Optics Comm.* **119**, 256 (1995).

[7] C. D. Nabors, R. C. Eckardt, W. J. Kozlovsky and R. L. Byer, *Optics Lett.* **14**, 20, 1134 (1989).

[8] Peter Lichtenberg Hansen and P. Buchhave, *Optics Lett.* **22**, 14, 1074 (1997).

[9] G. M. Gibson, M. H. Dunn and M. J. Padgett, *Optics Lett.* **23**, 1, 40 (1998).

[10] A. J. Henderson, M. J. Padgett, J. Zhang, W. Sibbett and M. H. Dunn, *Optics Lett.* **20**, 9, 1029 (1995).

[11] R. S. Conroy, C. F. Rae, G. J. Friel, M. H. Dunn, and B. D. Sinclair, *Optics Lett.* **23**, 17, 1348 (1998).

7 Temperature tuned difference frequency mixing in periodically poled $KTiOPO_4$

The work detailed in this chapter was carried out in collaboration with Graham Turnbull at the University of St. Andrews.

7.1 Introduction

The use of periodically-poled materials for quasi-phase-matching (QPM) has recently had a considerable impact in the field of nonlinear optics [1]. QPM permits access to the highest nonlinear coefficients of a material (e.g. d_{33} in $LiNbO_3$, $KTiOPO_4$, $RbTiOAsO_4$), and hence can provide greater conversion efficiency than with traditional birefringent phase-matching. In addition, with suitable grating selection, essentially any wavelength combination within the transparency range of the material may be phase-matched in a non-critical geometry.

While the pioneering work into QPM focused principally on periodically-poled lithium niobate (PPLN), recently other materials, notably periodically-poled $KTiOPO_4$ (PPKTP) and its isomorphs, have been successfully developed. PPKTP has been demonstrated in the efficient frequency doubling of both pulsed and continuous-wave Nd:YAG lasers [2], [3] second-harmonic generation with simultaneous femtosecond pulse compression [4], and femtosecond OPOs for photon division [5]. In

cw applications periodically poled $RbTiOAsO_4$ (PPRTA) has been used in a singly resonant OPO [6].

Flux grown KTP, a now well established nonlinear optical material, has been successfully poled using millimetre thick samples [7]. KTP has the advantages of a higher laser damage threshold and higher resistance to photorefractive damage than PPLN. It has a coercive field ~10 times lower than that of $LiNbO_3$ which allows fine pitch gratings to be easily produced due to limited domain broadening during poling [7]. These properties, along with room temperature operation, make PPKTP an attractive alternative material to PPLN for a wide range of applications.

This chapter reports what is believed to be the first demonstration of difference-frequency generation (DFG) in PPKTP. Importantly, while conventional birefringent phase-matching in KTP is insensitive to crystal temperature QPM in KTP demonstrates a useful degree of temperature tuning. It can be shown from theory that the degree of temperature tunability varies with pump wavelength. Hence one can anticipate the application of PPKTP to widely temperature-tunable DFG and high average power OPOs.

7.2 Experimental configuration

The single-grating periodically poled crystal was fabricated by H. Karlsson and F. Laurell [8]. This crystal was prepared from a 9mm long x 1mm thick sample of flux grown KTP by patterning a photoresist grating with a period of $\Lambda = 9.55\mu m$ upon

the c- face. The sample was first ion-exchanged in 100% $RbNO_3$ on the c- side for 3.5 hours at 355°C prior to patterning, in order to create a low-conductive RTP layer at the surface where the domains can easily nucleate [7]. The sample was then poled by applying three 6 ms long pulses at 2.5kV. The electrodes were KCl on the c- side and a uniform Aluminium film on the c+ side. The poled interaction length of the crystal is 5mm with the end faces polished and left uncoated.

The experimental set up is as shown in figure 7.1. The PPKTP crystal was pumped by two collinear, continuous-wave laser beams, one at a fixed wavelength $\lambda_p = 523$nm, the other λ_s tunable around 760nm. The source at 523nm is an all-solid-state, diode-pumped, Nd:YLF laser with an intracavity KTP doubler giving an output power of a few hundred milliwatts.

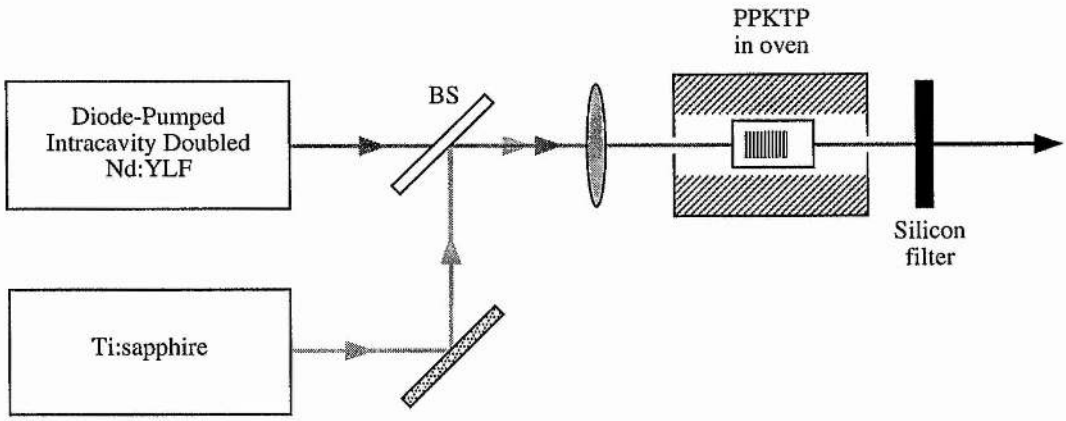

Figure 7.1 *Schematic of the experimental setup (BS, Beamsplitter).*

The tunable source is a Ti:sapphire laser configured as a standing-wave bow-tie resonator, and is itself pumped by an argon-ion laser. A three-plate birefringent tuner allows coarse tuning of the multi-axial-mode (~20GHz bandwidth) output from 750 to 850 nm. When operating around 760nm, the Ti:sapphire laser provides an output power of a few hundred milliwatts.

The two beams were combined using a dichroic coated beamsplitter which transmits the green light and reflects the red. The combined beams were then focused into the crystal using a single 50mm focal length lens, resulting in beam waists of 11.5μm and 16.9μm for the green and red beams respectively. The PPKTP was mounted in a temperature controlled oven which could vary the crystal temperature from room temperature to over 100°C.

Figure 7.2 shows the tuning range of the generated wavelength as the PPKTP crystal temperature is varied over a range of 80°C, while simultaneously tuning the Ti:sapphire wavelength to maintain optimum conversion. Over this temperature range the Ti:sapphire wavelength is varied from 767nm to 755nm, corresponding to a DFG wavelength λ_i variation of 1649nm to 1707nm. The corresponding tuning rate for the generated wavelength is 0.73nm/°C. This is consistent with the value calculated from the $\frac{\partial n}{\partial T}$ data from Wiechmann et al. [9]. $\frac{\partial \lambda_i}{\partial T}$ is calculated from the quasi-phase-matching condition

$$\frac{n_p(T)}{\lambda_p} = \frac{n_s(T)}{\lambda_s} + \frac{n_i(T)}{\lambda_i} + \frac{1}{\Lambda}, \qquad [7.1]$$

where $n(T) = n(25^\circ C) + \frac{\partial n}{\partial T}(T - 25^\circ C)$ and T is the crystal temperature.

The uncertainty in published Sellmeier data for KTP and the uncertainty in grating period results in predicted wavelengths that are offset from the experimental results. However, Sellmeier data published by Fan et al. [10] predicted the closest wavelengths which were within ~9nm at Ti:sapphire wavelengths.

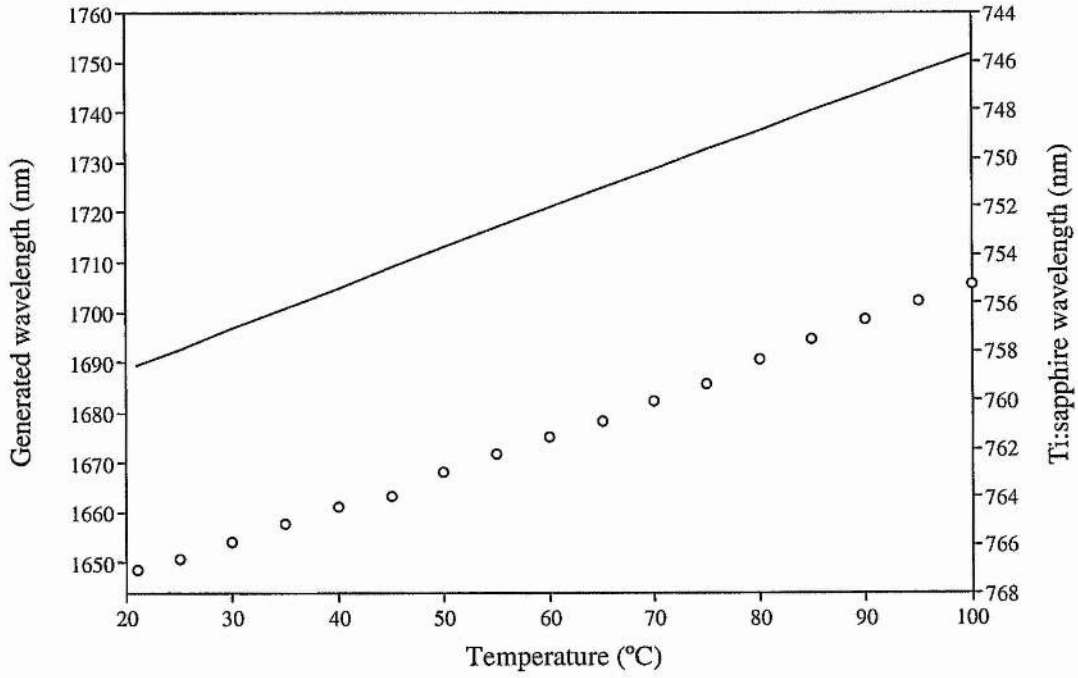

Figure 7.2 *Temperature tuning of PPKTP. The solid line shows the predicted temperature tuning based on ref. 9.*

The temperature acceptance-bandwidth of the interaction was then measured by fixing the Ti:sapphire wavelength while the crystal temperature was varied. Figure 7.3 shows two experimental bandwidth measurements, together with a theoretical

curve based on the temperature-dependent index data from [9]. Experimental data for two different Ti:sapphire wavelengths (and hence different temperatures of peak conversion) are shown; the circles and diamonds correspond to Ti:sapphire wavelengths of 761nm and 753nm and peak temperatures of 63°C and 111°C, respectively.

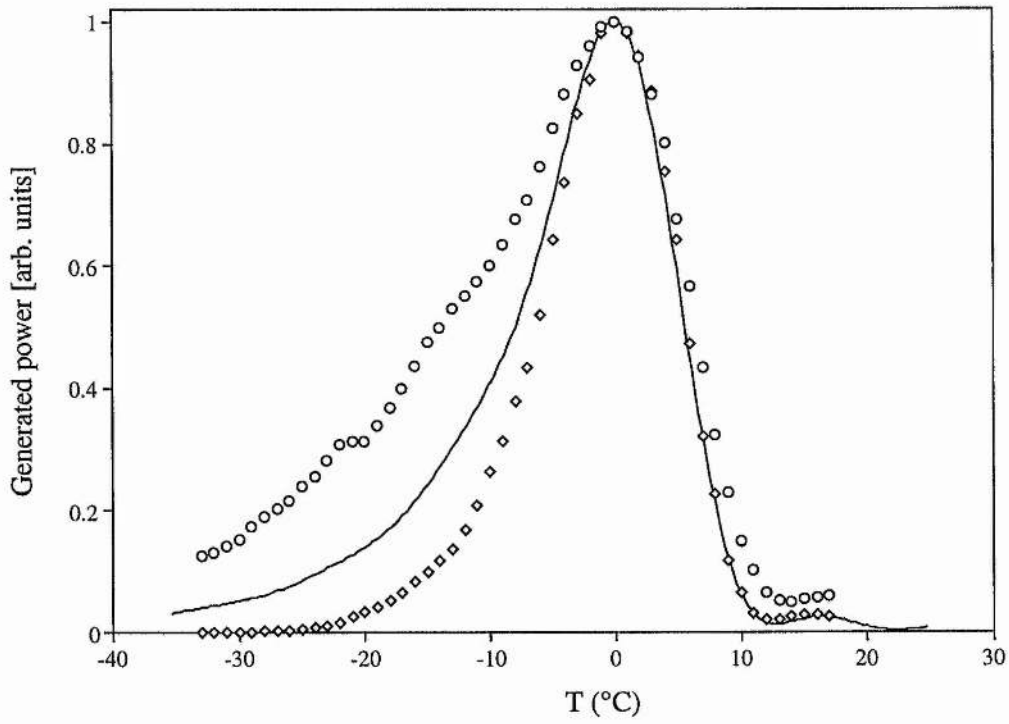

Figure 7.3 *Temperature acceptance-bandwidth of PPKTP. Solid line shows the theoretical prediction based on ref. 12. Experimental curves, circles and diamonds, correspond to temperatures of 63°C and 111°C, corresponding to Ti:sapphire wavelengths of 761nm and 753nm respectively.*

It is well known that for the case of tightly focused Gaussian beams, the acceptance-bandwidth curve deviates from the ideal sinc^2 shape associated with collimated beams, and, for example comprehensive analyses have been carried out by Boyd and Kleinman, [11] and Guha et al. [12]. The tight focusing of the red, $\xi_s = 1.34$, and green, $\xi_p = 1.75$, beams has resulted in the asymmetry of the experimental data as shown in figure 7.3. The theoretical curve in figure 7.3 is a normalised plot of the function h_s as defined in equation (15) in ref. [12], as a function of temperature (assuming small depletion of the waves at λ_p and λ_s). In ref. 12, h_s is defined as a function which shows the relative DFG efficiency, as a function of phase mismatch, for the general case of unequal confocal beam parameters. The present calculation is based on a Ti:sapphire wavelength of 767nm, a poled interaction length of 5mm, and the above beam focusing parameters. In order to plot h_s as a function of temperature in the present case, the phase-mismatch Δk has been related to the temperature deviation, ΔT, from the phase-matching temperature by

$$\Delta k = 2\pi\left(\frac{1}{\lambda_p}\frac{\partial n_p}{\partial T} - \frac{1}{\lambda_s}\frac{\partial n_s}{\partial T} - \frac{1}{\lambda_i}\frac{\partial n_i}{\partial T}\right)\Delta T \quad , \qquad [7.2]$$

where the $\frac{\partial n}{\partial T}$ values are from ref. [9].

The asymmetry observed in figure 7.3 results from a spread in the wavevectors in the focussed beams. Different wavevector components phase-match at different temperatures resulting in the broadening of the temperature acceptance bandwidth as

well as an offset in maximum conversion from Δk =0. In this experiment the maximum conversion occurs at Δk = -5.5 cm^{-1} (ΔT = 4 °C).

The theory in ref. 12 predicts a FWHM temperature acceptance-bandwidth of 6.9°C-cm which is close to the experimental values of 6.0°C-cm and 10°C-cm. This agreement suggests that the full 5mm interaction length is contributing to the DFG process. The difference between the two experimental bandwidths is not explained by the theory in ref. 12 which predicts similar bandwidths for each case. It should be noted that, strictly, this theory describes only deviations from conventional phase-matching and does not include the periodic domain inversion of the PPKTP. An improved model which includes the periodic-poling may explain this difference. Otherwise the discrepancy could be due to a thermal gradient between the crystal and thermocouple inside the oven.

The power of the DFG wavelength was measured using a calibrated germanium photo-detector, after the input beams had been removed by a silicon blocking filter. For input powers of 240mW at 523nm and 340mW at 767nm, a maximum generated power of 12μW at 1644nm was observed. These measurements, along with the measured beam waists of 11.5μm and 16.9μm for the green and red beams respectively, allows the value of the effective d_{33} coefficient to be estimated. A simplified calculation based on a plane wave approximation results in an effective d_{33} of ~5pm/V. This calculation assumes that the pump and signal beams are not substantially depleted by conversion to idler. However, a more detailed calculation based on eqn. (10) in ref. [13] results in an effective d_{33} value of ~4pm/V.

The theoretical predictions based on data by Fan et al. have been extended to determine the degree of tunability for OPOs based on PPKTP. Using a Nd:YAG laser @ 1064nm as the pump source, one can predict accessible wavelengths ranging from ~1.6μm up to the transparency limit of KTP. This is obtainable using a single grating and a temperature variation of ~200°C.

7.3 Summary and conclusions

In summary difference frequency generation and temperature tuning of PPKTP has been demonstrated. A temperature tuning rate of 0.73nm/°C was observed for the generated wavelength, a useful rate compared to the rapid tuning observed in PPLN. A generated power of 12μW (1.6μm) was obtained for input powers of 240mW (523nm) and 340mW (767nm). The value of the effective d_{33} coefficient was estimated to be ~5pm/V. From these studies, and experimental data, one can anticipate that PPKTP will prove to be a significant nonlinear material for the near- and mid-infrared, not only for DFG but also for OPOs, and having considerable flexibility through a combination of grating-period and temperature tuning. Indeed, sensitivity to temperature tuning can be engineered to suit requirements through appropriate design of grating period [1]. The high damage threshold of the bulk material together with the relatively large aperture available with PPKTP should allow, in particular, future application to high average-power, pulsed and cw tunable OPO's.

7.4 References

[1] Martin M. Fejer, G. A. Magel, Dieter H. Jundt and R. L. Byer, *IEEE J. Quant. Elect.* **28**, 11, 2631 (1992).

[2] A. Englander, R. Lavi, M. Katz, M. Oron, D. Eger, E. Lebiush, G. Rosenman and A. Skliar, *Optics Lett.* **22**, 21, 1598 (1997).

[3] A. Arie, G. Rosenman, A. Korenfeld, A. Skliar, M. Oron, M. Katz and D. Eger, *Optics Lett.* **23**, 1, 28 (1998).

[4] D. T. Reid, P. Loza-Alvarez, M. Ebrahimzadeh, E. U. Rafailov, P. Faller, D. J. Birkin, W. Sibbett, H. Karlsson and F. Laurell, *CLEO 98 Technical Digest, Optical Society of America* **CME3**, 17 (1998).

[5] Tolga Kartaloglu, Kahraman G. Köprülü, Orhan Aytür, Michael Sundheimer and W. P. Risk, *Optics Lett.* **23**, 1, 61 (1998).

[6] T. J. Edwards, G. A. Turnbull, M. H. Dunn and M. Ebrahimzadeh, *Optics Lett.* **23**, 11, 837 (1998).

[7] H. Karlsson and F. Laurell, *Appl. Phys. Lett.* **71**, 24, 3474 (1997).

[8] The crystal was fabricated by H. Karlsson and F. Laurell, Institute of Optical Research, Stockholm, Sweden.

[9] W. Wiechmann, S. Kubota, T. Fukui and H. Masuda, *Optics Letters* **18**, 15, 1208 (1993).

[10] Tso Yee Fan, C. E. Huang, B. Q. Hu, R. C. Eckardt, Y. X. Fan, Robert L. Byer and R. S. Feigelson, *Appl. Optics* **26**, 12, 2390 (1987).

[11] G. D. Boyd and D. A. Kleinman, *Appl. Phys.* **39**, 8, 3597 (1968).

[12] Shekhar Guha, Fei-jain Wu and J. Falk, *IEEE J. Quant. Elect.* **QE-18**, 5, 907 (1982).

[13] J. A. C. Terry, Y. Cui, Y. Yang, W. Sibbett and M. H. Dunn, *J. Opt. Soc. Am. B* **11**, 5, 758 (1994).

8 A continuous-wave optical parametric oscillator based on periodically poled KTiOPO4 and its application to spectroscopy.

8.1 Introduction

This chapter reports a cw DRO based on the nonlinear material periodically poled $KTiOPO_4$ (PPKTP). As discussed in chapter 7 Quasi-phase-matching (QPM) in periodically-poled materials offers advantages over traditional birefringent phase-matching for their use in nonlinear optical processes. Such materials have recently had a considerable impact in the field of nonlinear optics [1, 2]. PPKTP [3] is an attractive material for OPOs pumped by cw visible sources where the advantages of high laser damage threshold, low susceptibility to thermal lensing, and operation at room temperature without photorefractive damage, are particularly important.

PPKTP has recently been demonstrated in a near degenerate, cw, doubly-resonant OPO (DRO) [4]. This chapter reports a cw, DRO based on PPKTP that has been purposely designed as a smoothly tunable, single-frequency, source operating around 1.65μm for spectroscopic applications. Importantly, while conventional birefringent phase-matching in KTP is insensitive to crystal temperature, it has been shown previously that in the case of QPM, KTP demonstrates a useful degree of temperature tuning [5].

8.2 Stability requirements for single mode-pair operation of DROs

The cavity length stability requirements for DROs, with regard to obtaining single mode-pair output, have been discussed in chapter 2 and ref. [6]. In summary, easily stabilised operation of a DRO can be achieved when the mismatch in the signal and idler free spectral ranges, ΔFSR, is large compared to the widths of the signal and idler modes. Under this condition, detuning the cavity length results in discrete output peaks, corresponding to individual mode-pairs, which provides a clear feature upon which to lock the output of the OPO and ensure single-frequency operation.

The requirement for easily stabilised operation on a single mode-pair is therefore

$$\Delta L_{hop} > \Delta L_{stab}, \qquad [8.1]$$

$$\text{where } \Delta L_{hop} \approx \frac{\Delta FSR}{2\,FSR}\lambda_p, \text{ and } \Delta L_{stab} < \frac{\lambda_p}{4}\left(\frac{1}{F_s}+\frac{1}{F_i}\right).$$

In the case of QPM in PPKTP, where the pump, signal, and idler waves have the same linear polarisation, the FSRs of the signal and idler fields are dependent on the dispersive property of the material alone. Therefore operation at signal and idler wavelengths away from degeneracy is essential to obtain the necessary ΔFSR to ensure easily stabilised operation on a single mode-pair. For operation of the idler wavelength at 1.65μm we determine the range of output coupling such that equation 8.1 is satisfied.

Previously Henderson et al. [6] demonstrated single mode-pair operation of a cw DRO based on a bulk KTP crystal configured for near-degenerate, type-II, critical phase-matching. Type-II phase-matching results in a large ΔFSR even for operation near frequency degeneracy.

Figure 8.1 shows the calculated values for ΔL_{hop} and ΔL_{stab} for various values of signal and idler wavelengths. The calculations are based on a pump wavelength of 523nm, a cavity length of 15mm, a crystal length of 9mm, and an estimated maximum roundtrip power loss of 2%. For a 1% output coupling it can be seen that equation 8.1 is not satisfied for idler wavelengths below 1.2μm. However, for operation at an idler wavelength of 1.65μm it can be seen that equation 8.1 is adequately satisfied for all three values of output coupling.

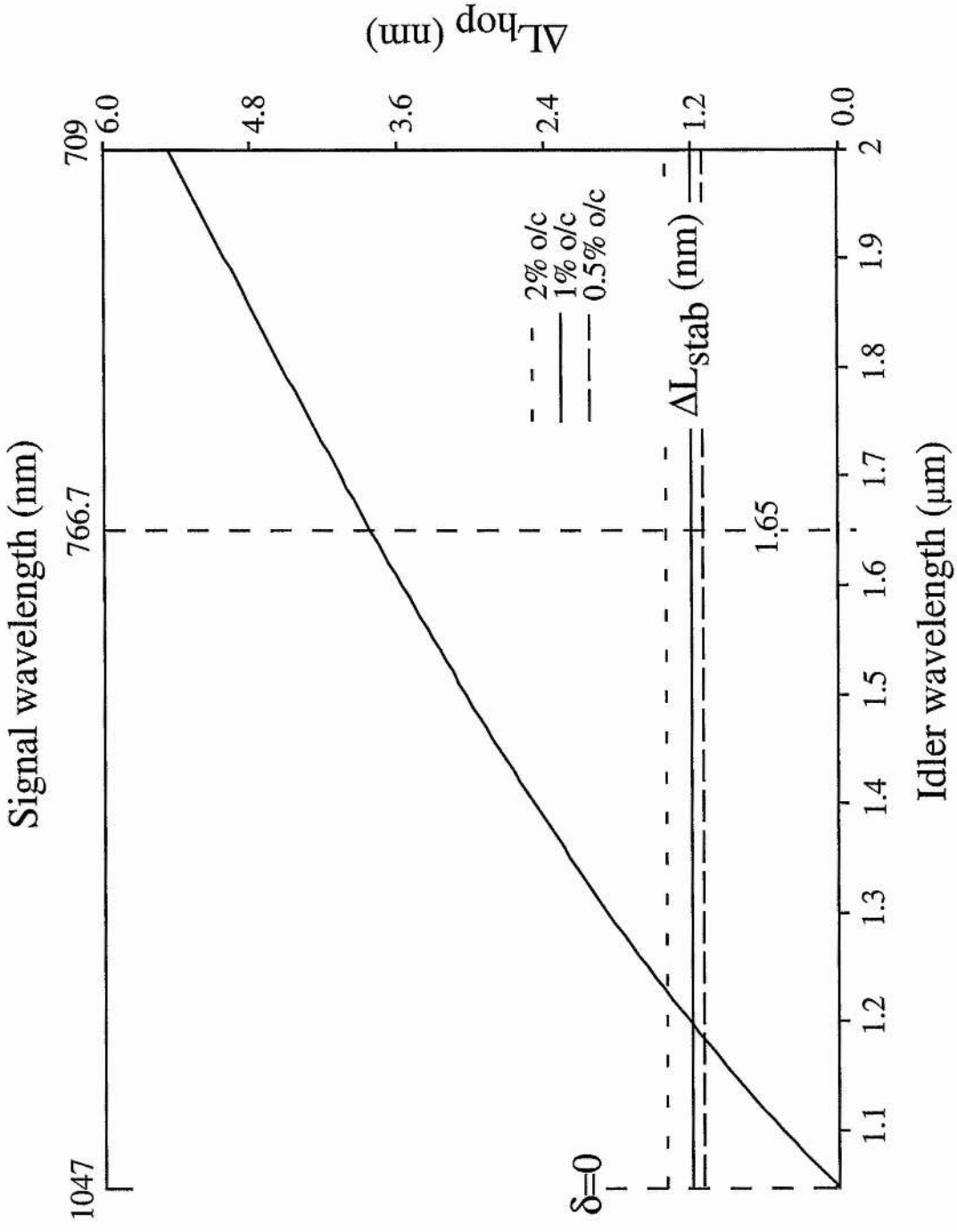

Figure 8.1 *Calculated values for ΔL_{hop} and ΔL_{stab} for various values of signal and idler wavelengths. For operation at an idler wavelength of 1.65μm the condition $\Delta L_{hop} > \Delta L_{stab}$ is adequately satisfied all three values of output coupling.*

8.3 Experimental configuration

The single-grating periodically poled crystal (9mm long x 1mm thick) was prepared as reported earlier [5] with the end faces polished and AR coated at the pump, signal, and idler wavelengths.

The experimental configuration of the OPO is shown in figure 8.2. The pump source operating at $\lambda_p = 523$nm is an all-solid-state, diode-pumped Nd:YLF laser with an intracavity KTP frequency-doubler giving an output power of ~200mW. Smooth tuning of the pump laser, over a range of ~10GHz, is achieved by piezoelectric control of the cavity length. The OPO is based on a 9mm long, 1mm aperture, PPKTP crystal located in a linear cavity, 15mm in length. The mirrors have radius of curvature r=15mm and are coated for high reflectivity at the signal wavelength λ_s around 766nm, and 99% reflectivity at the idler wavelength $\lambda_i = 1.65\mu$m thus forming a doubly-resonant oscillator. A servo-control system, stabilising the cavity length, maintains a constant output power and operation on a single signal and idler mode-pair. Temperature tuning of the output frequency is achieved using a Peltier heat pump which can vary the PPKTP crystal temperature from room temperature up to a maximum of 80 °C.

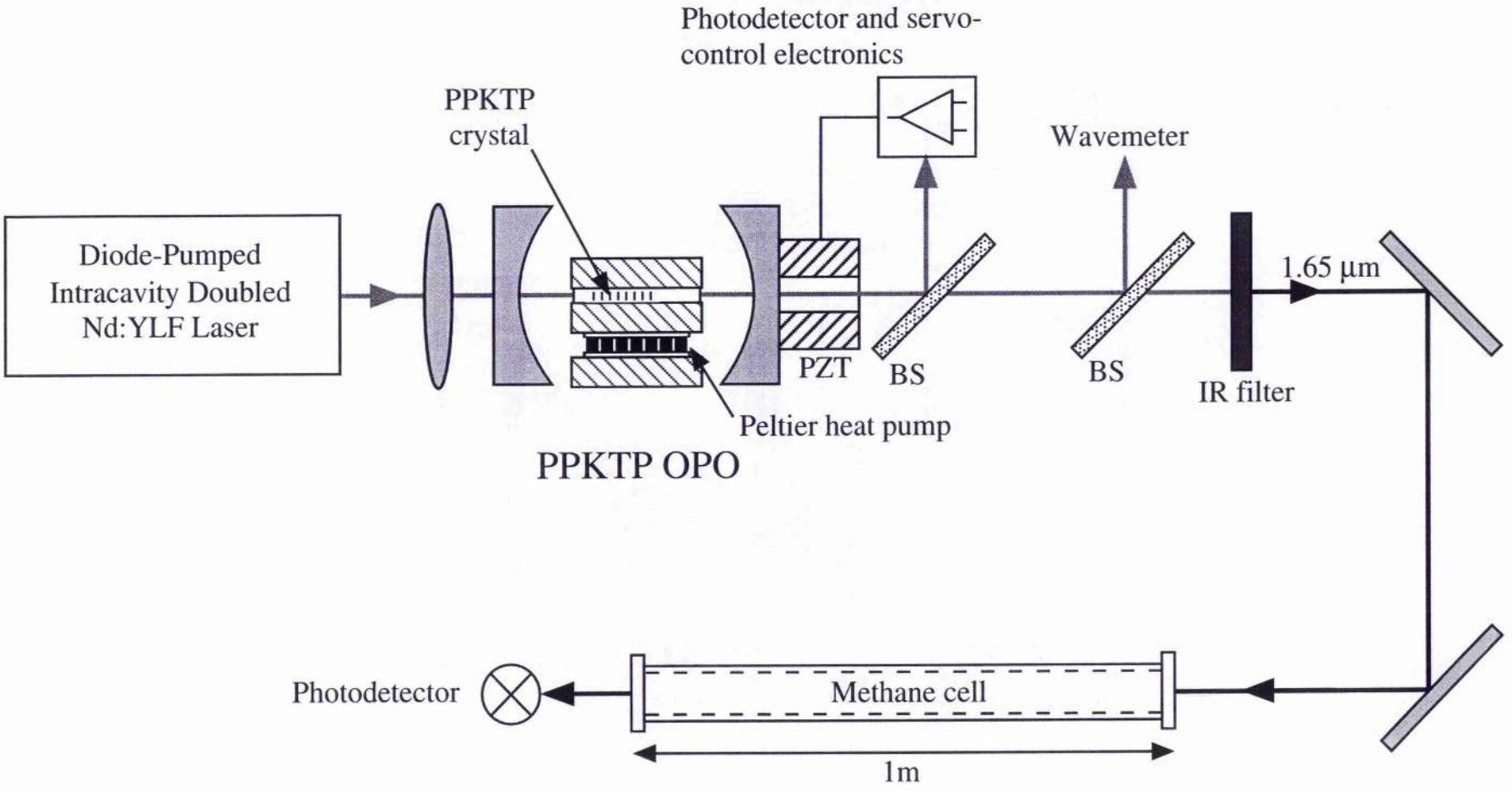

Figure 8.2

Schematic of the experimental layout. The temperature of the PPKTP crystal is varied using a Peltier heat pump. A beamsplitter (BS) provides a signal for the cavity length servo system.

The output of the OPO was temperature tuned by varying the PPKTP crystal temperature from 20°C to 55°C (see figure 8.3). In this case the temperature tuning range was limited by the mirror coatings. Over this temperature range the signal wavelength varies from 769.14nm to 763.44nm, monitored using a wavemeter and corresponds to an idler wavelength λ_i variation of 1639.17nm to 1665.67nm. The corresponding temperature tuning rate for the idler wavelength is 0.73nm/°C, which is consistent with the value obtained previously from a difference-frequency mixing experiment [5] and from the value calculated from the $\frac{\partial n}{\partial T}$ data of Wiechmann et al. [7].

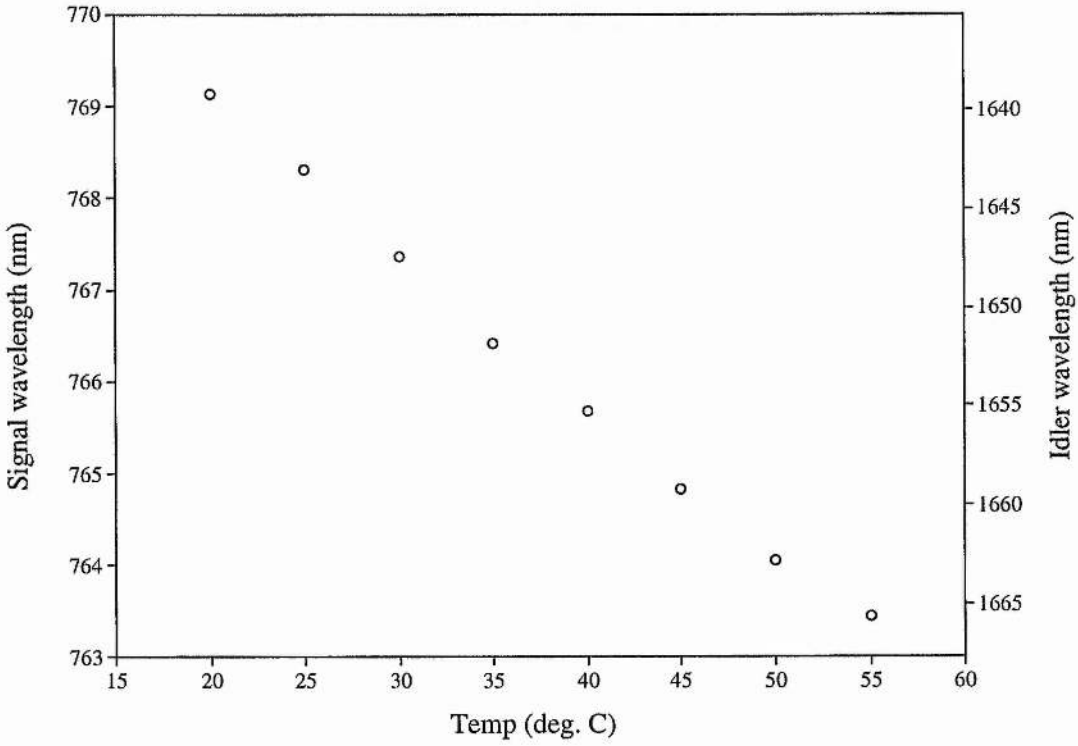

Figure 8.3 *Temperature tuning of PPKTP. The tuning range was limited by the mirror coatings.*

The power of the idler wavelength was measured using a calibrated germanium photo-detector, after the transmitted pump beam had been removed by an IR filter. An experimental pump power threshold of only 25mW was observed. For an input pump power of ~200mW at 523nm, a useful output power of 10mW at 1644nm was observed. The OPO operated on a single signal and idler mode-pair, confirmed using a Fabry-Perot interferometer (see figure 8.4), that was smoothly tuned by smoothly tuning the pump laser. The ratio of the tuning ranges of the signal and idler frequencies, $\Delta\nu_s$ and $\Delta\nu_i$ respectively, is given by

$$\frac{\Delta\nu_s}{\Delta\nu_i} = \frac{\lambda_i}{\lambda_s}. \qquad [8.2]$$

Hence, continuously tuning of the pump laser over ~10GHz resulted in the signal wavelength tuning over ~7GHz, monitored using a wavemeter, corresponding to the tuning of the idler wavelength over ~3GHz (see figure 8.5). The smooth tuning range of the OPO is limited by the smooth tuning range of the pump laser.

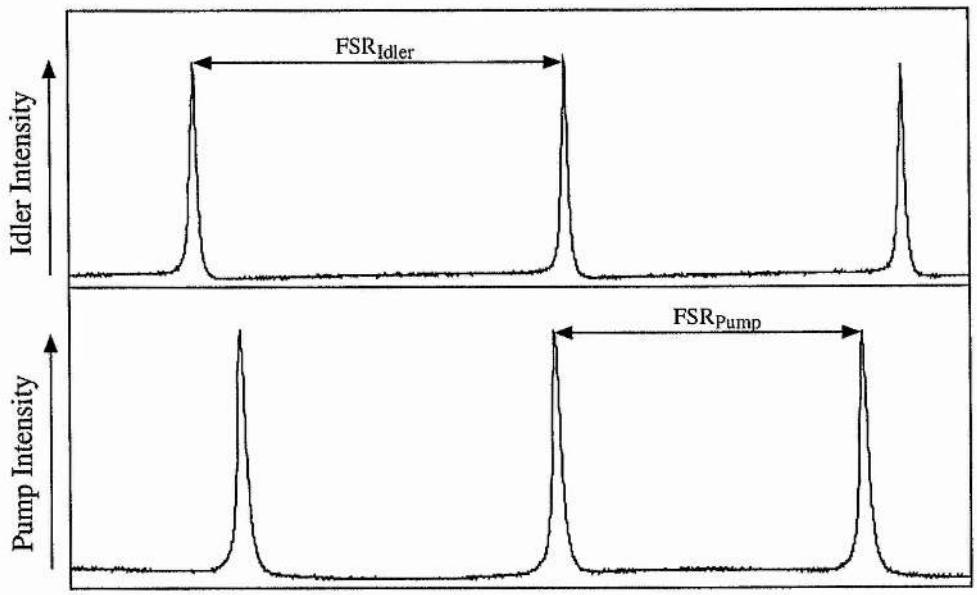

Figure 8.4 *When using a single-frequency pump source, the OPO operates on a single signal and idler mode-pair. Monitored on a scanning Fabry-Perot Interferometer.*

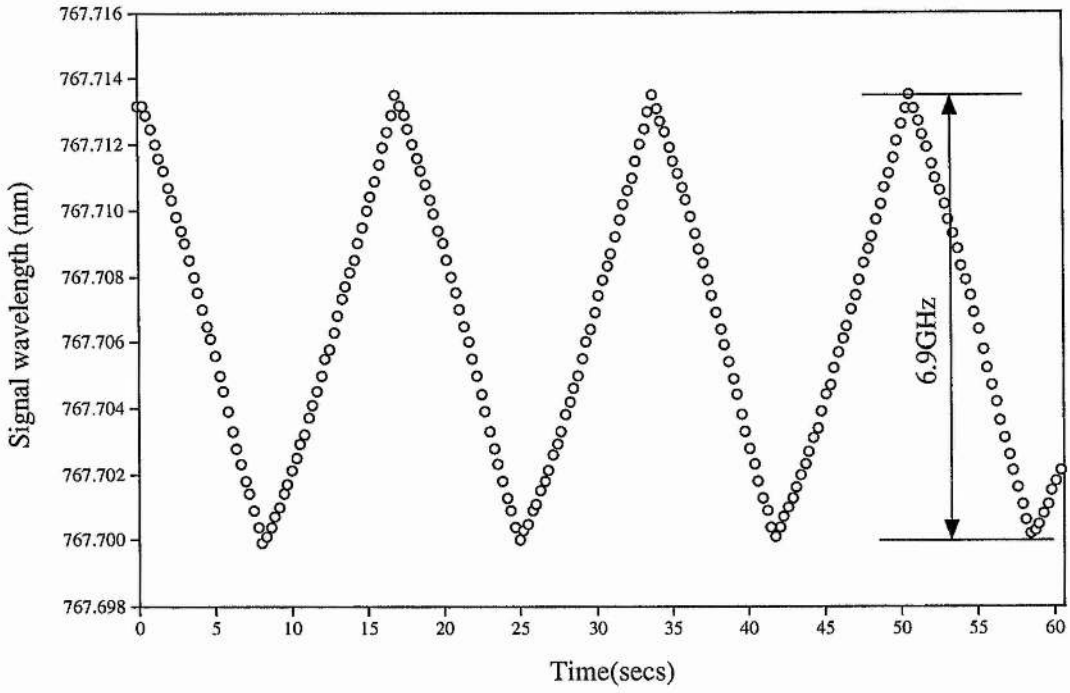

Figure 8.5 *A single signal and idler mode pair can be smoothly tuned by smoothly tuning the pump laser. Tuning the pump laser over ~10GHz results in the signal tuning over ~7GHz (recorded using a wavemeter). This corresponds to the tuning of the idler over ~3GHz.*

To demonstrate the practicality of the OPO we recorded the absorption spectrum of methane around 1649nm. The output of the OPO passes through a gas cell having a path length of 1 meter and containing methane at a pressure of 50 torr. The output idler wavelength is scanned over 3GHz then back again by scanning the pump laser. Figure 8.6 shows the transmitted OPO output power recorded as a function of frequency using a photodiode. The absorption feature is predominantly Doppler broadened (Doppler width calculated to be 560MHz). The wavelength of the idler is

determined by measuring the pump and signal wavelengths using a wavemeter. Temperature tuning the OPO crystal allows different spectral regions to be accessed.

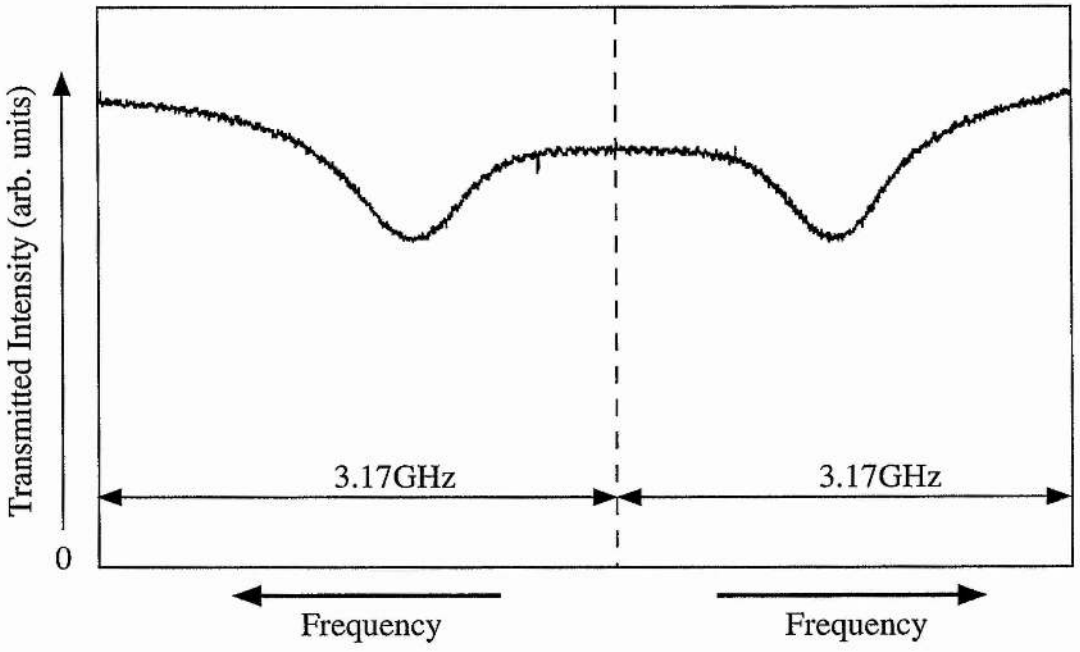

Figure 8.6 *Absorption spectrum of a methane transition around 1649nm. The output of the OPO is scanned over 3.17GHz by tuning the pump laser.*

8.4 Summary and conclusions

In summary a single frequency cw OPO based on PPKTP has been demonstrated. The OPO operated with a low pump power threshold of 25mW and an output power of 10mW (1.65μm), for an input pump power of ~200mW (523nm). The single frequency output of the OPO was smoothly tuned over ~3GHz by smoothly tuning the pump laser. The idler wavelength was temperature tuned from 1639.17nm to

1665.67nm by varying the crystal temperature from 20 to 55°C, limited to the bandwidth of the mirror coatings. The relatively lower temperature tuning rate of PPKTP compared to PPLN, along with its high photorefractive damage threshold, makes PPKTP an attractive nonlinear material for CW-OPOs operating at room temperature. The suitability of the OPO as a spectroscopic source was demonstrated by recording the absorption spectrum of methane around 1649nm.

8.5 References

1 Martin M. Fejer, G. A. Magel, Dieter H. Jundt and R. L. Byer, *IEEE J. Quant. Elect.* **28**, 11, 2631 (1992).

2 Lawrence E. Myers and Walter. R. Bosenberg, *IEEE J. Quant. Elect.*, **33**, 10, 1663 (1997).

3 H. Karlsson and F. Laurell, *Appl. Phys. Lett.* **71**, 24, 3474 (1997).

4 A. Garashi, A. Arie, G. Rosenman and A. Skliar, Conference on Lasers and Electro-Optics-Europe (Post Deadline papers) September 1998, CPD1.10, (1998).

5 G. M. Gibson, G. A. Turnbull, M. Ebrahimzadeh, M. H. Dunn, H. Karlsson, G. Arvidsson and F. Laurell, *Appl. Phys. B*, **67**, 5, 675 (1998).

6 A. J. Henderson, M. J. Padgett, F. G. Colville, J. Zhang and M. H. Dunn, *Optics Comm.* **119**, 256 (1995).

7 W. Wiechmann, S. Kubota, T. Fukui and H. Masuda, *Optics Letters* **18**, 15, 1208 (1993).

9 Summary and Conclusions

This thesis details the work relating to stable, cw, continuously frequency tunable, OPOs. A doubly-resonant OPO has been demonstrated, operating on a single pair of signal and idler modes, which was smoothly tunable by smoothly tuning the pump laser. The frequency selective property of DROs results in single mode-pair operation of devices having the combination of simple cavity design and low pump power threshold. Mode-hoping within DROs has been shown to be a reliable method of selecting different signal and idler mode-pairs within the phase-matched bandwidth.

The suitability of the DRO as a spectroscopic source was demonstrated by using the device to record the transmission spectrum of cesium molecules in the 1μm spectral region. The output of the OPO was scanned over~4GHz which was limited only by the tuning range of the pump laser. A combination of angle-tuning and controlled mode-hops allowed these scans to be centered at different frequencies throughout the phase-matched bandwidth allowing a larger spectral coverage.

The advantage of the low pump power threshold associated with DROs has also been demonstrated by using an ultra-compact, frequency-doubled, microchip laser as the pump source. In this case, the DRO not only has an advantage in terms of its low threshold but also in its ability to operate on a single mode-pair even when pumped by a multilongitudinal mode laser.

The suitability of the new nonlinear material Periodically Poled KTP (PPKTP), within frequency conversion applications, was assessed by a difference frequency generation experiment. PPKTP demonstrated a significant degree of temperature tuning which is more useful than the rapid tuning rate observed with PPLN. The use of such engineered nonlinear materials has the advantage of providing greater flexibility through the design of their gratings.

PPKTP was demonstrated to be a suitable material for use in cw OPOs. The flexibility of grating engineered phase matching in periodically poled materials allowed a DRO to be specifically designed as a spectroscopic source for methane around 1.65μm. The DRO was based on PPKTP and operated on a single mode-pair which was continuously tunable through its tunable pump source. The mismatch in the free spectral ranges of the signal and idler fields was shown to be an important factor in the easy stabilisation of this device. The OPO was demonstrated by recording the transmission spectrum of methane near 1649nm.

The combination of compact, low threshold, DROs and the flexibility in the choice of pump lasers should provide very compact sources of tunable, coherent, radiation for low power applications. This in combination with the recent demonstrations of engineered nonlinear materials, in particular periodically poled crystals, should provide even greater efficiency opening up the possibility of stable, tunable OPOs directly pumped by commercial laser diodes.

10 Appendices

Appendix A. Program Listing

Appendix B. Summary of Pump Power Thresholds

Appendix C. Error Signal Circuit for Stabilising DROs

Appendix D. Publications/Conferences

10.1 Appendix A. Program Listing

The following program listing is used to model the dynamic behaviour of a DRO as detailed in chapter 4. The model calculates the signal and idler fields as they build up from the spontaneous parametric fluorescence. The main inputs to the model are Cavity length, crystal length, pump level above threshold, and rate of change of cavity length.

```
/*****************************************************************/
/*                    OPO DYNAMICAL BEHAVIOUR                    */
/*****************************************************************/


#include <complex.h>

#include <iostream.h>

#include <stdlib.h>

#include <fp.h>

#include <Files.h>

#include <StandardFile.h>

#include <stdio.h>


/*******************************/

/*      OPO model parameters       */

/*******************************/


#define h                6.626075e-34

#define C                3e8

#define wavelengthP      523e-9          // Wavelength of pump

#define wavelengthSI     1047e-9         // Wavelength of sig/idler

#define D                30e-6           // Beam waist

#define l                6e-3            // Crystal length

                                                  (physical length)

#define PI               3.1415927

#define Eo               8.854e-12       // Permittivity of a vacuum

#define deff             3.2e-12         // Effective nonlinear coefficient
```

```
#define NoSegs      1e1      // Number of segments of the OPO
                             crystal

#define ns          1.7445   // Signal refractive index
#define ni          1.8302   // Idler refractive index
#define np          1.7879   // Pump refractive index

/* Reflection Coeficients (amplitude) */

#define rPi         0.7      // Reflectivity input mirror (pump)
#define rPo         0.68     // Reflectivity output mirror (pump)
#define rSi         0.999    // Reflectivity input mirror (signal)
#define rSo         0.9975   // Reflectivity output mirror (signal)
#define rIi         0.999    // Reflectivity input mirror (idler)
#define rIo         0.9975   // Reflectivity output mirror (idler)

/* Losses (amplitude) */

#define LP          0.1      // Single pass loss (pump)
#define LS          0.1      // Single pass loss (signal)
#define LI          0.1      // Single pass loss (idler)

/* parameters (change for each experiment) */

#define Lphs        11e-3    // Cavity length (physical)
#define plotpoints  1e3      // Number of points to plot
```

```
#define tmax            5e-6        // Maximum time interval (scan time)
#define p               1.75        // Pumping level (No of times threshold
                                                                    power)
#define scanrate        278.5e-6    // Scan rate in m/sec


int main()
{
FILE *filePointer;

long        tCounter;
double      V, Vp, deltat, deltaLhop, rTripTime, t, z, a, b, X, J, L, time, modeVol,
            NoPoints, Ph, TPi, TPo, TSo, pSpace, Pratio, Pa, Pb, Pc, theta, FSR, deltav,
            Beta, F;
complex     alphaSf, alphaSb, alphaIf, alphaIb, alphaPf, alphaPb, alphaPinc, alphaSfold,
            alphaSbold, alphaIfold, alphaIbold, alphaPfold, alphaPbold, alphaSinit,
            alphaIinit;

F = (2*PI)/(log(1/(rSi*rSi))+log(1/(rSo*rSo))+(2*log(1/(1-(LS*LS)))));
L = Lphs + (((ns+ni)/2)-1)*l;
deltaLhop = (wavelengthP/2)*((ni-ns)*l)/L;
modeVol = PI*pow(D,2)*L;
Vp = C/wavelengthP;
V = C/wavelengthSI;
rTripTime = 2*(L/C);
```

```
deltat = rTripTime;

NoPoints = tmax/deltat;

pSpace = NoPoints/plotpoints;


TPi = sqrt(1-(rPi*rPi));

TPo = sqrt(1-(rPo*rPo));

TSo = sqrt(1-(rSo*rSo));


X = sqrt((pow(deff,2)*pow(PI,2)*l*pow(Vp,4)*h)/(2*Eo*pow(C,4)*pow(np,2)));


// Set of equations to calculate the threshold and hence pump level


Pa = (pow((2*X),2)*(sqrt(1-(rPi*rPi))*sqrt(1-(LP*LP)))*rPo)/(1-(rPo*rPi*
                                                        (1-(LP*LP))));

Pb = ((2*X)*sqrt(1-(rPi*rPi))*(1+(rPo*sqrt(1-(LP*LP)))))/(1-(rPo*rPi*(1-(LP*LP))));

Pc = 1-(1/(rSo*rSi*(1-(LS*LS))));


alphaPinc = sqrt(p)*(-Pb+sqrt((Pb*Pb)-(4*Pa*Pc)))/(2*Pa);


alphaPb = alphaPinc*TPi;


theta = wavelengthSI/(PI*D);

FSR = C/(2*L);

deltav = FSR/F;

Beta = ((h/(2*PI))*pow(2*PI*V,5)*ni*deff*deff)/(PI*PI*pow(C,5)*ns*np*Eo);
```

```
Pratio = Beta*l*l*0.5*theta*theta*(PI/2)*deltav;

alphaSinit = alphaPinc*sqrt(Pratio*(Vp/V));
alphaIinit = alphaPinc*sqrt(Pratio*(Vp/V));

alphaSb = alphaSinit;
alphaIb = alphaIinit;

printf("OPO Results \n");
filePointer = fopen("Expt?","w");

t = -1;
time = deltat*(t + 1);

cout << "Starting value of alphaS " << alphaSb << '\n';
cout << "Starting value of alphaI " << alphaIb << '\n';

fprintf(filePointer,"OPO Model Parameters \t");
fprintf(filePointer,"Signal Power \t");
fprintf(filePointer,"Pump Power \t");
// fprintf(filePointer,"Phase \t");
fprintf(filePointer,"Time \n");
fprintf(filePointer,"Number of data points %.3e \n", NoPoints);
fprintf(filePointer,"Point spacing %.3e \n", pSpace);
fprintf(filePointer,"Points Plotted %.3e \n", plotpoints);
```

```
fprintf(filePointer,"Max time %.3e \n", tmax);
fprintf(filePointer,"Scanrate %.3e \n", scanrate);
fprintf(filePointer,"Cavity Length (physical) %.3e \n", Lphs);
fprintf(filePointer,"Cavity Length (optical) %.3e \n", L);
// fprintf(filePointer,"Delta t %.3e \n", deltat);
fprintf(filePointer,"NoSegments (crystal) %.3e \n", NoSegs);
// fprintf(filePointer,"Hoptime %.3e \n", hoptime);
fprintf(filePointer,"DeltaLhop %.3e \n", deltaLhop);
fprintf(filePointer,"Pump frequency %.3e \n", Vp);
fprintf(filePointer,"Signal frequency %.3e \n", V);
fprintf(filePointer,"theta %.3e \n", theta);
fprintf(filePointer,"Beta %.3e \n", Beta);
fprintf(filePointer,"deltav %.3e \n", deltav);
fprintf(filePointer,"FSR %.3e \n", FSR);
fprintf(filePointer,"Finesse %.3e \n", F);
fprintf(filePointer,"Pratio %.3e \n", Pratio);
// fprintf(filePointer,"Mode Volume %.3e \n", modeVol);
fprintf(filePointer,"Beta %.3e \n", Beta);
fprintf(filePointer,"X %.3e \n", X);
fprintf(filePointer,"AlphaSo %.3e ", real(alphaSb));
fprintf(filePointer," i %.3e \n", imag(alphaSb));
fprintf(filePointer,"AlphaIo %.3e ", real(alphaIb));
fprintf(filePointer," i %.3e \n", imag(alphaIb));
fprintf(filePointer,"Threshold Pump Power %.3e \n",
                                    pow(abs((alphaPinc/sqrt(p))),2)*h*Vp);
```

```
// fprintf(filePointer,"AlphaPinc %.3e \n", alphaPinc);
fprintf(filePointer,"Inc Pump Power %.3e \n", pow(abs(alphaPinc),2)*h*Vp);
fprintf(filePointer,"Round trip time %.3e \n\n\t", rTripTime);

z = 0;
a = 0;
b = 0;

for (tCounter=0; tCounter<NoPoints; tCounter++)
{
t = tCounter;
time = deltat*(t + 1);

Ph = ((-4*PI/wavelengthSI)*(tmax*scanrate)) +
                                ((8*PI/wavelengthSI)*(tmax*scanrate)*(t/NoPoints));

alphaPfold = alphaPb;
alphaSfold = alphaSb;
alphaIfold = alphaIb;

for(a=0; a<NoSegs; a++)
{
alphaPf = (alphaPfold - (2*(X/(NoSegs))*alphaSfold*alphaIfold));

alphaSf = (alphaSfold + (2*(X/(NoSegs))*alphaPfold*conj(alphaIfold)));
```

```
alphaIf = (alphaIfold + (2*(X/(NoSegs))*alphaPfold*conj(alphaSfold)));

alphaPfold = alphaPf;
alphaSfold = alphaSf;
alphaIfold = alphaIf;
}

alphaPf = alphaPfold*exp(complex(0,Ph*2))*rPo*sqrt(1 - (LP*LP));
alphaSf = alphaSfold*exp(complex(0,Ph))*rSo*sqrt(1 - (LS*LS));
alphaIf = alphaIfold*exp(complex(0,Ph))*rIo*sqrt(1 - (LI*LI));

alphaPbold = alphaPf;
alphaSbold = alphaSf;
alphaIbold = alphaIf;

for(b=0; b<NoSegs; b++)
{
alphaPb = (alphaPbold - (2*(X/(NoSegs))*alphaSbold*alphaIbold));

alphaSb = (alphaSbold + (2*(X/(NoSegs))*alphaPbold*conj(alphaIbold)));

alphaIb = (alphaIbold + (2*(X/(NoSegs))*alphaPbold*conj(alphaSbold)));

alphaPbold = alphaPb;
```

```
alphaSbold = alphaSb;

alphaIbold = alphaIb;

}


alphaPb = alphaPbold*exp(complex(0,Ph*2))*rPi*sqrt(1 - (LP*LP)) +
                                                    (TPi*alphaPinc);

alphaSb = alphaSbold*exp(complex(0,Ph))*rSi*sqrt(1 - (LS*LS));

alphaIb = alphaIbold*exp(complex(0,Ph))*rIi*sqrt(1 - (LI*LI));


// conditional statements to maintain alpha to be at least alpha start


if(abs(alphaSb) < abs(alphaSinit))

{

alphaSb = alphaSinit;

}


if(abs(alphaIb) < abs(alphaIinit))

{

alphaIb = alphaIinit;

}


alphaPfold = alphaPb;

alphaSfold = alphaSb;

alphaIfold = alphaIb;
```

```
z = z + 1;

// conditional statements to only plot every pSpace points

if(z > pSpace-1)
{
z = 0;
fprintf(filePointer,"%.3e\t",  pow(((abs(alphaSf)*TSo)/rSo),2)*h*V);
fprintf(filePointer,"%.3e\t",  pow(((abs(alphaPf)*TPo)/rPo),2)*h*Vp);
// fprintf(filePointer,"%.3e\t", Ph);
fprintf(filePointer,"%.3e\n\t", time);
}

// conditional statements to only plot first 100 points

/*
if (z<100)
{
fprintf(filePointer,"%.3e\t", pow(((abs(alphaSf)*TSo)/rSo),2)*h*V);
fprintf(filePointer,"%.3e\t", pow(((abs(alphaPf)*TPo)/rPo),2)*h*Vp);
fprintf(filePointer,"%.3e\n\t", time);
}
*/
}
```

```
    fclose(filePointer);

    return EXIT_SUCCESS;

}
```

10.2 Appendix B. Summary of Pump Power Thresholds

Assuming confocal focusing and no mirror dephasing

	Pump Power Threshold	Typical Values
DRO with single pass pump	$P_{threshold} = K\frac{\pi^2}{F_s F_i}$	10's mW
DRO with pump enhancement	$P_{threshold} = K\frac{\pi^2}{4F_s F_i Enh_p}$	milliwatts
SRO with single pass pump	$P_{threshold} = K\frac{\pi}{F_i}$	Watts
SRO with pump enhancement	$P_{threshold} = K\frac{\pi}{2F_i Enh_p}$	100's mW

$$K = \frac{n_p^2 \varepsilon_o c^4}{2\pi^2 L_{crystal} \left|d_{eff}\right|^2 \left(1-\delta^2\right)^2 \nu_p^3}$$

$Enh_p = \frac{2\gamma_p F_p^2}{\pi^2}$ is the maximum enhancement of the pump field inside the cavity.

10.3 Appendix C. Error Signal Circuit for Stabilising DROs

The electronic circuit shown overleaf generates the error signal for stabilising a DRO. The OPO is slightly detuned from optimum power which is monitored on a standard photodiode. The output of the photodiode is subtracted from a voltage reference to give a +ve or -ve error signal, dependent on whether the cavity length is increased or decreased (0 volts for a perfectly locked cavity). The resulting signal is then integrated to give a control voltage, controlling the cavity length such that the error signal is minimised.

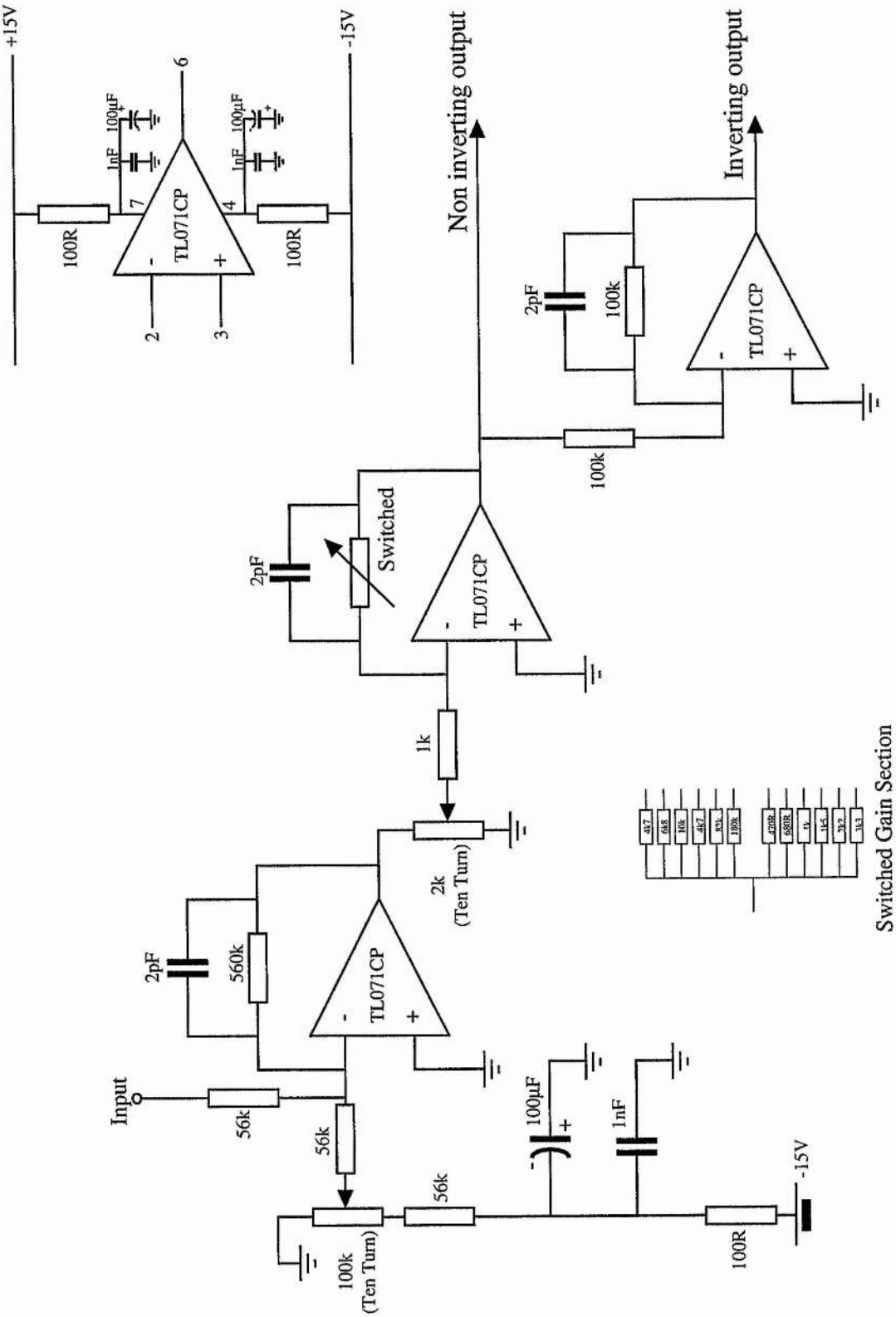

Schematic of error signal and pre-amp circuit.

10.4 Appendix D. Publications/Conferences

Publications

"Dynamic behaviour of a doubly resonant optical parametric oscillator," G. M. Gibson, G. R. Morrison, P. L. Hansen, M. H. Dunn, and M. J. Padgett, *Optics Communications* **136** (1997) p423-428.

"Application of a continuously tunable, cw optical parametric oscillator for high-resolution spectroscopy," G. M. Gibson, M. H. Dunn, and M. J. Padgett, *Optics Letters* **23**, 1, (1998) p40-42.

"Microchip laser-pumped continuous-wave doubly resonant optical parametric oscillator," G. M. Gibson, R. S. Conroy, A. J. Kemp, B. D. Sinclair, M. J. Padgett, and M. H. Dunn, *Optics Letters* **23**, 7, (1998) p517-518.

"Temperature-tuned difference-frequency mixing in periodically poled $KTiOPO_4$," G. M. Gibson, G. A. Turnbull, M. Ebrahimzadeh, M. H. Dunn, H. Karlsson, G. Arvidsson, F. Laurell, *Applied Physics B* **67**, 5, 675 (1998).

"Continuous-wave optical parametric oscillator based on periodically poled $KTiOPO_4$ and its application to spectroscopy," G. M. Gibson, M. Ebrahimzadeh, M. J. Padgett, and M. H. Dunn, *To be published in Optics Letters,* (1999).

Conferences

"Dynamic behaviour of a doubly resonant optical parametric oscillator," G. M. Gibson, G. R. Morrison, P. L. Hansen, M. H. Dunn, and M. J. Padgett, P17 in Lasers and Electro-Optics Society (LEOS) Scottish Chapter, 25th September (1996) Heriot-Watt University.

"Development of a continuous frequency tunable cw optical parametric oscillator," G. M. Gibson, M. H. Dunn, and M. J. Padgett, P6 in Lasers and Electro-Optics Society (LEOS) Scottish Chapter, 3rd September (1997) University of Strathclyde.

"The application of a continuously tunable, cw optical parametric oscillator for high-resolution spectroscopy," G. M. Gibson, M. H. Dunn, and M. J. Padgett, in The Thirteenth National Quantum Electronics conference (QE13) University of Wales, Cardiff. 1997 Technical Digest p20. (I.O.P., September 1997).

"The application of a continuously tunable, cw optical parametric oscillator for high-resolution spectroscopy," G. M. Gibson, M. H. Dunn, and M. J. Padgett, Paper CMK6 in Conference on Lasers and Elecro-optics (CLEO), 1998 Technical Digest series Vol. 6 (O.S.A., Washington D. C. 1998).

"Microchip laser-pumped continuous-wave doubly resonant optical parametric oscillator," G. M. Gibson, R. S. Conroy, A. J. Kemp, B. D. Sinclair, M. J. Padgett, and M. H. Dunn, Paper CTuM14 in Conference on Lasers and Elecro-optics (CLEO), 1998 Technical Digest series Vol. 6 (O.S.A., Washington D. C. 1998).